Novel Encapsulation of Water Soluble Active Ingredients to Achieve Their Controlled Release in Aqueous Environment

By

Cong Sui

A thesis submitted to
The University of Birmingham
for the degree of
DOCTOR OF PHILOSOPHY

School of Chemical Engineering
The University of Birmingham
July 2018

UNIVERSITYOF
BIRMINGHAM

University of Birmingham Research Archive

e-theses repository

Abstract

Encapsulation technology has been widely researched and applied to different industry sectors. There are vast examples of encapsulation for controlled release of hydrophilic or hydrophobic ingredients to the target place. However, it is still difficult to encapsulate the small water-soluble salts or molecules, which can achieve long-term sustained release or even no release in water. The objectives of the project is to encapsulate small water-soluble salts or molecules exhibiting sustained release or no release in the aqueous environment.

To achieve the target, three strategies were proposed here to encapsulate potassium chloride and allura red (dye) as model-small water soluble ions and molecules with low molar mass, respectively. A novel type of organic-inorganic composite solid microsphere, comprised of polystyrene sulfonate and silica ($PSS-SiO_2$) was developed here utilising the oppositely charged ion exchange resins to achieve a sustained release of K^+ ions in aqueous environment for over 48 hours. To the author's best knowledge, it exhibits >8 times longer than what had been achieved previously for the release of water soluble inorganic salts.

Furthermore, a novel type of melamine formaldehyde (MF) based microcapsules exhibiting a desirable barrier property has been developed to encapsulate KCl and allura red *via* an *in situ* polymerisation method. They showed a sustained release of KCl and allura red for 12 h and >10 days in aqueous environment, respectively. As far as the author knows, it had not been possible to fabricate MF microcapsules with hydrophilic ingredients encapsulated, achieving a sustained release of payload in water. This work expands MF based materials from the encapsulation of hydrophobic ingredients to hydrophilic ones. The developed MF formation method may provide a new way to deliver different types of water soluble ingredients, which can have applications in various areas of scientific research and industry.

Finally, a novel formulation for encapsulation of KCl and allura red has been developed based on the formation of melamine formaldehyde-octadecyltrichlorosilane-melamine formaldehyde (MOM) microcapsules, achieving no release in aqueous environment for 1 month. The key to provide the proper barrier to entrap the active ingredients is profited from the sandwich of the hydrophobic intervening layer between two melamine formaldehyde shells. It is a breakthrough to prevent the leakage of small water soluble ingredients from the carrier, which is of great significance for their long-term storage until they are delivered to a target place via triggered release in many applications. Also, it is the first time to fabricate the microcapsules with a hydrophobic layer embedded in the shell materials, applied in the delivery of hydrophilic active ingredients.

Acknowledgements

I would like to thank all of the following people who have made this thesis possible.

Firstly, I would like to express my immense gratitude and appreciation to Prof. Zhibing Zhang and Prof. Shuhong Yu in University of Science and Technology of China (USTC) for providing the 3+3 dual doctorate degree program to me, building a bridge between the two universities. I will never forget their invaluable guidance, plentiful resources, inspiration and support during my PhD research. I also thank Prof. Jon Preece as my secondary supervisor for his support, patience, kindness, careful thought and valuable insight in my research.

I would like to thank Dr Fideline Tchuenbou-Magaia for her patience, generous help and support during my research programme. I feel grateful to Cheryl Powell for her kind help with using a flame photometer. I am thankful to Frank Biddlestone for his generous help in supporting the FT-IR measurements. I would like to thank Chuan Li, Geng Qiao and Daniel Smith for their help in using STA equipment, and also thank Rui Wang for her help in using a freeze drier. Thanks go to Paul Stanley and Theresa Morris for their kind help in training, sample preparation and operation of electron microscopes.

I really feel grateful to Mingming Du and Jiayi Du for their timely help to send me chemicals from the UK to China when I was doing some experimental work at USTC. Thanks to all of the members of Micromanipulation and Encapsulation Research Group, Yu Lab in USTC and all of the students in G2 for their care and help.

I acknowledge the studentship provided by College of Engineering & Physical Sciences, the University of Birmingham.

The scientific research is full of challenge, but thanksgiving goes to Master Chin Kung and Khenpo Sodargye for teaching me the dharma. I can be peaceful to see the ups and downs in my research life. Also, I am thankful to Lulu, Jinshan, Frank Lee, Rongrong, Qun, Emma, Na

Li, etc. for spending a joyful and memorable time with me, which I will never forget. I am really grateful to Mrs Yuanxian Bei, Mr Wei Zhang and Mrs Yuhui Chang for taking care of me and making me feel at home.

The last but not the least, I show my deepest gratitude towards my parents for their love, unwavering support and guidance. I also feel grateful to my wife for her love, trust and the proper time coming up to my life. In this way, I can focus on my research and finish the experimental work on time before I met her.

Table of Contents

List of Figures

List of Schemes

List of Tables

Nomenclature

A   The detected absorbance value (-)

C   Concentration of the analyte (g ml^{-1})

c_l Velocity of light (m s^{-1})

d   Lattice spacing in a crystal (Å)

d_i Diameter of the calculated particles (m)

D_{10} Diameter under 10 % of the cumulative volume of the particles (m)

D_{50} Diameter under 50 % of the cumulative volume of the particles (m)

D_{90} Diameter under 90 % of the cumulative volume of the particles (m)

D_{32} Sauter mean diameter (m)

D_{43} Volume mean diameter (m)

E   Young's modulus (Pa)

ΔE Energy absorbed in a molecule from ground state to excited state during the electronic transition process (J)

F   Force (N)

h   Planck's constant (J s)

l   Path length of the cuvette (cm)

I_0 Intensity of the incident radiation (W m^{-2})

I   Intensity of the emergent radiation (W m^{-2})

R   Diameter of the particle (m)

v   Poisson's ratio (-)

υ   Frequency of radiation (counts/s)

$\overline{υ}$ Wave number of radiation (-)

Greek Symbol

ε   Molar absorptivity (L mol^{-1} cm^{-1})

λ   Wavelength of the radiation (nm)

φ A constant representing the characteristic of the system (-)

θ   Diffraction angle (º)

θ Water contact angle (º)

γ_{lv} Interfacial tension of the liquid-vapor (N/m)

γ_{sl} Interfacial tension of the solid-liquid (N/m)

γ_{sv} Interfacial tension of the solid-vapor (N/m)

δ   Displacement (μm)

List of Publications

Peer-reviewed papers:

1. **Cong Sui**, Jon Preece* and Zhibing Zhang* Novel Polystyrene Sulfonate-Silica Microspheres as a Carrier of a Water Soluble Inorganic Salt (KCl) for Its Sustained Release, via a Dual-Release Mechanism. *RSC advances*, **2017**, 7, 478-481.

2. **Cong Sui**, Jon A Preece, Shu-Hong Yu and Zhibing Zhang* Novel Encapsualtion of Water Soluble Inorganic or Organic Ingredients in Melamine Formaldehyde Microcapsules to Achieve Their Sustained Release in Aqueous Environment. *RSC advances*, **2018**, 8, 29495-29498.

Conference abstracts:

1. **Cong Sui** and Zhibing Zhang[*] Calcium-Based Shellac Microcapsule Synthesis and Encapsulation of Water Soluble Molecules. *12th UK Particle Technology Forum 2014*, 16-17 September 2014 Manchester, UK.

2. **Cong Sui** and Zhibing Zhang[*] Encapsulation of Small Water Soluble Molecules to Control Their Release in Aqueous Environment. *ChemEngDayUK 2015*, 8-9 April 2015, Sheffield, UK.

3. **Cong Sui** and Zhibing Zhang[*] Encapsulation of Potassium Chloride as a Model Small Water Soluble Molecule to Achieve Its Sustained Release in Aqueous Environment. *Joint Conference of 5th UK-China and 13th UK Particle Technology Forum*, Leeds, 12-15 July 2015, Leeds, UK.

4. **Cong Sui**, Jon A Preece, and Zhibing Zhang[*] Novel Microencapsulation of Small Water Soluble Ingredients to Achieve Sustained Release in Aqueous Environment. *ChemEngDayUK 2018*, 27 March 2018, Leeds, UK.

Patent:

Cong Sui, Jon Preece and Zhibing Zhang. Non-permeable microcapsules. UK Patent Application No 1801212.0.

Abbreviations

AFM	Atomic force microscope
CLSM	Confocal laser scanning microscopy
DLS	Dynamic light scattering
DIW	Deionised water
DSC	Differential scanning calorimetry
EDTA	Ethylenediaminetetraacetic acid
EDX	Energy disperse X-ray
ESEM	Environmental scanning electron microscopy
FMCGs	Fast moving consumer goods
FT-IR	Fourier-transform infrared
HRTEM	High resolution transmission electron microscope
ICP-EMS	Inductively coupled plasma emission spectroscopy
IFP	Interfacial polymerisation
KCl	Potassium chloride
LbL	Layer-by-Layer
MF	Melamine formaldehyde
MFP	Melamine formaldehyde precondensate
MOM	Melamine formaldehyde-octadecyltrichlorosilane-melamine formaldehyde
NaCl	Sodium chloride
O/W	Oil-in-water

PAH   Poly(allylamine hydrochloride)

PCL   Poly(Ɛ-caprolactone)

PGPR   Polyglycerol polyricinoleate

PSS   Poly(sodium 4-styrenesulfonate)

SAM   Self-assembled monolayer

SEM   Scanning electron microscopy

SLS   Static Light Scattering

TEM   Transmission electron microscopy

TEOS   Tetraethyl orthosilicate

TGA   Thermogravimetric analysis

W/O   Water-in-oil

W-O-W   Water-in-oil-in-water

XPS   X-ray photoelectron spectroscopy

XRD   X-Ray Diffraction

Chapter 1 Introduction

1.1   Background

Microencapsulation is considered to be an excellent technology to control delivery of active ingredients for a range of industrial sectors including printing, household care, beauty care, agrochemicals and pharmaceuticals.[1-3] Various techniques have been developed based on the emulsion containing water-in-oil (W/O) emulsion and oil-in-water (O/W) emulsion in terms of the encapsulation methodology. Generally, the hydrophilic active ingredients were delivered based on the formation of water-in-oil (W/O) emulsion, while the hydrophobic ones were encapsulated relied on the formation of oil-in-water (O/W) emulsion. Also, many techniques have been developed based on the formation of multi-emulsions applied in various fields of study. The designed microcapsules exhibit many functionalities e.g. mask of the odor and taste, enhancement of stability, sustained release of encapsulated ingredients, etc.

It is useful in many industrial applications to be able to design microspheres/microcapsules comprising an encapsulation material with proper barrier to the hydrophilic active ingredients. It is advantageous for the designed microspheres/microcapsules to exhibit sustained release in water phase. Specifically, it is beneficial to prevent the release of hydrophilic ingredients with low molar mass in an aqueous environment, e.g. pure water. The microcapsules may be designed to comprise a shell material that is stable in particular environments, but degrades upon exposure to a particular stimulus, for example, one or more of heat, shear stress, or change in pH, to release the core substance. The encapsulation of low molecular weight and hydrophilic compounds would be advantageous for a number of applications, including their use as delivery agents in foods, dentifrices and other personal care products or household products. For example, in cleaning products of liquid such as laundry detergent, it would be advantageous for the active ingredients (e.g. bleach) to remain in microcapsules during storage

on the shelf, but to be released due to fracture caused by mechanical stress during the laundry cycle for them to offer cleaning performances.

1.2   Challenges and objectives

There are vast examples of encapsulation for controlled release of hydrophilic or hydrophobic ingredients to the target place. However, it is still difficult to encapsulate the small water soluble molecules or salts, achieving long-term sustained release or even no release in aqueous environment, since the small water soluble ingredients are easy to leak out from the shell of microcapsules, attributed to their small molecular size and water soluble. There are some publications reporting their achievements in the sustained release of small water soluble ingredients, but the release time is still limited. Moreover, the fabrications of microcapsules by some hydrophobic materials were exhibited to be potential candidates for the sustained release of small active ingredients[4-6], but they might be difficult to be well dispersed in aqueous phase. The objectives of the project are to encapsulate small water soluble salts or molecules displaying sustained release or no release in the aqueous environment.

1.3   Proposed solution and thesis layout

To achieve the target, three strategies were proposed here to encapsulate potassium chloride ($M_w = 74.5$ g·mol^{-1}) and allura red (dye, $M_w = 496.42$ g·mol^{-1}) as models of small water soluble ions and molecules with low molar mass, respectively.

(1) *An ion exchange resin was utilised to hinder the release of K$^+$ ions.* Herein, a novel type of organic-inorganic composite solid microsphere, comprised of polystyrene sulfonate and silica (PSS-SiO$_2$), has been synthesised from polystyrene sulfonic acid and tetraethyl ortrhosilicate. It reveals a sustained release of K$^+$ ions in aqueous environment for over 48 hours. (**Chapter 4**)

(2) *Melamine formaldehyde based materials as a shell of microcapsules offered a proper barrier to the encapsulated active ingredients.* A novel type of melamine formaldehyde based microcapsules formed with a desirable barrier, has been used to encapsulate water soluble ingredients, including potassium chloride (KCl) and allura red (dye) as models of inorganic salt and organic molecule, respectively, *via* a facile method, and it has shown a sustained release of KCl and allura red for 12 h and 10 days in aqueous environment, respectively. (**Chapter 5**)

(3) *Formation of hydrophobic intervening layer between the two melamine formaldehyde shells.* A novel approach to encapsulate KCl and allura red has been developed based on the formation of melamine formaldehyde-octadecyltrichlorosilane-melamine formaldehyde (MOM) microcapsules, which prevent their release in aqueous environment for 1 month. The key for the MOM microcapsules to provide the excellent barrier to entrap the active ingredients is profited from the embedment of the hydrophobic intervening layer between two melamine formaldehyde shells. (**Chapter 6**).

The thesis contains 7 chapters as listed below:

Chapter 2. This chapter provides an introduction of microencapsulation technology as well as literature reviews about encapsulation methodologies, controlled release and the commonly used characterisation techniques in the encapsulation fields of research.

Chapter 3. The materials, methods and characterisations of the fabricated microspheres/microcapsules used in this project are described in detail.

The results and discussions of my projects are presented in Chapter 4-6, and the conclusions and the future works are stated in Chapter 7.

Chapter 4. A novel type of organic-inorganic composite solid microsphere comprised of polystyrene sulfonate and silica (PSS-SiO$_2$) was developed, which has been synthesised from

polystyrene sulfonic acid and tetraethyl ortrhosilicate as shown in Scheme 1.1. The microspheres were used to encapsulate a low molar mass (<100 Da) inorganic salt (KCl), which achieved sustained release (>48 hours) of the salt in an aqueous dispersion of the microspheres, which had hitherto not been possible. A novel dual-release mechanism of the salt from the microspheres was proposed (Scheme 1.2), which led to the sustained release. Such approach may have potential applicability for the controlled and prolonged release of other active ingredients.
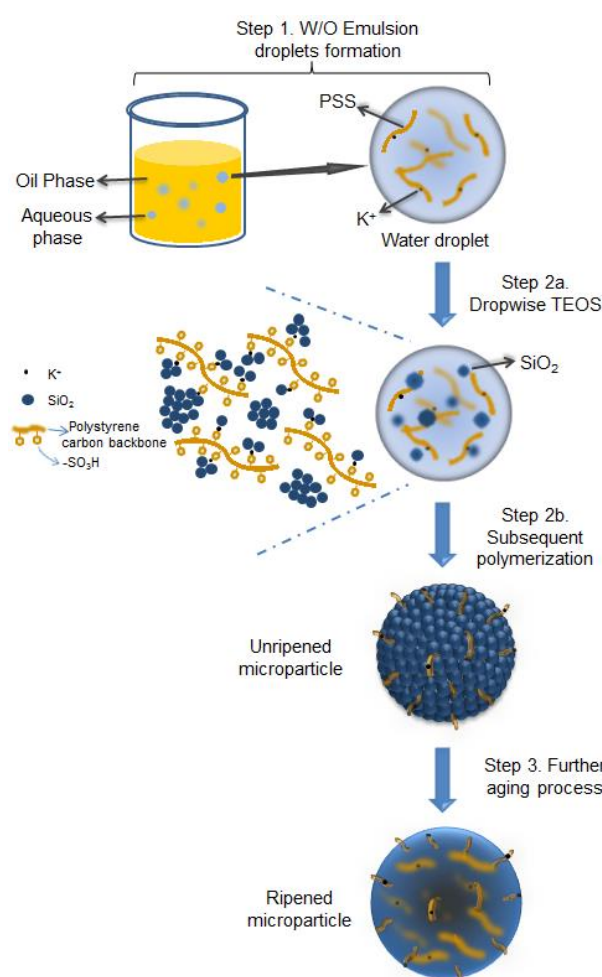
Scheme 1.1 Illustration of PSS-SiO$_2$ microspheres synthesis with KCl encapsulated *via* acid catalysed reaction.

Scheme 1.2 Schematic of the ions dual-release process from the PSS-0.7SiO$_2$ microspheres in an aqueous environment.

Chapter 5. A novel type of melamine formaldehyde (MF) based microspheres/microcapsules with a desirable barrier has been developed to encapsulate water soluble ingredients, including potassium chloride (KCl) and allura red (dye) as models of inorganic salt and organic molecule, respectively, *via* a W/O emulsion method as displayed in Scheme 1.3, and the prepared microspheres/microcapsules have showed sustained releases of KCl and allura red for 12 h and 10 days in aqueous environment, respectively.
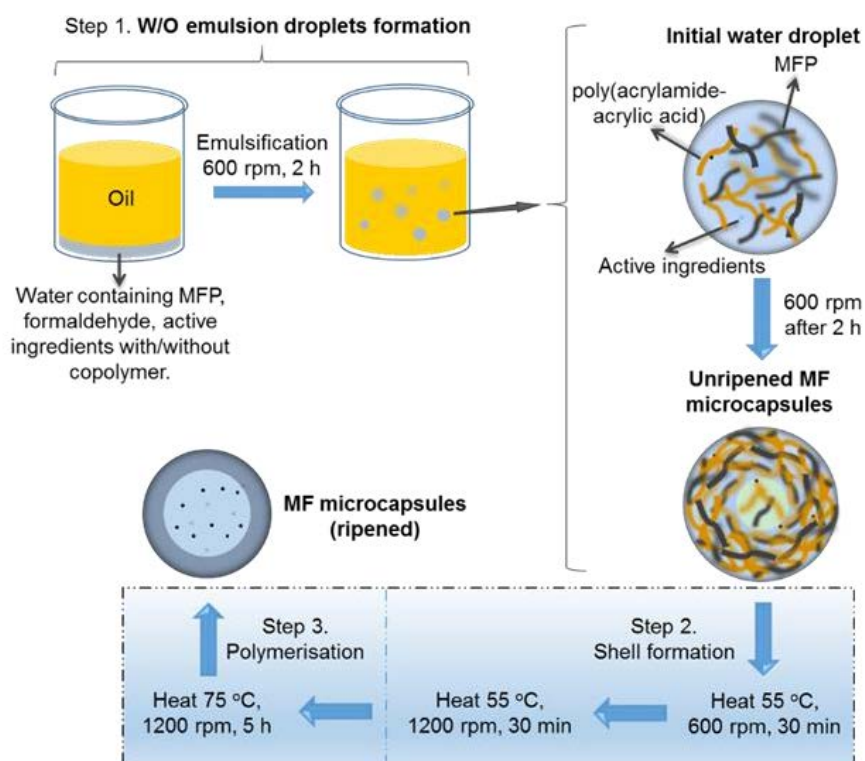
Scheme 1.3 Illustration of MF microcapsules synthesised *via* an *in situ* polymerisation process with water soluble ingredients (KCl salt/allura red molecules) encapsulated.

Chapter 6. A novel approach for encapsulation of small water-soluble ingredients including K$^+$ ions and allura red molecules has been developed based on the formation of melamine formaldehyde-octadecyltrichlorosilane-melamine formaldehyde (MOM) microcapsules, achieving no release in aqueous environment for 1 month (Scheme 1.4). The key to provide the proper barrier property to entrap the active ingredients is profited from the sandwich of the hydrophobic material between the two melamine formaldehyde shells.
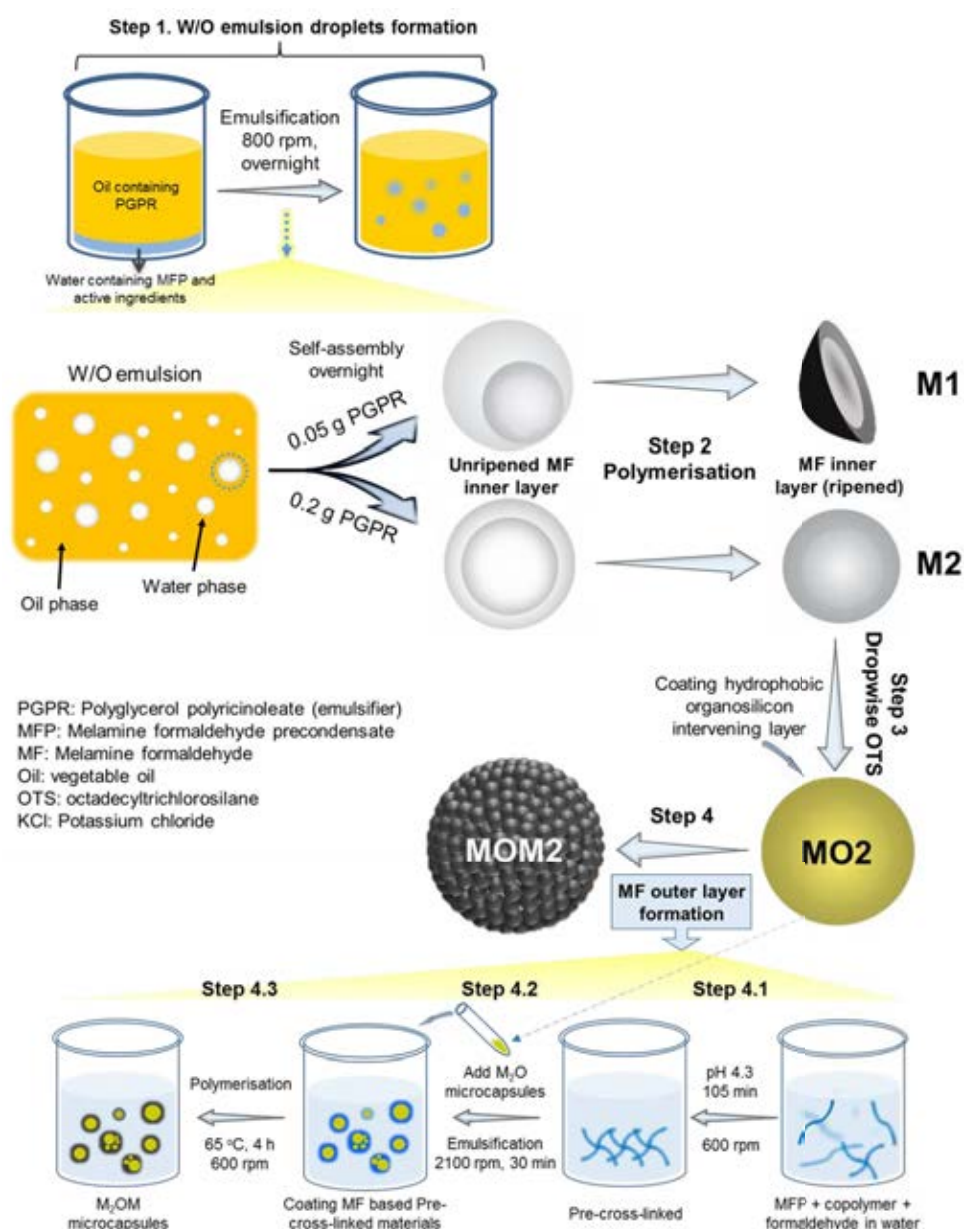
Scheme 1.4 Simple fabrication scheme of the M$_2$OM microcapsules with an active ingredient encapsulated via two in-situ polymerisation steps and one dropwise coating step.

Chapter 7. The conclusions are drawn from the results presented in Chapter 4-6 for this project, followed by potential future works.

Chapter 2 Literature Review

2.1 Introduction: microencapsulation

Microencapsulation is a technology to encapsulate active ingredients into solid shell materials, providing miniature reservoirs and leading to the separation of active ingredients from the surroundings. The pioneering work of microencapsulation started from 1950s, applied to the formation of the pressure-sensitive carbonless copy paper,[7] was then developed to a widely used technology among agriculture, cosmetics, food, medicine and so on.[8] This technology offers a way to store or deliver the active ingredients in solid powder. The target ingredients, namely core materials can be small solid particles, liquid droplets, gas bubbles, ranging from bioactive substances to synthetic chemicals.[9-11] Normally, the formed solid capsules are assigned to be nanocapsules (<1 μm), microcapsules (1-1000 μm) and macrocapsules (>1 mm) in terms of the sizes.[12] Broadly, the structure can be categorised into four types: matrix with active ingredient embedded, core-shell, multicore-shell and core-multishell (Scheme 2.1).[13]
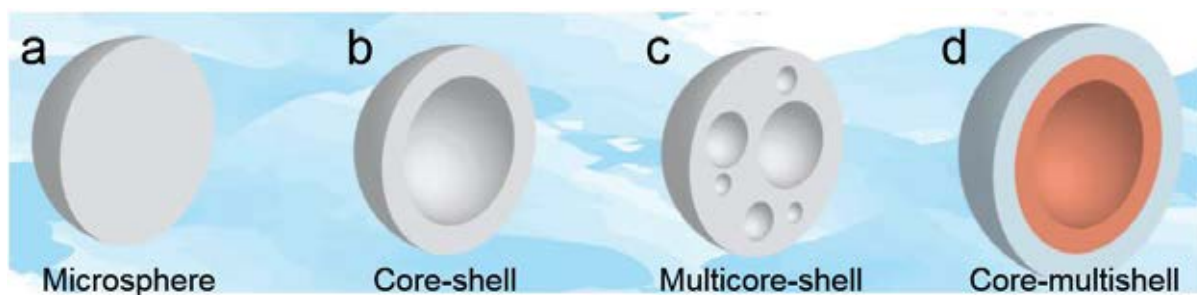
Scheme 2.1 Four types of microcapsule structures: (a) microsphere (matrix), (b) core-shell microcapsule, (c) multicore-shell microcapsule and (d) core-multishell microcapsule.[13]

2.1.1 Main advantages of microencapsulation

- Microencapsulation can provide a means to achieve a sustained release or prolonged release of active ingredients.

- It can mask the odor and taste of many ingredients, such as drug, and further enhance its acceptability to the user.

- For the active ingredients sensitive to gas (O_2, CO_2), liquid (water) or light, it is an effective way to stabilise them.

- The shelf life of some products can be enhanced.

- Liquids can be conveniently converted to dry solid powders.

- Incompatible substances can be easily separated and handled by microencapsulation.

- Regarding to the volatile molecules, encapsulation technology offers a way to minimise the evaporation of the molecules.

- Biocompatibility can be improved for the toxic or irritant products after being encapsulated.

- It can achieved targeted delivery of active ingredients.

2.1.2 Shell materials

The shell material is normally chosen as the one with the capability of forming a film, which can be cohesive with the core material. It can be inorganic, organic or hybrid materials.[14-16] Moreover, small particles or rods can also be used to stabilise the emulsions (oil-water mixture) and further form the microcapsules even without forming the film.[17,18] Some key factors need to be taken into considerations:

- The expected properties and requirements of the final products.

- Inert toward the core material (active ingredient).

- The cost of the whole encapsulation process.

- The biocompatibility of the shell material for food and pharma applications (whether it is approved by FDA).

The ideal shell material should display the following features:

- Non-reactivity between the active ingredients and the shell materials.

- Low permeability of the shell material during the encapsulation process or the storage of the active ingredients.

- The capability to allow a solvent to evaporate if it is used to dissolve the shell material during the encapsulation process.

- The ability to protect the active ingredients against the environment (e.g., pH, oxidation, moisture, light).

- Excellent rheology characteristics to disperse or emulsify the actives during the encapsulation process.

- Cheap and safe to use.[19]

Classifications of shell materials:

1. **Water-soluble materials:** e.g. Polyacrylic acid, Poly(styrenesulfonate), Gelatin, Polyvinyl alcohol, Gum Arabic, Arabinogalactan, Starch, Methylcellulose, Polyvinylpyrrolidone, Hydroxyethylcellulose, Maltodextrins, Carboxymethylcellulose.

2. **Water-insoluble materials:** Poly(lactideco-glycolide), Ethylcellulose, Cellulose nitrate, Silicones, Polyethylene, Polymethacrylate, Poly (Ethylene-Vinyl acetate), Polyurea Melamine, Aminoplasts, Polyamide (Nylon).

3. **Waxes and lipids:** Glyceryl stearates, Paraffin, Stearyl alcohol, Carnauba, Stearic acid, Hydrogenated vegetable oils, Beeswax, Spermaceti.

4. **Enteric resins:** Zein, Shellac, Cellulose acetate phthalate.[20]

2.2   Encapsulation methodologies

Microencapsulation is a technology learned from the nature. Vast examples of encapsulates (capsules) such as spores, cells, seeds, eggs and seashells, widely exist all over the world.[21] Nowadays, the encapsulation technology has been realised using many different methods, which can be categorised into physico-chemical approaches (coacervation, co-crystallisation, polymerisation, self-assembly etc.) and mechanical approaches (spray drying, extrusion, freeze drying etc.) as is shown in Scheme 2.2.[22] The most widely used approaches are extrusion and spray drying, meanwhile coacervation and freeze drying are also commonly used in industry.[23,24]
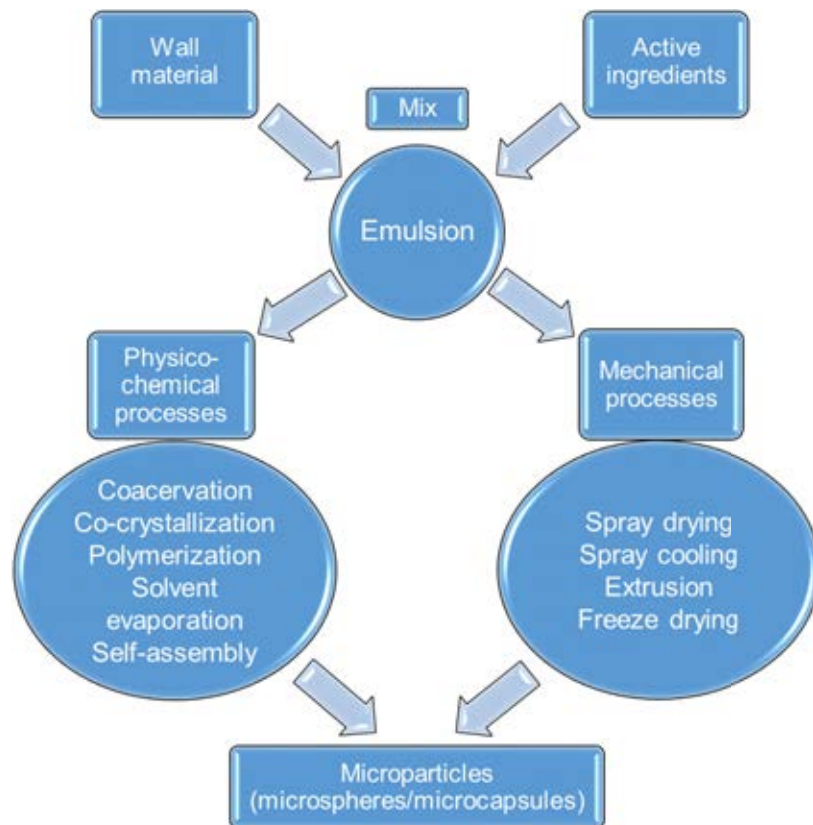
Scheme 2.2 A schematic demonstration of encapsulation processes.[22]

2.2.1 Coacervation

Coacervation, named phase separation is the first example used in the field of microencapsulation for the fabrication of carbonless copy paper by Green and Scheicher in 1950s.[25] It involves the precipitation or separation of the polymer from the liquid *via* the change of pH.[26] Briefly, the core material (active ingredient) initially disperses in the immiscible solvent (solubility < 2 % v/v), and the emulsion is thus formed. The core active is emulsified in the dispersion *via* agitation, and their size and size distribution are determined by stirring speed, stirrer type, viscosity and interfacial tension. This process can be proceeded with or without an emulsifier, and also the core material should prevent from reacting with the dispersant, regarding to the experimental design. The polymer then precipitates from the solution after the change of pH, and gradually forms a continuous film. The shell material is finally solidified with the active core encapsulated. This process can be described by Scheme 2.3.[27] Regarding to the types of polymer involved, the process is categorised into simple and complex coacervation. The simple coacervation just relates to one type of polymer, while the complex one involves two or more types.[8]
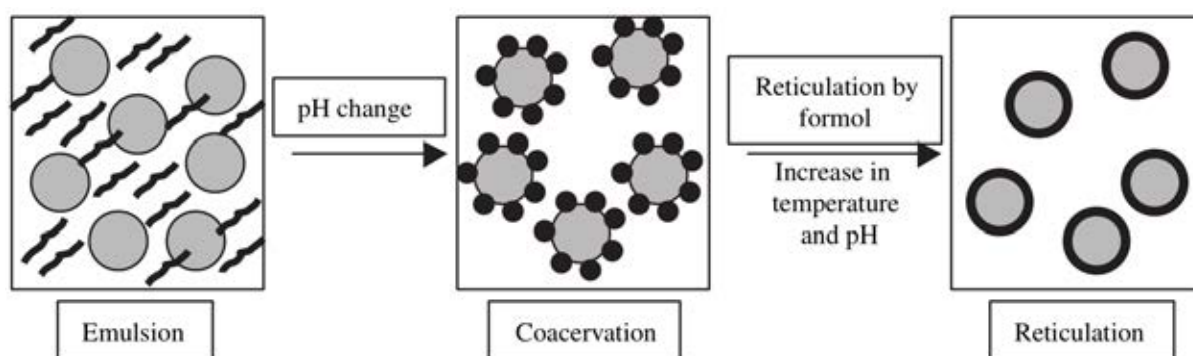
Scheme 2.3 A schematic representation of complex coacervation process.[27] Formol is assigned to formaldehyde.

2.2.2 Co-crystallisation

Co-crystallisation as a new encapsulation technique has been used in food engineering, utilising e.g. melted sucrose at high temperature to entrap the active ingredients. The sucrose liquid at supersaturated concentration tends to crystallise, forming aggregates with the size range of 3-30 μm.[28] The key factors to determine success of the process are the rates of nucleation and crystallisation. However, rare successful example could be found, and also this technique is not suitable for the encapsulation of bioactive substances including cells, enzyme, etc. due to the high temperature applied during the manufacturing process.[28]

2.2.3 *In situ* polymerisation

In situ polymerisation has exceeded the pioneering technique coacervation, and become a popular method in the last decade in terms of publications (Fig. 2.1).[29] All of the reactants containing monomers or oligomers are in the same phase (mostly the continuous phase) and result in the depositions of the polymers onto the interphase, forming the microcapsules with smooth surface and spherical shape. This technique exhibits many advantages including simple, fast, as well as highly cross-linked shell leading to a compact shell, which is ideal for the encapsulation of small molecules.
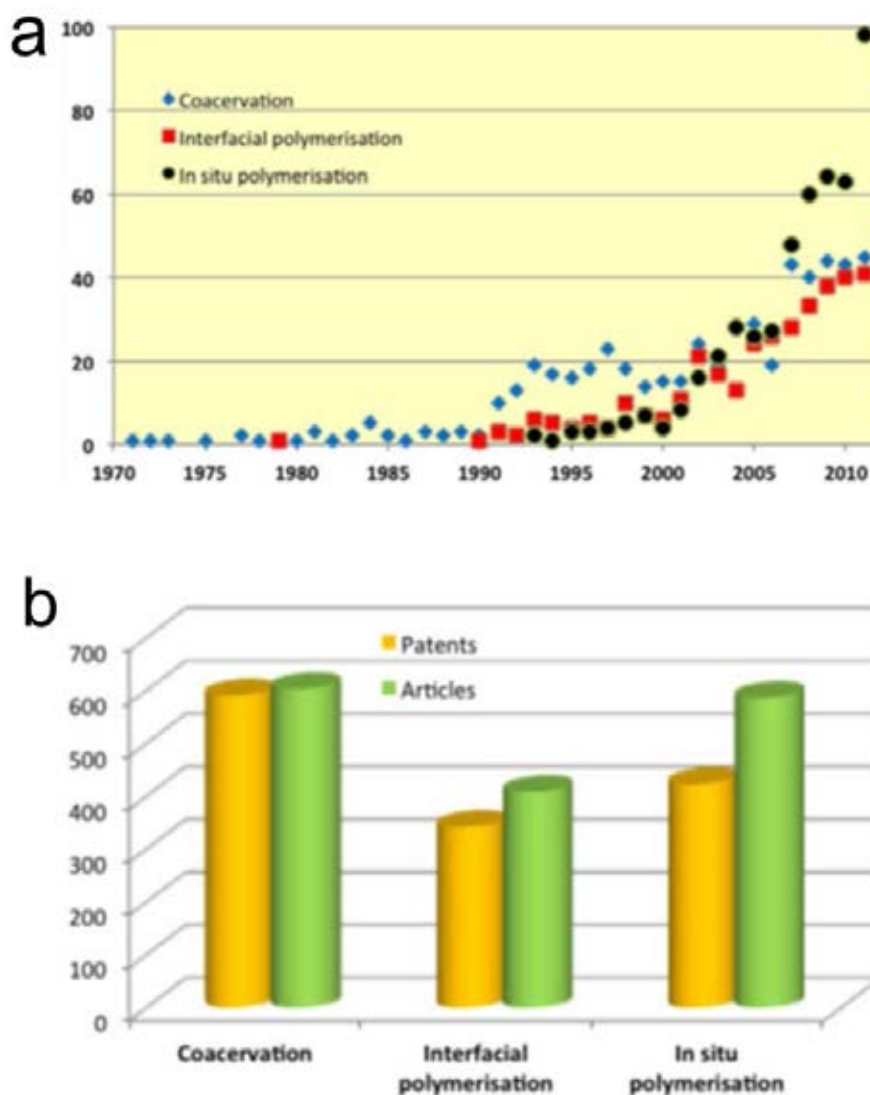
Fig. 2.1 (a) Scientific publications, (b) articles and patents for the coacervation, interfacial polymerisation and *in situ* polymerisation fields of research.[29]

Regarding to the shell material, the optimum polymer is aminoplast, containing melamine formaldehyde[30], urea formaldehyde[31], urea melamine formaldehyde[32], resorcinol modified melamine formaldehyde[33], epoxy resin with ketimine[34] as well as polyamine, polyols and substituted methylene moieties[35]. Scheme 2.4 illustrates formation of the melamine formaldehyde (MF) microcapsules in a typical *in situ* polymerisation process. Herein, the polymer precondensate was initially dissolved in water to form the continous phase (Step 1). The core oil was poured into the shell solution (Step 2) and emulsified to form the unripened

microcapsules (Step 3). The MF shell was further solidified forming the microcapsules with oil encapsulated (Step 4).[36]
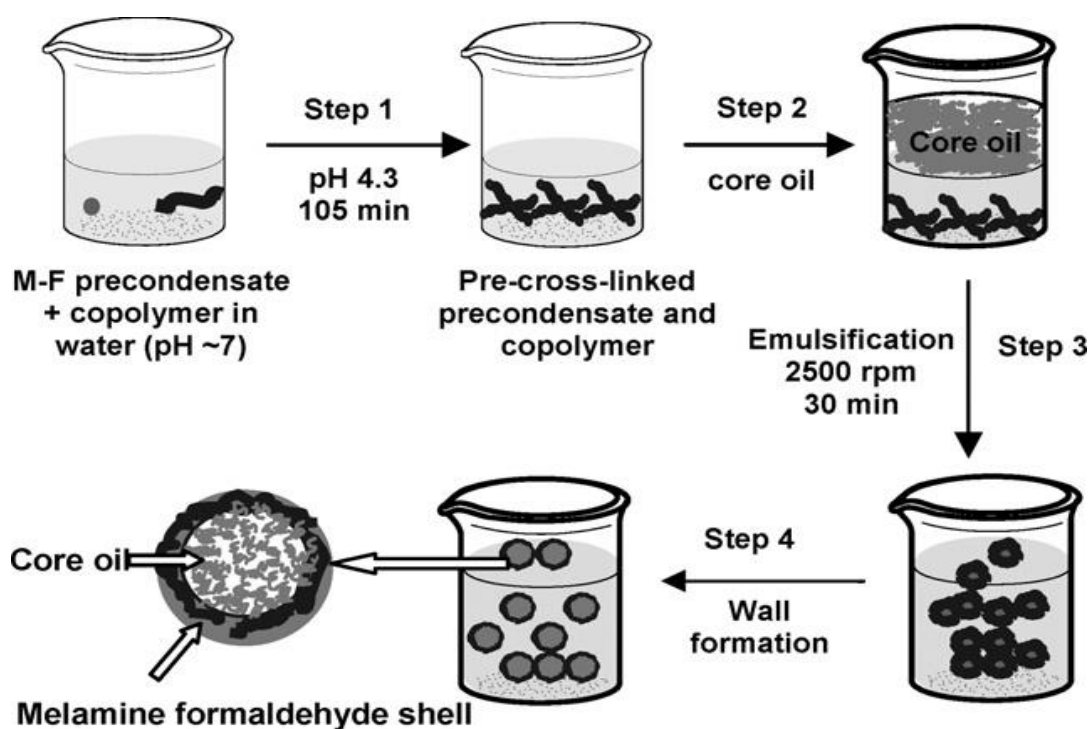
Scheme 2.4 Synthesis strategy of melamine formaldehyde microcapsules with oil encapsulated *via in situ* polymerisation method.[36]

The advantages of *in situ* polymerisation are high payload and narrow size range,[37] whereas this technique displays two inevitable problems. Firstly, the same amount of shell solution was used to produce microcapsules with different sizes within one batch.[38,39] The larger microcapsules tend to form thinner shell relative to its size, while the smaller microcapsules exhibit comparatively thicker and stronger shell. This has a significant impact on the mechanical property and release profile. Moreover, the free formaldehyde in the final products needs to be removed in terms of health and enivironment consideration.[40] Fortunately, some researchers have reported some efficient ways to reduce the free formaldehyde.[40,41]

In situ polymerisation technique has been widely used in many fields of scientifc research and industries. The most commonly used carbonless copy paper as the pioneering product to

encapsulate dye, has now been developed into scratch-and-sniff paper with fragrance encapsulated. The microcapsules formed by *in situ* polymerisation have also been applied to textile products such as antimicrobial towels, insoles, scented shirt and pantyhose (Fig. 2.2)[42]. The microcapsules would break up and release out the encapsulated ingredients under compression.
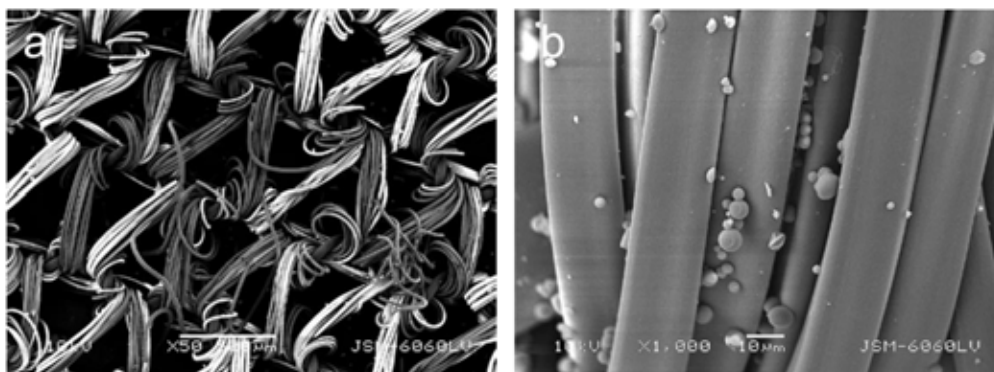
Fig. 2.2 SEM images of textile modified with urea formaldehyde microcapsules containing dicyclopentadiene. (a) 50×, (b) 1000×[42].

2.2.4 Interfacial polymerisation

Interfacial polymerisation (IFP) as another microencapsulation method has been widely used in industries, which is very similar to the previous *in situ* polymerisation method. For the IFP, both of the two reactants dissolve in two respective immiscible phases, rather than dissolve in a single phase for *in situ* polymerisation method. The commercial microcapsules synthesised by IFP are normally in the size range of 20-30 μm, and the larger capsules can also be obtained by this method.[43] The benefits of IFP technique has been summarised below:[44]

- Simple and stable process.
- Low cost and scalable.
- Controllable size and shell thickness.
- Excellent chemical and mechanical properties of microcapsule shell.

- High encapsulation efficiency.

Historically, the initial reactions were under harsh conditions (acid or alkaline environment, high temperature and toxic solvents). In this way, the IFP technique was just confined to the encapsulation of relative stable active ingredients. However, recent developments have taken place in the field of IFP, enabling its application to biomedicine such as the encapsulation of cofactors, enzymes and cells.[45]

2.2.5 Solvent evaporation

Solvent evaporation is a common technique in microencapsulation, especially for the encapsulation of bioactivator in pharmaceuticals. This technique exhibits many merits such as fast fabrication process, less operation skills required, good process reproducibility and controllable size range from nanoscale to microscale.[46] In order to achieve the controlled size ranges, the experimental conditions and suitable solvent type need to be carefully considered. The optimum encapsulation process is to realise high payload, high encapsulation efficiency and low residual solvent in the microparticles.[47] The formulation and processing conditions of the technique need to be optimised to achieve the different release profiles of active ingredient.

Generally, solvent evaporation method consists of four steps as shown in Scheme 2.5.[47] Active compound was initially dispersed in the solution of matrix material. The as-prepared solution was emulsified into the immiscible phase (continuous phase), forming the droplets with the active compound. The dispersant solvent was then removed by evaporation, and the polymer solidified with active encapsulated. The solid product was finally harvested from the continuous phase and dried into powder. The evaporation process can be facilitated by elevated temperature or reduced pressure.[48,49]

bioactive compound (micronised or dissolved)

dissolved matrix material

"drug/matrix dispersion"

① Incorporation of the bioactive compound

continuous phase

② Droplet formation

further cont. phase or additional extraction agents (extraction)

adapt p, T (evaporation)

③ Solvent removal

④ Microsphere harvest (and drying)
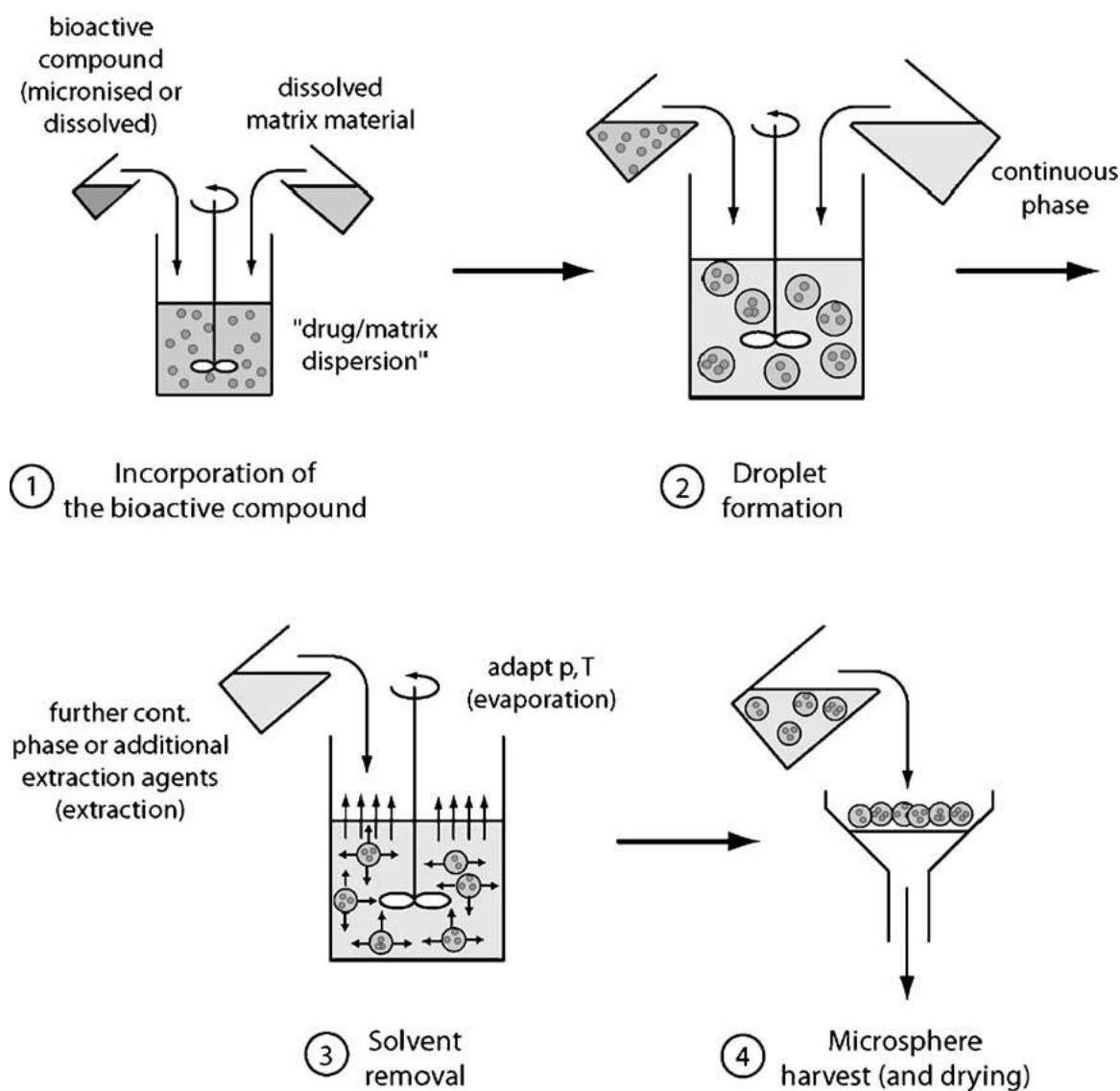
Scheme 2.5 Schematic overview of the principal process of the solvent evaporation technique.[47]

With respect to the encapsulation of water soluble active ingredients, the encapsulation efficiency is comparatively low for the particles synthesised by W/O emulsion solvent evaporation method, since the ingredients dissolved in solvent tend to lose away before the solidification of the polymer. The multi-emulsion method has been introduced and combined with the solvent evaporation means emerging as an innovative encapsulation technique to solve the above problem.[50-52]

2.2.6 Self-assembly technique

Plenty of methods to form multi-layers of charged materials were categorised into self-assembly research area. The most widely used self-assembly technique was Layer-by-Layer (LbL) pioneered by Sukhorukov, Donath, Caruso, Mohwald etc. in terms of the encapsulation.[53,54] In addition, many types of encapsulation including the encapsulation of solid and liquid core, achieved by LbL have been developed since late 1990s.[53,55] These techniques can be emulsion-based or sacrificial template-based.[13]

2.2.6.1 Emulsion-based Layer-by-Layer (LbL) technique

Many kinds of liquid actives containing aqueous phase and oil phase were successfully encapsulated by LbL adsorption of different charged materials onto the surface of the core. However, regarding to the encapsulation of water soluble ingredients, this method was subjected to the low encapsulation efficiency, because the encapsulated ingredients in inner aqueous core may likely be lost, subjected to the external aqueous phase of polymers for LbL.[13] Generally, the hydrophobic actives were preferably encapsulated *via* o/w emulsion followed by the depositions of the different charged materials.[56]
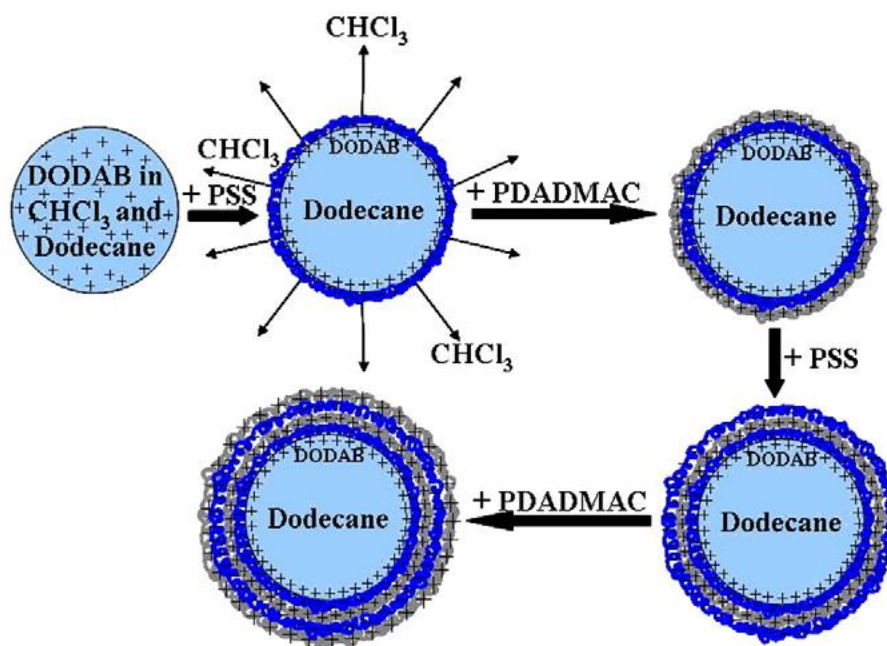
Scheme 2.6 A schematic demonstration of encapsulation of liquid actives *via* Emulsion-based LbL technique.[63,64] DODAB: Didodecyldimethylammonium bromide, PSS: poly(sodium 4-styrenesulfonate), PDADMAC: poly(diallyldimethylammonium chloride) and $CHCl_3$: chloroform.

In general, the hydrophobic liquid with dissolved material was initially emulsified *via* standard mixing or ultrasonic as shown in Scheme 2.6.[56,57] The oppositely charged polymer was deposited onto the surface of the first polyelectrolyte layer of the core. Successively, the oppositely charged polymers were alternatively deposited onto the surface of the capsules, forming a LbL structure, until a desired number of layers was achieved.

2.2.6.2 Template sacrificed method

Formation of microcapsules utilising sacrificial templates is another way to encapsulate actives. The core as the template was then eliminated by applying extreme conditions, such as high or low pH, oxidation, organic solvent etc. In order to protect the actives, harsh conditions should be avoided during the encapsulation process.[58] In brief, a porous core was formed initially as a template and the oppositely charged polymers were then adsorbed onto the core *via* electric

interactions as shown in Scheme 2.7.[58-60] The core was dissolved by adding ethylenediaminetetraacetic acid (EDTA) solution, forming the cross-linked microcapsules.
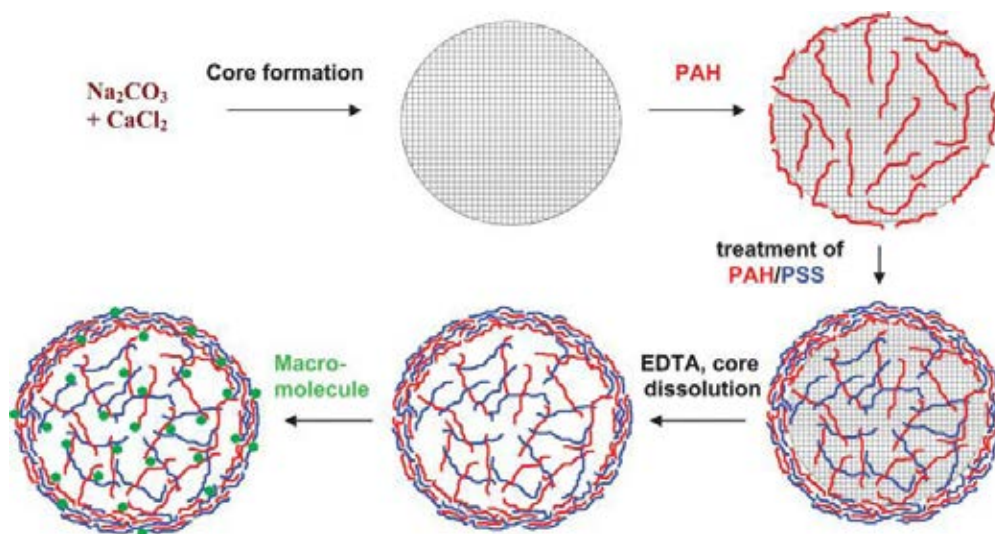
Scheme 2.7 A schematic demonstration of microencapsulation of macromolecules *via* elimination of calcium carbonate core by adding EDTA.[58-60] PAH: poly(allylamine hydrochloride).

2.3   Release of active ingredients

2.3.1 Release mechanism

The active ingredients encapsulated in the microcapsules should be delivered to the target place and released in a controllable way, including sustained release, delayed release and triggered release. The release rate is generally determined by the following factors:[61]

- Shell properties: density, shell thickness, crystallinity and degree of cross-linking.
- Microcapsule properties: size, mechanical property, structure of the microcapsules.
- Storage environments: temperature, pH, moisture.

The release mechanisms mainly contain four types:

2.3.1.1 Rupture

The microcapsules with active ingredients encapsulated can be ruptured by applying extra force, including pressure or shear force. The ingredients are then released out after rupture. Carbonless copy paper as one of the pioneering commercial applications in the field utilised the pressure to release out the encapsulated dye (Scheme 2.8). The encapsulated dye underneath the top layer paper can be released out and react with the reagent coated on the bottom layer paper, after the pressure is applied on the top layer paper. Many other applications can also be found in fragrance[62], tooth paste[63] and so on.
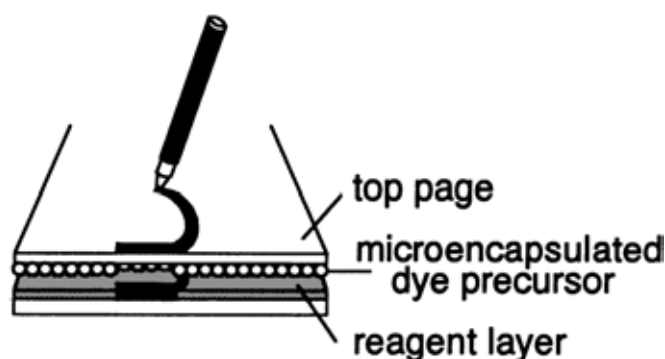
Scheme 2.8 Illustration of the mechanism to form a replica *via* the microencapsulation of dye in the carbonless copy paper.[64]

2.3.1.2 Diffusion

Diffusion is a process for active ingredients to diffuse from the high concentration side to the low side by random movement through the shell or the matrix of the microcapsule. Briefly, the active ingredients can be dissolved at the high concentration side, and then diffuse to the outside of the microcapsules through the shell or the matrix of the microcapsules. The diffusion process can be defined as the diffusivity and described by the Fick`s law.

The diffusion process is determined by the factors below:

- Size distribution and morphology of the microcapsules.

- Molecular weight, polarity and solubility of the active ingredients.

- The porosity of the materials of microcapsules.

- The thickness of the microcapsule shell.

- Environmental temperature.

2.3.1.3 Degradation

The active ingredients encapsulated by the shell materials or embedded in the matrixes homogeneously are released out based on the degradation of the shell or matrix. Normally, the damage of the capsule material is prior to the release of ingredients. It can be triggered by changing temperature[65], pH[66], salinity[67], humidity[68] or applying ultrasound[69], electric[70], photo[71,72], chemical[73], magnetic field[74] and biological[75] etc.. The state of capsule material is changed and the active ingredients are then released out.

2.3.2 Sustained release

Regarding the sustained release of the encapsulated ingredients, there have been many reviews reporting these achievements.[76-78] The main advantages of sustained release are offering the special release rates of active ingredients according to the certain aims, e.g. decrease of the daily administrations, minimisation of side effects and improvements of compliance.[79] The encapsulation of water soluble ingredients is meaningful, including the small water soluble salts,[80-82] small water soluble molecules[83] and biomacromolecules[84,85]. Generally, the delivery matrix can be hydrophilic[79] or hydrophobic[86] to deliver the active ingredients to the target place.

The mechanism for the hydrophilic matrix to achieve the sustained release is classified into three types, including the matrix erosion, incorporation of opposite charged ion exchange resins with the active ingredients and physically entrapment.[87] Regarding the matrix erosion dominated release, the surface layer of particles tends to be hydrated when they are in contact with water environment, leading to their transformation of crystalline state to the "rubbery"

state. The encapsulated ingredients are concomitantly released out *via* matrix erosion, leading to the entry of water molecules and the exit of ingredient molecules.[88] The second type is the incorporation of oppositely charged ion exchange resins with the active ingredients in the microparticles matrix. The active ingredients are interacted with the oppositely charged resins within the microparticle matrix. In this case, the release rate of active ingredients is thus delayed, attributed to the interaction between resin and active ingredient. The final type of mechanism, diffusion-controlled release is determined by the diffusion of active ingredients entrapped in the matrix. This type of release is mainly dominated by the diffusion of the active ingredients, when the matrix swelling and erosion are all eliminated. It can avoid any irreproducibility in terms of the erosion rate and the balance between the diffusion and erosion processes.[87]

2.3.2.1 Small water soluble molecules

The delivery of small water soluble molecules, such as drugs, dyes, tea polyphenol extracts and peroxide have been widely used in the encapsulation fields of research. The release profiles displayed a sustained release from minutes to days, and the size ranges of the microcapsules are from several nanometers to millimeters.

Drugs

Regarding the drug delivery, the encapsulation of small water soluble molecules has attracted a lot of attentions, aiming to achieve a sustained release.[76-79,86] The encapsulation of 5-fluorouracil as an anticancer drug displayed a 12-hour sustained release *in vitro*, *via* the synthesis of polyacrylamide microparticles.[89] Procainamide hydrochloride as a kind of water soluble model drug was encapsulated in polyelectrolyte microcapsules, but it just released for several hours in water at 22 $^{\circ}$C.[90] The encapsulation of doxorubicin as a water soluble anticancer drug achieved a sustained release for days *via* the formation of Aerosol OT^{TM}-

alginate nanoparticles[91] and inorganic amorphous calcium carbonate (ACC) coated with silica nanoparticles.[92] Unfortunately, the particles of the nanosize still limit their applications in industries due to the safety concern.[93]

Dyestuffs

The encapsulations of water soluble dye molecules, eg. Methyl Orange,[94] Rhodamine B,[95] Allura Red,[96] 6-carboxyfluorescein[90] are highly demanded in the dyestuff and food industries. Allura Red was encapsulated by the fabrication of colloidosomes with latex nanoparticles (diameter ≈ 153 nm) embedded in the calcium carbonate shell (Scheme 2.9). The formed colloidosomes displayed rough surface with the microparticle size of no more than 10 μm. The release profiles were studied by shear, dilution and addition of acid, and the formed colloidosomes demonstrate a 20 % dye release for more than 150 h by dilution with water.[96] However, the encapsulation efficiency of the enzyme amylase as a model of large water soluble molecules shows just 25-30 %, after the final wash by water leading to the leakage of a large amount of encapsulated water soluble molecules. In addition, the shell is sealed by the interaction between the encapsulated CO_3^{2-} and external Ca^{2+} ions, which reveals the system may not provide a proper barrier to the small water soluble ions. The method may thus be not suitable for the encapsulation of other types of small water soluble ions such as Ca^{2+} and K^+ to offer a prolonged release.
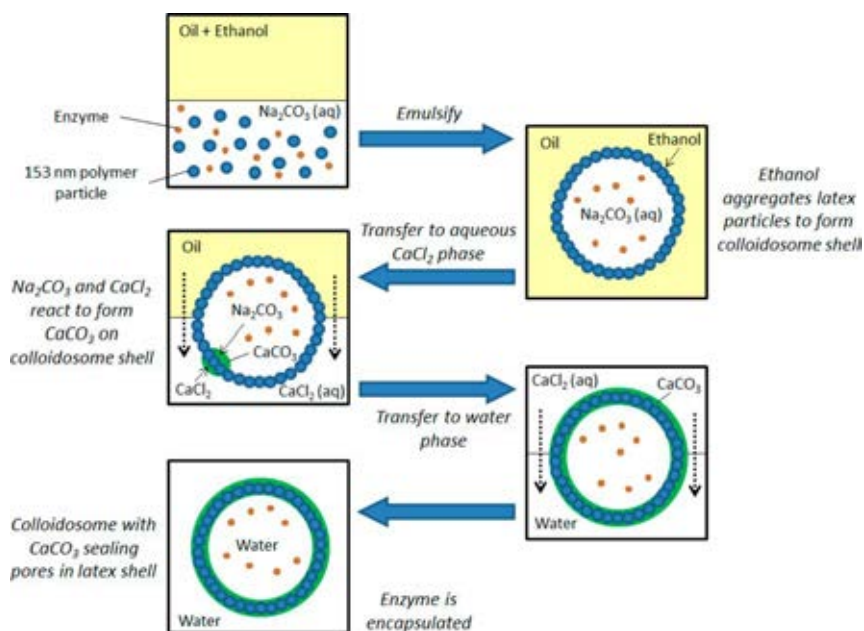
Scheme 2.9 Illustration of the mechanism to form the CaCO$_3$ sealed colloidosomes with active ingredients encapsulated in the aqueous core.[96]

Polyphenol extracts

The encapsulation of polyphenol extracted from tea, fruit or vegetable can be widely used in health promotion, such as antioxidant, anticancer, anti-inflammation, diabetes care and longevity.[83,97] The polyphenol extracts are compounds, whose major structures are shown below in Scheme 2.10.[97] The polyphenol extracts were encapsulated by formation of nanoparticles, nanofibers, nanoliposomes and microparticles.[83]
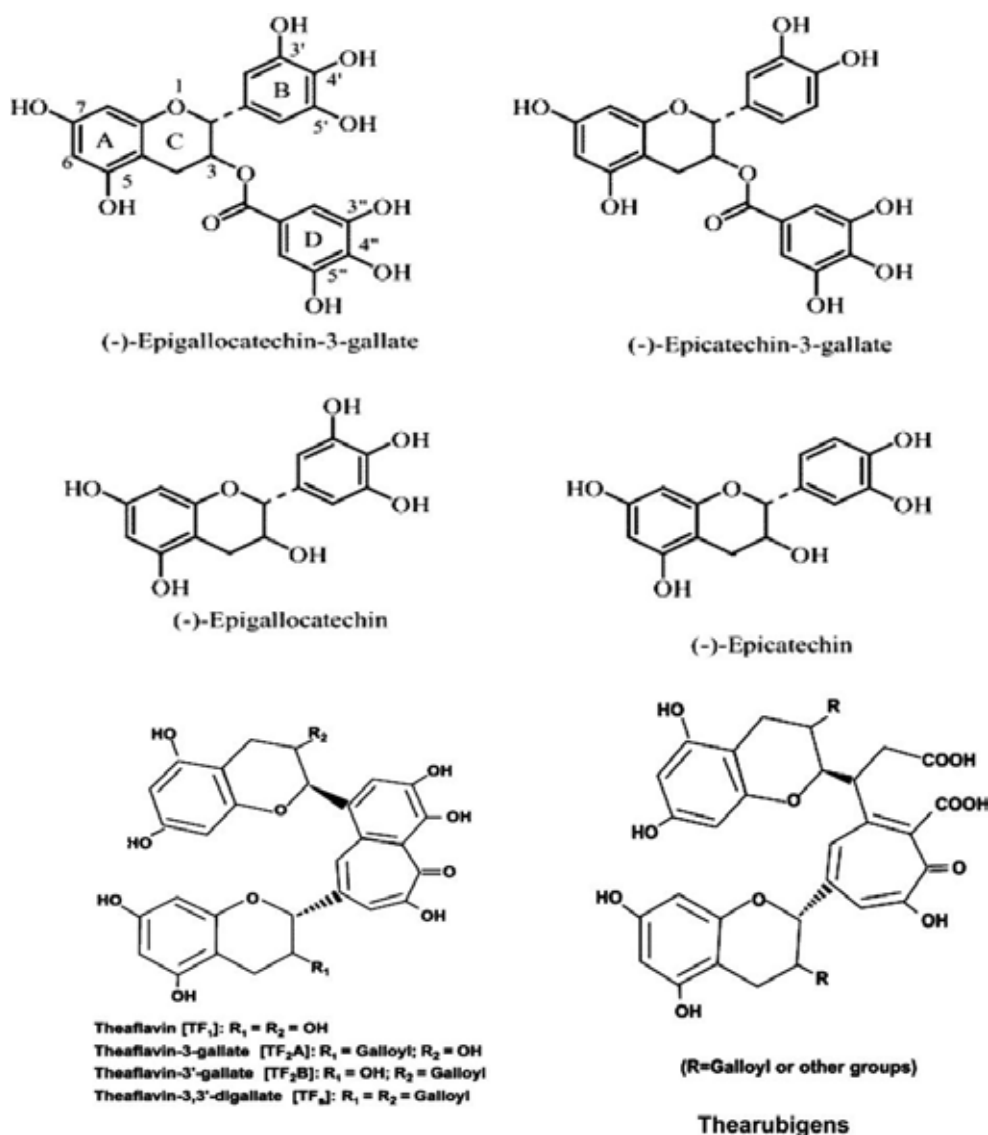
Scheme 2.10 The chemical structures of the major polyphenol compounds.[97]

The polyphenols were encapsulated by the synthesis of layer-by-layer-coated gelatin nanoparticles[98] and gelatin-dextran biopolymeric nanoparticles[99] displaying a fast release in water within 1 day. The tea polyphenols delivered by chitosan nanoparticles only revealed a 2-day release.[100] The theaflavin and epigallocatechin-3-gallate encapsulated by the fabrication of poly(lactide-co-glycolide) (PLGA) nanoparticles demonstrated a sustained release for 10 days, but the encapsulation efficiency just displayed ∼18 % and 26 %, respectively.[101] Furthermore, the nanosize of the particles is still a limitation for their applications due to the safety concern.[93]

The controlled release of green tea polyphenols was achieved over 160 h by the formation of poly(ε-caprolactone) (PCL)/multi-walled carbon nanotube composite nanofibers.[102] The drawback is the use of PCL needed to be dissolved in toxic organic solvent CH_2Cl_2, which leads to the waste removal problem and the potentially harmful residues left in the final products. Also, the paper does not report the encapsulation efficiency and payload, which are important parameters for the encapsulation.

The tea polyphenols were also reported to be delivered by nanoliposome system *via* dynamic high-pressure microfluidisation method[103], the thin film ultrasonic dispersion method[104] and extrusion with porous membrane[105,106]. The prolonged releases of encapsulated polyphenols in nanoliposomes just showed up to 24 h in aqueous environment. The fast release of the entrapped ingredients is a significant disadvantage of the liposome system, and also the low payload, low reproducibility and instability of storage are drawbacks needed to be concerned.[83]

The polyphenols were encapsulated by ethyl cellulose microcapsules[107], chitosan microspheres[108], kafirin microparticles[109], lactose or hypromellose microspheres[110] and PCL particles[111], displaying a sustained release from 1 h to 24 h. Unfortunately, the release time is still not long enough for the delivery of many types of water soluble ingredients, and these carriers cannot be widely used in industrial applications.

Peroxide

The encapsulation of peroxide is still challenging due to its low stability, incompatible with many kinds of chemicals and easy to react with many organic solvents. The reported carriers for the encapsulation of peroxide are calcium-shellac microspheres[112,113], silica xerogels[114], PLGA and PCL mixtures[115], etc. However, there are very rare successful examples of encapsulation of peroxide, achieving a sustained release in water,[115] although successful

encapsulation and controlled release of peroxide can have applications in different industrial products, such as toothpaste, chewing gum.[102]

2.3.2.2 Small water soluble salts

Inorganic salts

Various types of small water soluble inorganic salts containing potassium[116], magnesium[117] and lithium[118], have been reported to be encapsulated by different methods, and further applied in food, medicine, fertiliser, etc. The encapsulation of potassium permanganate ($KMnO_4$) by waxy polymers with the size range of 60 μm to 2 mm, and the release tests were performed in DIW on an orbital shaker at room temperature, exhibiting an average long-term release of 27 days, ranging from 3 to 80 days.[4] When $KMnO_4$ was encapsulated in Paraffin wax, the times for 90 % of their payloads to release out were estimated to be 1.6 months, 19.3 years, and 472 years, based on the particles fabricated with mass ratios of paraffin wax to $KMnO_4$ showing 1:1, 2:1 and 5:1, respectively.[5] The estimated release time was calculated relied on the experimental release data proceeded in water fitted to a previous linearized model. However, the particles formed by waxy polymers still displayed hydrophobic property, which cannot be well dispersed in aqueous phase, limiting the application ranges. The size range from several microns to several millimetres are also another problem which needs to be concerned.

Regarding the encapsulation of potassium chloride (KCl) in ethylcellulose[119] and Eudragit[120] microspheres with a size distribution of 180 to 830 μm in diameter as well as the saturated polyglycolyed glycerides matrices[121] with unknown size range, they showed a sustained release of KCl for 6 hours in water. Whereas, the size distributions of the formed microspheres are still large, and the prolonged release time may be attributed to the large particle size. The commercial fertilizer NPK6-20-30 granules coated by various polymers including polysulfone,

polyacrylonitrile and cellulose acetate, which displayed sizes in the millimetre range, displayed the release of 31.8 % of NH_4^+, 16.7 % of P_2O_5, and 11.6 % of K^+ after 5 h.[122]

The lithium carbonate as a kind of commonly used anti maniac drug has been investigated to be loaded in different types of waxes/fat microspheres, exhibiting an 8-hour prolonged release, but the hydrophobic properties of the wax materials are still a limitation for the dispersibility of the formed microspheres in aqueous environment.[118] Magnesium ions loaded in the water-in-oil-in-water (W-O-W) emulsions have been widely investigated in the food industries in terms of the sustained release.[123-126]

Organic salts

The organic salts such as citrate anions and bisphosphonate can have pharmaceutical applications. The citrate anions were intercalated in magnesium aluminium layered double hydroxides with unknown size distribution for the sustained release of citrate ions up to 12 h.[117] The alendronate as a hydrophilic low MW bisphosphonate was encapsulated in PLGA nanoparticles offering a sustained release for 240 min in water.[127]

2.4   Characterisations of microcapsules

Encapsulation of active ingredients has been widely used in a range of industry sectors for decades. It is essential to determine and characterise their properties precisely, including morphology, size, physicochemical and mechanical properties during their formulation processes and storage, relating to their specific applications. The desirable properties vary depending on the corresponding applications. For instance, the fragrance molecules encapsulated in the microcapsules are aimed to achieve a prolonged release of fresh scent after use on clothing in the perfume industry. The release profile of the fragrance molecules is dominated by the thickness, porosity and composition of the microcapsule shell material. This

design criteria to achieve a sustained release, can also be applied in the pharmaceutical and agrochemical industry sectors. Regarding the laundry products, the microcapsules containing fragrance are normally designed to be intact and adhesive to clothing, and ruptured by mechanical force applied after drying process. The mechanical properties of the microcapsules are therefore vital to control the release of active ingredients.

Herein, plenty of techniques for the characterisations of the properties of microparticles will be discussed in the encapsulation fields of research, covering the determinations of morphology, size distribution, mechanical property and the release profiles of encapsulated active ingredients.

2.4.1 Morphology

The morphology of materials containing shape, size, and structure is a very important property in the characterisations of materials. The microstructure of materials strongly affects the physical and chemical properties of the materials, especially for them on the nanoscale.[128] For example, the surface structure can affect the wettability of materials surface from hydrophobic to hydrophilic state.[129] The characterisations of the morphology of the synthesised microcapsules are very important, since it is strongly related to their other properties.

Various types of microscopes are commonly used to determine the morphology of the microcapsules, which can be generally divided into non-destructive source and physical probe scanning. Regarding the non-destructive source based microscopes, various waves exhibiting different wavelengths are used to irradiate the sample, whose signal is collected, recreating a magnified image of the sample. Electron and visible light are commonly used source for the microscope. The resolution of the microscope is limited by the wavelength of the source, and it is enhanced with the utilisation of the wave with shorter wavelengths. The electron microscope thus has higher magnification than the optical microscope due to the shorter

wavelength of electron.[130] Other waves with longer wavelengths are also applied in the microscopy, such as ultraviolet microscopy, infrared microscopy to generate topochemical image, but they are seldom used on the nanoscale or microscale due to their limited resolutions.[131] Magnetic field is also exploited in the microscopy fields of study, but mostly it is applied in medical imaging.[132] Regarding the scanning probe microscopes, the most widely used microscope is atomic force microscopy (AFM), using the physical probe to detect the surface of the sample at the atomic level. The performance of AFM can be improved by exploiting the other elements such as ultrasonic, electromagnetic wave, magnetic force, etc.[133-135]

Generally, optical microscopy, confocal laser scanning microscopy (CLSM), scanning electron microscopy (SEM), transmission electron microscopy (TEM) and AFM are the most commonly used microscopy in terms of the characterisations of microcapsules. Optical microscopy using visible light as the source is cheap and easy to operate, but the resolution is still limited.[136] CLSM is widely used in the characterisations of the microcapsules in terms of the measurements of shell thickness, due to its enhanced resolution. SEM or environmental scanning electron microscopy (ESEM) is usually used to observe the microstructure of the microcapsule samples.[30,137] In addition, the CLSM and ESEM can be used in the observation of dried or liquid samples. TEM are also used to characterise the microcapsules[137], but it is mostly used in the observation of cross-section of the microcapsules.[36] The samples need to be embedded in the resin and cut into ultra-thin slice. Besides, AFM is also applied to obtain the topographic image of microcapsules.[138]

2.4.2 Size and size distributions

Size and size distribution are fundamental physical properties for the characterisations of microcapsules, and they are strongly related to the other properties of the final products, such

as payloads, flow properties, surface adhesion and mechanical properties. Generally, the microcapsules formed by microfluidics exhibit narrow size distributions compared with the one obtained by stirred vessel. Various techniques are developed to be used in the charactersations of microcapsules as summarised in Table 2.1, and they can be classified into two categories: laser diffraction method and microscopy. Among all of the techniques in Table 2.1, laser diffraction[139] and microscopy combined with image analysis[140] are mostly popular ones in the characterisations of the microcapsules.

Table 2.1 Summary of the techniques for the characterisations of particle size.[141]

Light Interaction Methods	Laser Diffraction Single Particle Light Obscuration Single Particle Light Scattering Multi-Angle Light Scattering Photon Correlation Spectroscopy Fiber Optic Doppler Anemometry (FODA) Time of Flight
Microscopy Methods	Optical Microscopy and Imaging Analysis TEM, SEM and AFM
Electrical Property Methods	Differential Mobility Analyzer (DMA) Coulter (Electro zone) Principle Zeta Potential
Sorting and Classification Methods	Sieving and Screening Field Flow Fractionation (FFF) Air Classification Fluorescence Activated Cell Sorting
Sedimentation Methods	Centrifugal Sedimentation Photo Sedimentation X-ray Sedimentation

Dynamic light scattering (DLS) detecting the Brownian motion of the measured sample dispersed in the liquid is usually used in the characterisation of size distribution ranging from

1 nm to 1 μm,[142,143] while Static Light Scattering (SLS) namely laser diffraction measures the variations of the laser intensity, applying in the detection of size ranging from 10 nm to 3 mm.[144] However, a drawback of SLS method is that the knowledge of refractive index of the detected material is essential for the size measurement.

Microscopy is another commonly used technique for the size measurements of microcapsules on the individual level. Microscopy offers the real image of the microcapsules, but the obvious disadvantages are the time-consuming measurements and cannot provide the information on the bulk level easily.

2.4.3 Mechanical property

The mechanical property of a capsule is imparted by the choice of shell material, subjected to the shell thickness, physical structure of the shell, diameter of the capsule and chemical composition of the shell, and it exhibits the information of its capability.[144] For instance, in fast moving consumer goods (FMCGs), it is advantageous to release the active ingredients *via* fracture caused by mechanical force, but they need to be entrapped in the microcapsules before they are delivered to the target place. In this case, the mechanical property data are essential to study the stabilities of the formed microcapsules from different types of materials.

Regarding to the mechanical properties of the microcapsules, they normally can be determined either in bulk or individual level.[144] For the bulk mechanical test, it generally places emphasis on the resistance to hydrodynamic force, caused by shaking,[145] turbine rotor[146] and bubble column[147]. Regarding the individual level measurements, the commonly used techniques contain shear flow, tweezers, micropipette, atomic force microscope (AFM) and micromanipulation utilising two paralleled surfaces to press the capsules as shown in Scheme 2.11.
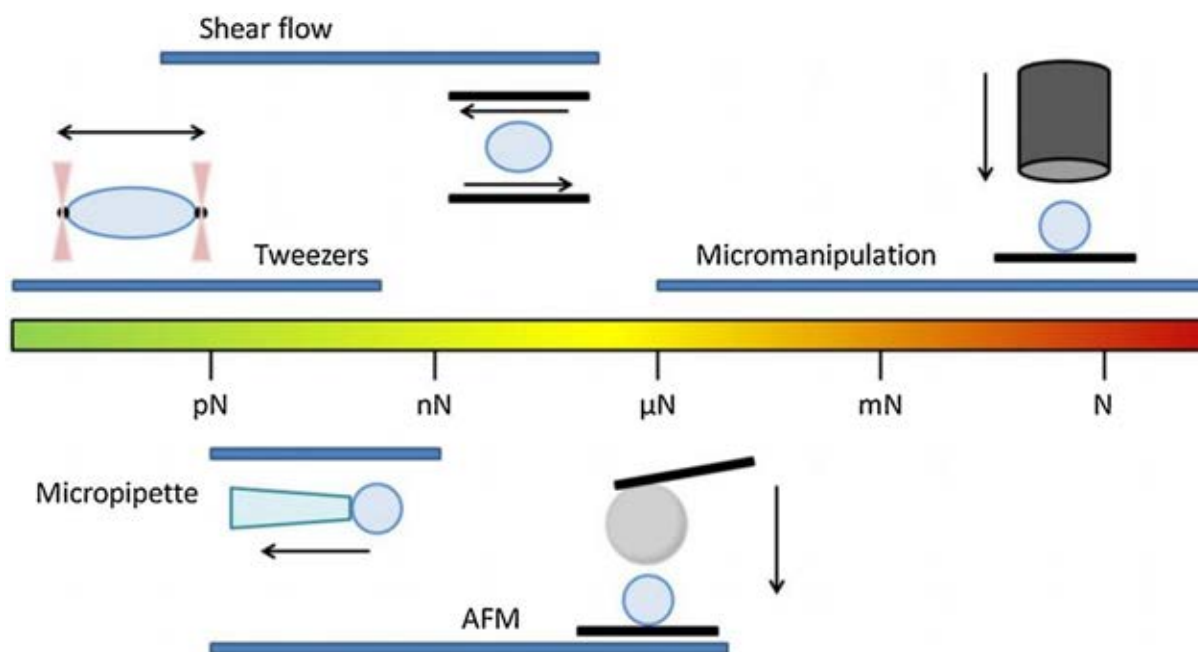
Scheme 2.11 Schematic representation of general techniques to measure the mechanical properties of single-particle with corresponded force range. Arrows represent the directions of forces applied.[148]

The tweezers, containing optical and magnetic ones as the most sensitive technique, measure the mechanical properties of biological samples with the force range below 50 pN. The optical tweezers usually named optical traps, utilise photons ejected from laser to afford an attraction or repulsion force considering the refractive index of the sample. The magnetic tweezers are used to measure the tensile force or torque generated by the biomolecules or polymers.[149] For the optical trap, the resolution is restricted to the optically homogeneous purified samples, since the trap stiffness relies on the optical intensity and its distribution, strongly affected by the optical property of the sample.[149] The optical trap also lacks of exclusivity and selectivity, while for the magnetic trap, the bandwidth, sensitivity and manipulation capacity are still unsatisfactory.[149] Moreover, the extra heat caused by the electromagnets causes a concern and needs to be further solved by advanced technology and development of theoretical research in the future.[149]

Shear flow technique is used to measure the mechanical properties of the capsule passing through the microfluidic channel.[150,151] The micropipette technique is developed to test the mechanical properties of biological capsules[152,153] and synthesised microcapsules[154-157] in a micropipette with similar principle to the shear flow technique. The elastic properties of the capsules or cells can be calculated *via* axisymmetric motion and deformation of the microcapsule.[144] The drawbacks of the above techniques are the limited applied force, which cannot break the capsules and provide the rupture characterisations, such as rupture force, displacement at rupture and rupture stress.

AFM is another powerful technique used in the measurements of the mechanical properties of individual particles. It can afford three abilities for mechanical measurements, including force measurements, imaging and manipulation. The AFM technique is generally categorised into colloidal probe and sharp tip in terms of the indentation. The colloidal probe AFM uses a large colloidal probe attached on the cantilever to measure the mechanical behaviour of the whole particle rather than a point, providing the whole geometric information of the particle.[158,159] Whereas, the sharp tip AFM offers the mechanical properties of the particles, providing a high resolution imaging of the materials, and even the exhibition of structural information on macromolecules, as well as the further compression to rupture.[160,161]

Micromanipulation was first invented by Zhang et al. to measure the rupture force of individual mammalian cells in 1991,[162] and was then developed to test a variety of samples, ranging from biological cells to artificial microcapsules.[163-167] Not only the rupture force, displacement at rupture, nominal rupture stress, deformation at rupture and Young's modulus can be calculated from the obtained data, but also loading and unloading of compression at small deformations (such as 10 % of the particle size) to a single capsule is possible, obtaining the intrinsic mechanical property of the capsule.[163] Notably, the force range of the micromanipulation technique can reach the orders of magnitude from nanoNewton to Newton, which is greater

than any other technique discussed in the chapter.[144] The micromanipulation technique exactly fills in the blank of the mechanical characterisation. The details of the technique is presented in Chapter 3, Section 3.4.7.

2.4.4 Quantification of release

Plenty of techniques are used in the determination of release of water soluble ingredients. Flame photometry and inductively coupled plasma emission spectroscopy (ICP-EMS) are both widely used techniques to measure the concentrations of some certain metallic elements. The sodium and potassium are normally measured quickly and accurately by flame photometry relative to the ICP-EMS.[168]

Regarding the molecules detections, UV-vis spectrophotometry, fluorescence spectrophotometry, gas chromatography (GC) and HPLC are commonly used techniques for the quantitative detection of various molecules.

UV-vis spectrophotometry attracts a lot of attentions due to its fast analysis and easy operation. UV-vis spectrophotometers generally contain three types, namely single-beam UV-vis spectrophotometer, double-beam-in-space UV-vis spectrophotometer and multichannel UV-visible spectrophotometer (Scheme 2.12).[169] Regarding the single-beam instrument, the complexity and performance varies greatly for different instruments. It has good light throughput, but the fluctuation of the source power needs to be concerned. For the double-beam instrument, the beam is split into two by the beam-splitter, each of which simultaneously passes through the sample cell and the reference standard cell, eventually recombines at same detector. The fluctuations of the source power, transducer and amplifier are thus removed from each measurement. The multichannel instrument is the most recent UV-visible spectrophotometer appeared on the market since 1980s. It alternatively sends the beam to the sample and the

reference standard cell before recombines at the photo-detector. The multichannel instrument

offers the merits of speed and reliability of measurements.[169]

(a)

(b)

(c)
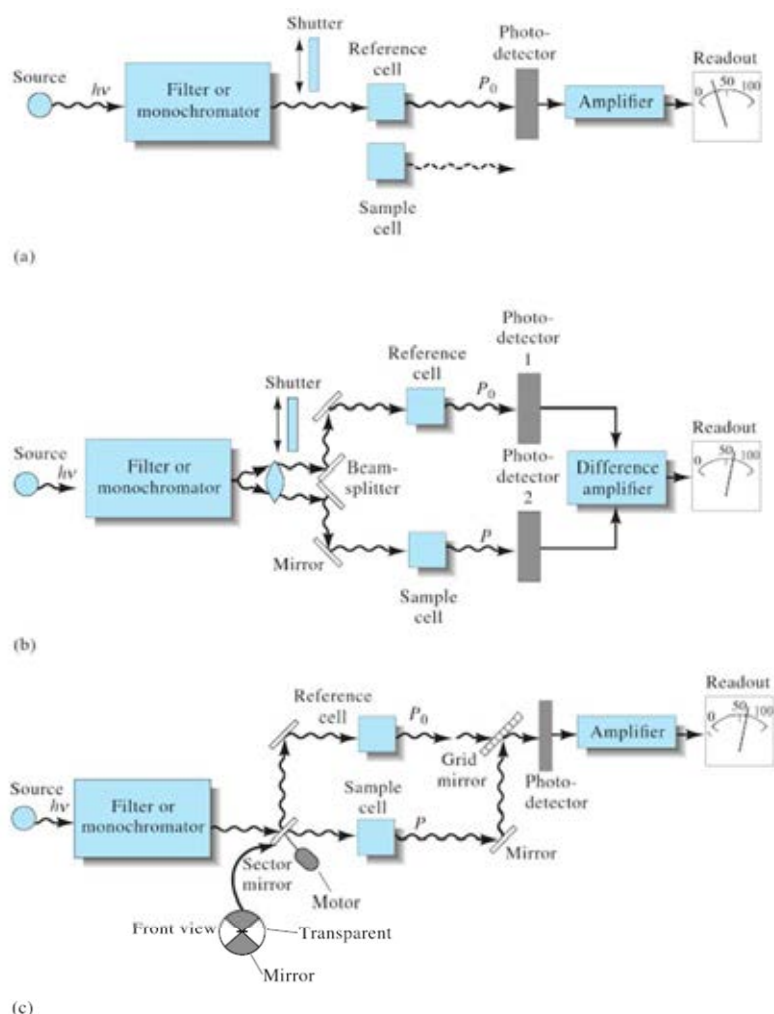
Scheme 2.12 Schematic diagram of the three types of UV-visible spectrophotometers, including (a) single-beam UV-vis spectrophotometer, (b) double-beam UV-vis spectrophotometer and (c) multichannel UV-vis spectrophotometer.[169]

Fluorescence spectrophotometry is another technique widely applied in the detections of molecules. This technique benefits from its high sensitivity, normally 10-1000 times higher than that of UV absorption spectroscopy, but its application is still limited to the detection of fluorescent materials.[170] GC and HPLC using similar principles are also widely used in many chemical separation, identification, and quantification. Many chemical compounds, including

drugs and metabolites, can be analysed by either gas chromatography (GC) or high-performance liquid chromatography (HPLC). Unfortunately, GC is just confined to detect the chemicals with low molecular weight and high stability at temperatures. HPLC offers a wide sample scope, but the cost is much more expensive than GC.

2.5   Summaries and discussions

This chapter presents the background of microencapsulation, following by literature reviews about encapsulation methodologies, release mechanisms of active ingredients and characterisations of microcapsules. The current challenge in the microencapsulation for controlled release of water soluble active ingredients with low molar mass is also stated here. There are plenty of techniques to characterise the microcapsules, each with their own advantages and limitations. In my project, the techniques for the characterisations of microcapsules will be introduced in details in Chapter 3.

Microencapsulation is a widely used technology to encapsulate active ingredients, delivering them to the target place. It can be achieved by plenty of methods, ranging from physic-chemical approaches (coacervation, co-crystallisation, polymerisation, self-assembly, etc.) to mechanical approaches (spray drying, extrusion, freeze drying, etc.). There are vast examples to achieve a sustained release of hydrophobic ingredients,[30,171,172] but it is still a challenge to encapsulate water soluble ingredients with low molar mass, displaying a sustained release or no release in aqueous environment. The small water soluble salts and molecules have been encapsulated by various ways including nanoliposomes, nanoparticles, nanofilbers and microparticles based on the literature review. However, it is still difficult to design a proper way to entrap the small water soluble ingredients with long-time release or even no release in aqueous environment, considering the proper size range on the microscale, payload, encapsulation efficiency, other physical and chemical properties, since the small water soluble

ingredients are easy to leak out from the shell of microcapsules, due to their small molecular size and water soluble. There are some researchers demonstrating their achievements in the sustained release of small water soluble ingredients, but the release time is still limited. Furthermore, the fabrications of microcapsules by some hydrophobic materials were exhibited to be potential candidates for the sustained release of small active ingredients, but they seemed to be difficult to be well dispersed in aqueous phase. To overcome the challenge is highly demanded to be extensively used in many fields of research, such as FMCGs, agrochemicals, printings, etc.

Inorganic, organic and inorganic-organic composite materials have been vastly applied in the encapsulation fields of research based on the literature review. Silica exhibits excellent physical properties including good biocompatibility, optical transparency and permeability, which made it a good candidate to be applied across vast fields of material, chemistry and engineering.[173,174] Melamine formaldehyde (MF) is a versatile chemical cross-linking agent and has been broadly used in diverse applications, due to its polycondensates providing tight seal, acid/alkaline resistance and mechanical and thermal stability.[175-177]

Interfacial polymerisation (IFP) and *in situ* polymerisation methods are very similar encapsulation methods and they both have been widely used in industries. The commercial microcapsules synthesised by IFP are normally in the size range of 20-30 μm, and the larger capsules can still be obtained by this method.[43] The merits of IFP are simple, stable, low cost, high encapsulation efficiency, controllable size and shell thickness, etc., while the *in situ* polymerisation method has the advantages of high payload and narrow size range as summarised in the literature review. Therefore, it is imperative to develop a proper technique to deliver water soluble ingredients with low molar mass, displaying a sustained release or no release in aqueous phase. Considering the end use, morphology, size, shell structure and

thickness, mechanical properties and release profiles are the most important characterisations

of the designed microparticles to be considered.

Chapter 3 Materials, Methods and Characterisations

3.1   Introduction

This chapter presents the materials and methods to synthesise the microspheres comprised of polystyrene sulfonate (PSS) and silica (PSS-SiO$_2$) as well as melamine formaldehyde (MF) based microcapsules/microspheres. A conventional mechanical stirring system with full baffles and standard configuration was used for the preparation of water in oil emulsions to form the microcapsules/microspheres. The physical, structural and mechanical properties of the formed microcapsules/microspheres were characterised, which include morphology, phase, composition, size distribution, mechanical property, wall structure and thickness of the synthesised microparticles as well as the release profiles of encapsulated active ingredients. The morphology of the formed microcapsules/microspheres was determined by an optical microscope and scanning electron microscope (SEM). The phase of the obtained materials was confirmed by X-Ray Diffraction (XRD) and Fourier-transform infrared spectroscopy (FT-IR), while the composition was characterised by thermogravimetric analysis (TGA), energy disperse X-ray (EDX) and X-ray photoelectron spectrometer (XPS). The size distribution parameters including SPAN and mean size of the formed microcapsules/microspheres were measured by a static light scattering (SLS) technique. The mechanical properties of the formed microparticles were measured by a micromanipulation technique utilising two paralleled surfaces to press the single microparticles.[163-167] The shell structure, thickness and elemental distribution of the formed microparticles were observed and measured by SEM and transmission electron microscopy (TEM) after the sample was embedded in the resin and cut by a microtome. Water contact angle was measured by a contact-angle-analysis system. The release rates of ions and molecules in an aqueous environment were measured by a flame photometer, inductively coupled plasma emission spectroscopy (ICP-EMS) and a UV-Vis

spectrophotometer. Details of these materials, methods and techniques are discussed in this chapter.

3.2 Materials

3.2.1 Materials for the fabrications of PSS-SiO₂ microspheres

Potassium chloride (KCl), sodium chloride (NaCl), poly(4-styrenesulfonic acid) (PSS) aqueous solution (M_w = ~75000, 18 wt. % in H_2O) and tetraethyl orthosilicate (TEOS) were purchased from sigma-Aldrich. Polyglycerol polyricinoleate (PGPR) was obtained from Palsgaard (Palsgaard 7130, Juelsminde, Denmark). Vegetable oil was bought from an Aldi store (Birmingham, UK), and hexane was ordered from Fisher Scientific, UK.

3.2.2 Materials for the fabrications of melamine formaldehyde (MF) based microcapsules/microspheres

Potassium chloride (KCl), allura red, poly(4-styrenesulfonic acid) (PSS), formaldehyde (37% (aq.) w/w) and octadecyltrichlorosilane were purchased from Sigma-Aldrich, UK. MF precondensate (70 % wt (aq), formaldehyde to melamine molar ratio 0.2) was obtained from British Industrial Plastics Ltd, Birmingham, UK. Poly (acrylamide-acrylic acid, sodium salt) was bought from Polyersciences, Inc., US. Shellac flakes were obtained from Syntapharm (Harke Group, Germany). Polyglycerol polyricinoleate (PGPR) was obtained from Palsgaard (Palsgaard 7130, Juelsminde, Denmark). Vegetable oil was bought from an Aldi store (Birmingham, UK), and hexane was ordered from Fisher Scientific, UK. All of the chemicals were analytical grade without further purification.

3.3 Methods

3.3.1 Synthesis of PSS-SiO₂ microparticles with KCl/NaCl encapsulated.

To the PSS solution (3 ml) was added KCl/NaCl (0.1 g), which allowed to be fully dissolved, followed by emulsification in vegetable oil (100 ml) containing dissolved polyglycerol polyricinoleate (PGPR) (0.8 g) (Scheme 3.1, Step 1). The emulsification process was proceeded via mechanical stirring at a speed of 200 rpm with a marine impeller (ϕ 44 mm) at half liquid depth position in a vessel (ϕ 65 mm × 95 mm) without baffles for 2 h. TEOS (1 ml) was then added dropwise *via* a pipette manually or syringe pump at an injection rate of 100 μl/min into the emulsion (Scheme 3.1, Step 2), which was stirred continuously for 4 h (Scheme 3.1, Step 3). The precipitate was centrifuged for 2 min at 4000 rpm (centrifugal force 1860 g), the supernatant decanted off, and the residue washed by hexane (35 ml x 3), and dried in a vacuum drier (Edwards High Vacuum Ltd, Manor Royal, Crawley, Sussex, UK) at room temperature for ~12 h, affording ~1 g of yellow microspheres.
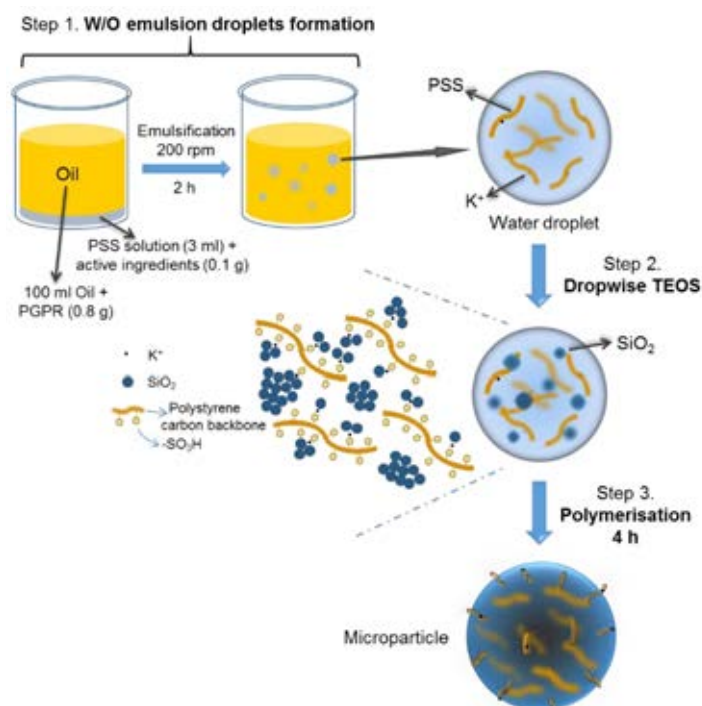
Scheme 3.1 Scheme of PSS-SiO₂ microspheres fabrication process with active ingredients encapsulated.

3.3.2 Synthesis of PSS-0.7SiO$_2$ microparticles with KCl encapsulated.

The same method as above was followed, but using 0.7 mL of TEOS, and afforded ~1 g of yellow microspheres.

3.3.3 Synthesis of MF^{wtc} and MF microcapsules with KCl/allura red encapsulated.

KCl/allura red powder (0.1 g), MF precondensate (MFP, 1.0 g), copolymer (0.232 g, poly(acrylamide-acrylic acid), sodium salt) and formaldehyde solution (200 μl/600 μl) were mixed in water (5 ml) homogeneously, and the aqueous solution was then adjusted by acetic acid to pH 4.3 (monitored by a pH meter) at room temperature (Scheme 3.2, Step 1). After the aqueous solution was mixed well, vegetable oil (400 ml) with polyglycerol polyricinoleate (0.8 g) was added immediately followed by stirring at 600 rpm for 2 h by a Rushton turbine (Φ 31 mm, in a vessel with standard configuration and full baffles) to form unripened MF microcapsules. The unripened MF microcapsules was heated to 55 ^{o}C, which was maintained for 30 min at the same stirring speed, and then stirred at 1200 rpm for another 30 min at the same temperature (Scheme 3.2, Step 2). After the temperature was adjusted to 75 ^{o}C for another 5 h heating, the ripened MF microcapsules were formed (Scheme 3.2, Step 3). Finally, NaOH solution (1 M, 2 ml) was added dropwise (100 μl/min) by a syringe pump into the above vessel for 2 h at a stirring speed of 600 rpm to terminate the polymerisation process. The precipitate was centrifuged for 2 min at 6000 rpm (centrifugal force 4427 g), the supernatant decanted off, and the residue washed by hexane (35 ml x 3), and dried in a vacuum drier at room temperature for ~12 h, affording ~1 g of MF microcapsules. The MF-KCl microcapsules (ripened) formed with different volumes of formaldehyde solution (200 μl and 600 μl) were named as MF-KCl (200 F) and MF-KCl (600 F), respectively, and the MF-dye microcapsules (ripened) formed with formaldehyde solution (200 μl) were named as MF-dye (200 F). For the synthesis of

MF^{wtc}-KCl microcapsules, the initial aqueous solution was prepared without adding copolymer, and the rest procedures were the same as the preparation of MF microcapsules.
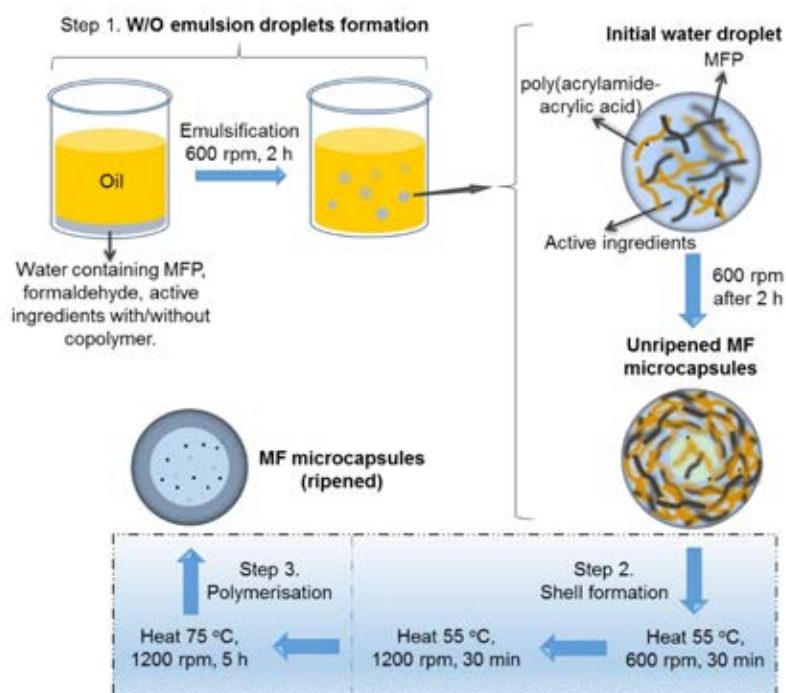
Scheme 3.2 Scheme of MF microcapsules fabrication process with active ingredients encapsulated.

3.3.4 Synthesis of MF-shellac microcapsules with KCl/allura red encapsulated.

KCl/allura red powder (0.1 g), MFP (1.0 g), copolymer (0.232 g, poly(acrylamide-acrylic acid), sodium salt) and formaldehyde solution (200 μl/600 μl) were mixed in water (5 ml) homogeneously, and the aqueous solution was then adjusted by acetic acid to pH 4.3 (monitored by a pH meter) at room temperature. After the aqueous solution was mixed well, vegetable oil (400 ml) with polyglycerol polyricinoleate (0.8 g) was added immediately followed by stirring at 600 rpm for 2 h by a Rushton turbine (Φ 31 mm, in a vessel with standard configuration and full baffles) to form W/O emulsion droplets. Shellac flake (2 g) dissolved in ethanol (1 ml) was then added dropwise into the above emulsion system at a stirring speed of

600 rpm for another 3 h. The emulsion was heated to 55 °C, which was maintained for 30 min at the same stirring speed, and then stirred at 1200 rpm for another 30 min at the same temperature. After the temperature was adjusted to 75 °C for another 5 h heating, the ripened MF microcapsules were finally formed. The precipitate was centrifuged for 2 min at 6000 rpm (centrifugal force 4427 g), the supernatant decanted off, and the residue washed by hexane (35 ml x 3), and dried in a vacuum drier at room temperature for ~12 h, affording ~1 g of MF microcapsules. The MF-shellac microspheres (ripened) formed with different volumes of formaldehyde solution (200 μl and 600 μl) were named as MF-shellac (200 F) and MF-shellac (600 F), respectively.

3.3.5 Synthesis of MF-PSS microspheres with KCl encapsulated.

KCl powder (0.1 g), MFP (1.0 g) and PSS solution (1 ml) were mixed in water (4 ml) homogeneously at room temperature. After the aqueous solution was mixed well, vegetable oil (400 ml) with PGPR (0.8 g) was added immediately followed by stirring at 600 rpm for 2 h by a Rushton turbine (Φ 31 mm, in a vessel with standard configuration and full baffles) to form unripened MF-PSS microspheres. The polymerisation process of the MF-PSS microspheres was the same as the one of MF microcapsules. Briefly, the unripened MF-PSS microspheres were heated at 55 °C at 600 rpm for 30 min and then increased to 1200 rpm, which was maintained for further 30 mins. The fully ripened MF-PSS microspheres were finally formed by heating at 75 °C at 1200 rpm for further 5 h. Finally, NaOH solution (1 M, 2 ml) was added dropwise (100 μl/min) into the above vessel for 2 h at a stirring speed of 600 rpm. The precipitate was centrifuged, washed by hexane (35 ml x 3), and dried in a vacuum drier at room temperature for ~12 h, affording ~1 g of MF-PSS microcapsules.

3.3.6 Synthesis of M_1 and M_2 microcapsules.

KCl (0.2 g)/allura red (0.1 g) and melamine formaldehyde precondensate (MFP, 1.0 g) were dispersed homogeneously in deionised water (DIW, 2 ml). The aqueous solution was then adjusted to pH 4.3 via adding acetic acid, which was then emulsified into vegetable oil (200 ml) with different amounts of PGPR (0.05 g and 0.2 g) at 800 rpm overnight (Scheme 3.3, Step 1). The temperature was raised to 60 $^{\circ}$C for 1 h at the same stirring conditions and it was then increased to 65 $^{\circ}$C, heating for 4 h at a stirring speed of 1000 rpm (Scheme 3.3, Step 2). The polymerisation process was finally terminated by adding NaOH solution (1 M, 1 ml) at a stirring speed of 2000 rpm for 30 min for further use. For the characterisation of the M microcapsule samples, they were then obtained by centrifugation (8000 rpm, centrifugal force 7871 g, 2 min) and washed by hexane for 3 times. The samples were dried overnight in a vacuum drier at room temperature. The ones fabricated with 0.05 g and 0.2 g PGPR were named as M_1 and M_2 microcapsules, respectively.

3.3.7 Synthesis of M_1O and M_2O microcapsules.

Octadecyltrichlorosilane (OTS, 1 ml) was added dropwise into the above emulsion at a stirring speed of 2000 rpm for 30 min at 35 $^{\circ}$C (Scheme 3.3, Step 3). The MF-OTS microcapsules were harvested by removing the free oil phase via centrifugation (8000 rpm, centrifugal force 4427 g, 2 min) ready for further use. For the characterisation, the samples were then obtained by the same procedure as M_1 and M_2 microcapsules. The ones fabricated using M_1 and M_2 microcapsules were designated as M_1O and M_2O microcapsules, respectively.

3.3.8 Synthesis of M_2OM microcapsules.

The MFP (5.0 g), formaldehyde solution (37% (aq.) w/w, 3 ml) and copolymer (poly(acrylamide-acrylic acid), 1.16 g) were dissolved in DIW (140 ml) at a stirring speed of 600 rpm for 105 min at pH 4.3 adjusted by acetic acid at room temperature (Scheme 3.3, Step

4.1). Half amount of the slurry of the formed M_2O microcapsules in vegetable oil was poured into the above aqueous solution, which was stirred at a speed of 2100 rpm for 30 min, forming an oil/water emulsion (Scheme 3.3, Step 4.2). The formed emulsion was then stirred at 600 rpm for 30 min before the temperature was raised to 65 °C, which was maintained for 4 h (Scheme 3.3, Step 4.3). The dispersion with microcapsules was then cooled down to room temperature and the polymerisation was terminated by adjusting pH to 12 via adding NaOH solution (1 M). The obtained microcapsules were harvested by centrifugation (8000 rpm, 2 min) and washed by DIW for 3 times. The formed MF-OTS-MF microcapsules were dried in a vacuum drier at 60 °C overnight, named as M_2OM microcapsules.
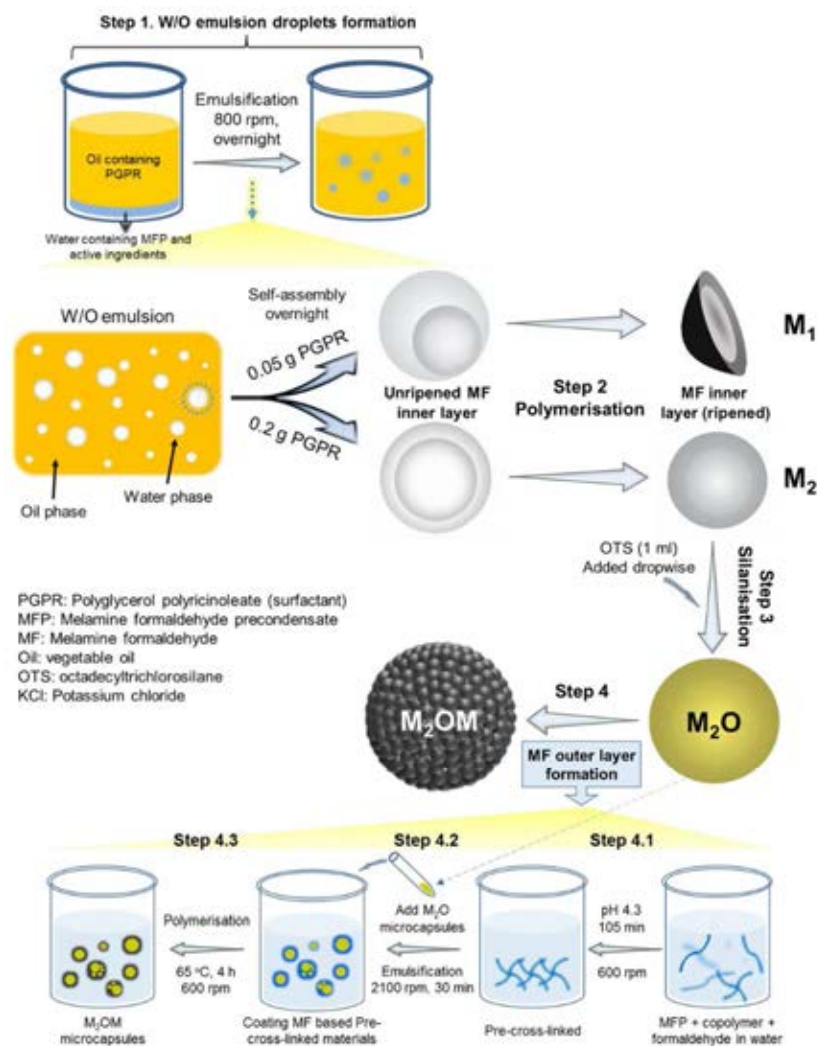
Scheme 3.3 Scheme of M_2OM microcapsules fabrication process with active ingredients encapsulated.

3.4   Characterisations of the formed microspheres/microcapsules

The morphologies and cross-sections of the prepared microparticles were observed with an optical microscope (301-371.011, Leica, Germany) and SEM (Philips XL-30 FEG ESEM or JSM-6700F). The cross-sections of the microcapsules were cut by a microtome (Reichert-Jung) and observed by SEM (Philips XL-30 FEG ESEM or JSM-6700F) and TEM (JEOL-1400). The size distribution, SPAN and the mean volumetric size (D_{43}) were measured by a laser light scattering technique (Mastersizer 2000, Malvern Instruments, UK). The phase of the sample was confirmed by a Bruker D8-Advance X-ray powder diffractometer using Cu Kα radiation (λ = 1.5406 Å), and the FT-IR spectrum was performed on a Thermo Electron Nicolet 8700 spectrometer. The composition was recorded on a thermogravimetric analysis (STA 449 F3, NETZSCH). The chemical composition of the sample was evaluated by an energy disperse X-ray microanalysis (EDX) (Oxford, Inca 300) in conjunction with SEM and an EDX detector (X-MAX 80 TLE, Oxford Instruments, Oxford, UK) connected with high resolution transmission electron microscope (HRTEM, Philips Tecnai F20) as well as X-ray photoelectron spectroscopy (XPS) obtained by an X-ray photoelectron spectrometer (ESCALab MKII) utilising Mg Kα radiation as an excitation source. Water contact angle measurements were carried out on a CAST 2.0 contact-angle-analysis system (Data-Physics, Germany). The mechanical properties of microspheres were determined by a micromanipulation technique. The concentration of K^+ and Na^+ ions were measured by the flame photometer, and the concentration of PSS and allura red were detected by a UV spectrophotometer at 254 nm and 504 nm, respectively (Cecil 2021 UV spectrophotometer).

3.4.1 Morphology (microscopy)

Microscopy established by Antonie van Leeuwenhoek was a technique utilising microscope to observe object under magnification,[178] especially for the one beyond the resolution range of our naked eyes. Herein, the morphologies of the samples were recorded by the optical and electron microscopes.

3.4.1.1   Optical microscopy

For the optical microscope, a beam of light was ejected by a light source towards the sample to create an enlarged image, utilising a system of lenses as shown in Scheme 3.1. The light gathered by the collector lens traveled through the field aperture and the aperture diaphragm, where the sample was focused *via* the condenser lens. The light diffracted or reflected by the sample was gathered by the objective lens, and projected onto an observer or a detector through the tube lens and the ocular. Herein, the morphology of the synthesised sample slurry was observed by an optical microscope (301-371.011, Leica, Germany). The image of the sample was magnified and recorded by the optical microscope connected with a computer installed with Leica QWin Pro V2.8 software (Leica Microsystems, UK). The image shows the morphology and size of the obtained microspheres/microcapsules. Fig. 3.1 shows a typical optical micrograph of the formed double emulsion droplets *via* a microfluidic method.
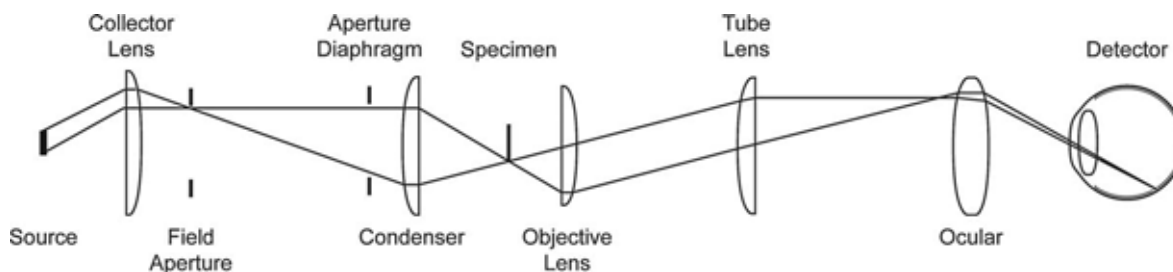
Scheme 3.4 The anatomy structure of an optical microscope.[179]
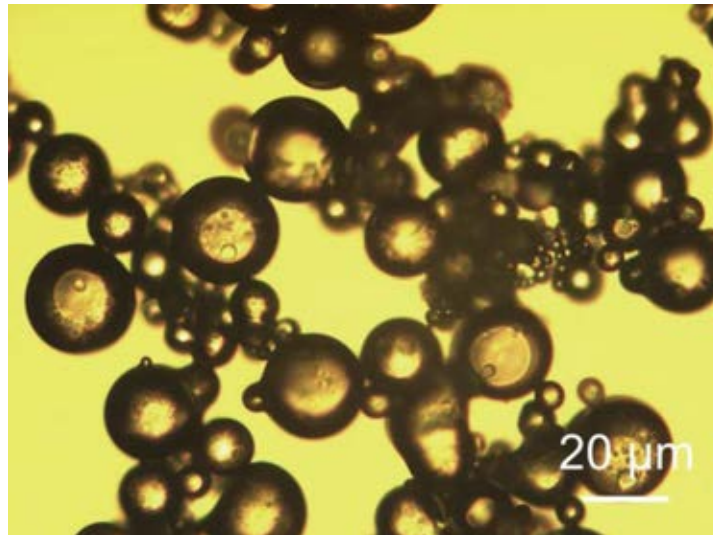
Fig. 3.1 The optical micrograph of the formed melamine formaldehyde microcapsules with aqueous phase encapsulated.

3.4.1.2 Scanning electron microscopy (SEM)

For the scanning electron microscope, it utilises a beam of accelerated electrons produced by an electron gun as the source to scan across an area of sample. The energy of the electron is lost after they interact with the sample, which is finally received by the monitor, recreating a magnified image of the sample with the properties of its topography and composition (Scheme 3.2). Generally, the atoms with higher numbers display brighter images than the ones with lower numbers, revealing elemental contrast images.[180]
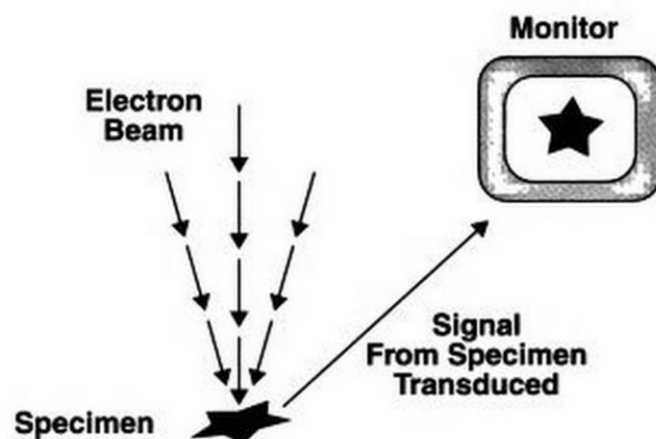
Scheme 3.5 The schematic illustration of scanning electron microscopy (SEM).[130]

The electron optical lens systems in the electron microscopes are similar to the glass lenses of the optical microscope. The resolution of the microscope is limited by the wavelength of the light or electron source. The electron microscope has higher magnification than the optical microscope due to the shorter wavelength of electron.[130] The electrons and X-rays ejected from the sample are then received by the monitor, generating an image.

The prepared dry sample was sputter coated with a thin layer of platinum by a sputter coater (SC-7640-Polaron) to offer the sample surface conductive before being loaded in SEM. The morphology of the prepared sample was observed by an SEM (Philips XL-30 FEG ESEM or JSM-6700F) under an accelerating voltage of 3.0 kV to 15.0 kV. A typical SEM image of the synthesised MF microcapsules with allura red (a kind of dye) encapsulated is displayed in Fig. 3.2.
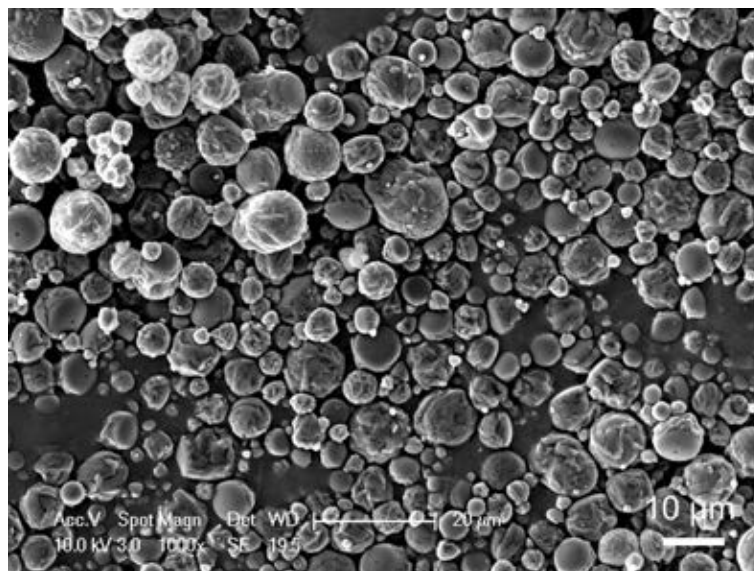
Fig. 3.2 The SEM image of the formed MF microcapsules with allura red encapsulated.

3.4.2 Shell structure and thickness

The shell structure and thickness are very important properties of the microcapsule. They can be observed and measured by SEM and TEM after the sample was embedded in the resin and cut by a microtome.

For the sample preparation, a small amount of sample is mixed with epon/araldite resin, which is polymerised at 60 °C overnight. A small trapezium shaped area is trimmed with a razor blade (approx. 0.3 mm × 0.3 mm). The face of the block is cut in an ultramicrotome (Ultracut E, Reichert-Jung, Austria) using a glass knife and the block further coated with Pt is mounted on an SEM stub before imaging. The typical SEM image of the cross-sections of the microcapsules is displayed in Fig. 3.3. The shell thickness of the microcapsules can be calculated based on the scale bar.
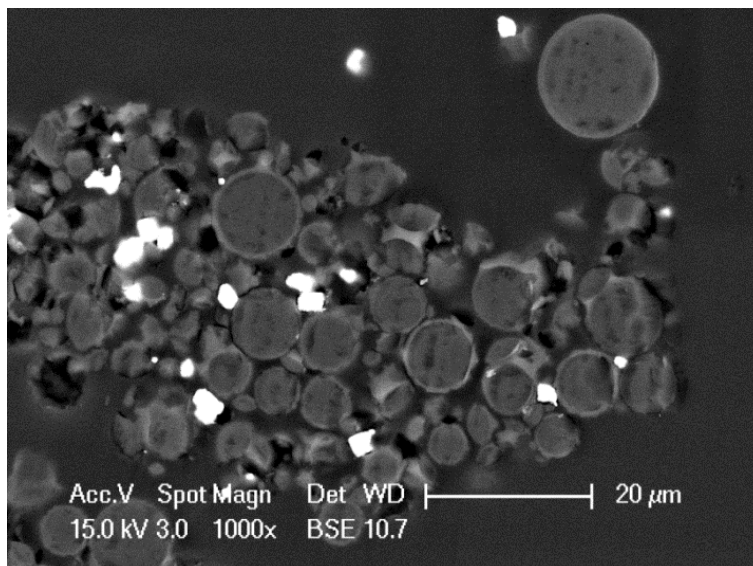
Fig. 3.3. A typical SEM image of the cross-sections of the melamine formaldehyde (MF) microcapsules.

In some cases, the SEM sample preparation process may cause the shrinkage and the artefact due to the dehydration and fixing, which can be solved by cold-stage SEM, namely cryo-SEM.[181] It can be used to observe the sample in fully hydrated and original state without further modifications, especially useful for the biological material observation and analysis. The sample is initially prepared below ambient temperature by plunged into liquid nitrogen. The cryo-fixed sample is then transferred into the cryo-preparation chamber under vacuum, where rupture can be applied if necessary. After further sputtered coating with metal, the sample is then sent to the SEM camber for imaging, where it remains frozen by adding liquid nitrogen periodically. The cryo-SEM is quick, cheap and relatively easy to operate. The typical image of the cryo-SEM is shown in Fig. 3.4.
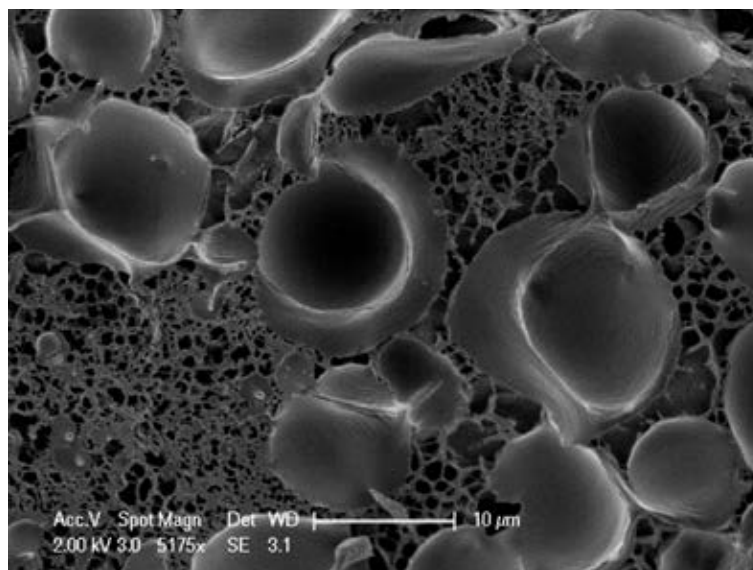
Fig. 3.4. A typical cryo-SEM image of the cross-sections of the formed melamine formaldehyde-shellac microspheres.

The shell structure and thickness of microcapsules/microspheres can be studied by transmission electron microscopy (TEM) after the sample was embedded in epon/araldite resin and cut by a microtome.[30] The ultra-thin slice with the thickness of approximately 80 nm was then made and coated with Pt for further observation. The sample slice was placed on carbon coated grids (G2500C, 2 mm × 1 mm slot, copper, 3.05 mm) observed by a TEM (JEOL-1400) at an acceleration voltage of 80 kV in vacuum conditions. The ultra-thin specimen was hit by a coherent beam produced by an electron gun and condenser lenses acquiring a magnified image by projector lenses in the TEM. The captured images of the cross-sections of the samples were finally analysed by ImageJ software (National Institute of Health, USA) installed in a computer. A typical image of the TEM is shown in Fig. 3.5.
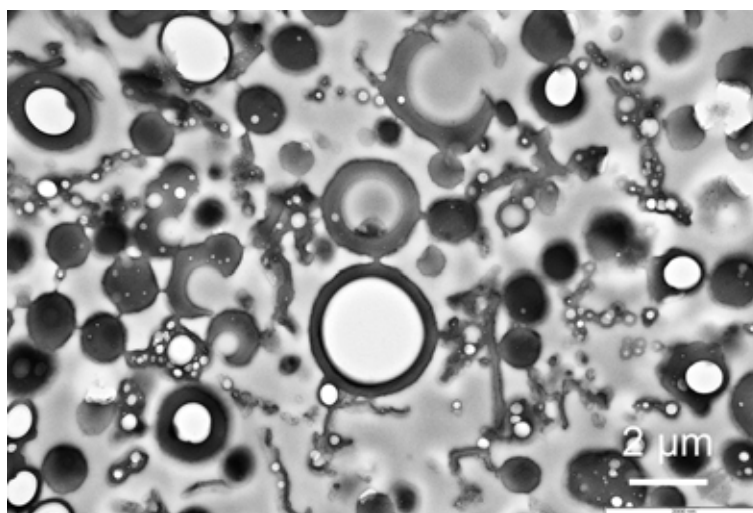
Fig. 3.5 A typical TEM image of the cross-sections of the formed melamine formaldehyde based microcapsules.

3.4.3 Size distribution (Static Light Scattering, SLS)

The size distribution of the particles can be determined by a static light scattering (SLS) technique, which is based on an optical instrument utilising laser to illuminate the particles. The diffraction pattern of the particles containing the information of the scattering angle, particle size and shape, is significantly related to their sizes, since the light diffraction occurs at a specific angle of the particles with different sizes.[182,183] The scattering angle and intensity are strongly dependent on the particle sizes. Large particles reveal low scattering angles with high intensities, whereas small ones display reversed properties as shown in Scheme 3.3.[184] In this way, the size distribution of the particles under low concentrations can be calculated by measuring their scattering angles and intensity, avoiding the false measurements of multiple scattering.[183,185]
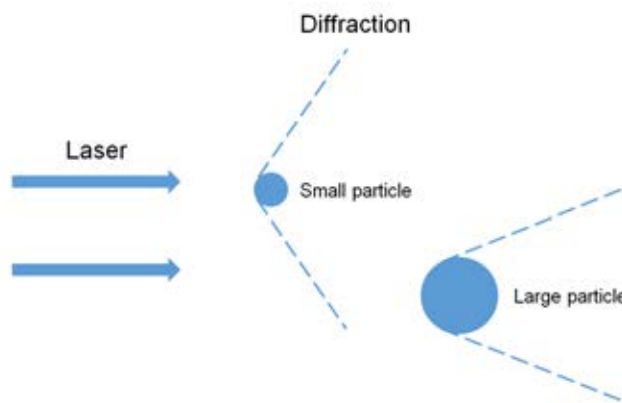
Scheme 3.6 The schematic representation of the scattering diffractions of the particles with different sizes.

A typical SLS instrument is constituted of a laser, a cuvette containing sample dispersion and one or more detectors as shown in Scheme 3.4. The laser is used to provide a stable and coherent light with fixed wavelength, illuminating the sample dispersion. The cuvette is to make sure the particles are dispersed homogeneously in the liquid. The scattering intensity is detected by photon detectors related to the scattering angle θ. The typical size distribution results of the formed melamine formaldehyde microcapsules measured by a SLS instrument (Mastersizer 2000, Malvern Instruments, UK) is shown in Fig. 3.6.
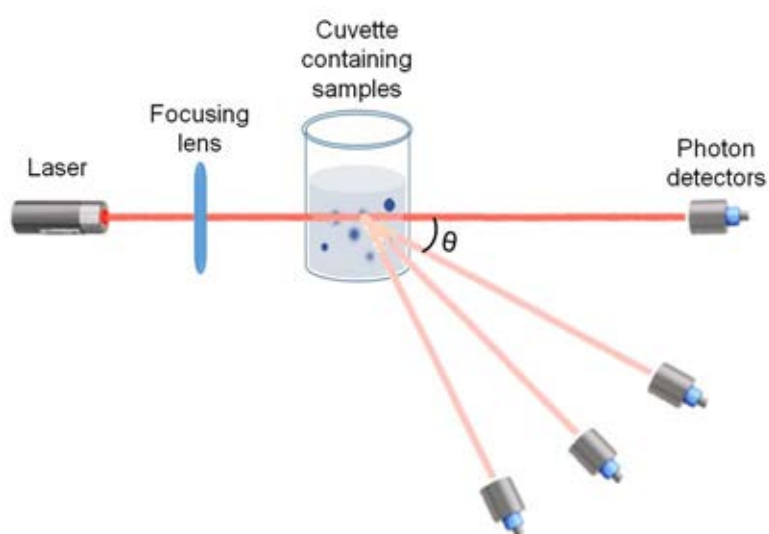
Scheme 3.7 Schematic demonstration of the dynamic static light scattering.
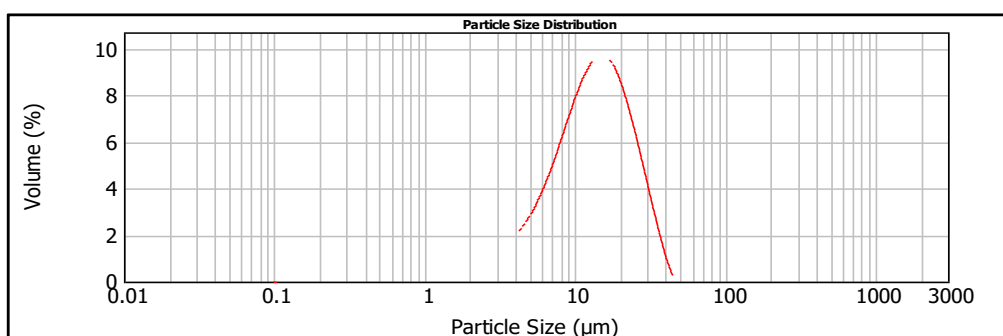
Fig. 3.6 A typical size distribution curve of melamine formaldehyde microcapsules *via* SLS equipment.

The data of SPAN value and mean size including the volume mean diameter D_{43} and the Sauter mean diameter D_{32} are defined by the following equations. D_{10}, D_{50} and D_{90} in the equations represent the diameter intercept for 10 %, 50 % and 90 % of the cumulative volume, respectively, and d_i is the diameter of the calculated particles.

$$\text{SPAN} = \frac{D_{90} - D_{10}}{D_{50}}$$

(Equation 3.1)

$$D_{43} = \frac{\sum_{i=1}^{i=n_i} d_i^4}{\sum_{i=1}^{i=n_i} d_i^3}$$

(Equation 3.2)

$$D_{32} = \frac{\sum_{i=1}^{i=n_i} d_i^3}{\sum_{i=1}^{i=n_i} d_i^2}$$

(Equation 3.3)

3.4.4 Phase

Phase is a physical feature of a matter such as solid, liquid and gas, including the crystal structure and phase composition, which can be characterised by X-Ray Diffraction (XRD) and Fourier-transform infrared spectroscopy (FT-IR).[186]

3.4.4.1 X-Ray Diffraction (XRD)

X-Ray diffraction as a non-destructive analytical technique utilises an X-ray beam to hit the sample for quantitative analysis of chemical structure based on Bragg's diffraction law.[187] The incident X-rays interact with the sample and produce the scattered rays, which can generate either destructive or constructive interference (Scheme 3.5). The diffraction peak can be formed and detected by photographic film, when the constructive interference is generated on

the condition of the Bragg`s Law ($n\lambda = 2d \sin \theta$). The Bragg`s Law correlates the wavelength of electromagnetic wave (X-ray) to the diffraction angle (θ) and the lattice spacing (d) in a crystal. The material with well-ordered atom structures can provide a diffraction pattern containing the information about atom position, bond angle, bond length, and spatial proximity of non-bonded atoms for materials capable of forming crystalline solids.[188] The obtained XRD pattern can reflect the crystalline or amorphous phase of the materials, even for the dopants, such as polymers in the crystalline material.[189] All of the possible directions of diffraction peaks would be attained and detected *via* a scanning under a range of 2θ angles. Herein, the phase of the prepared microspheres/microcapsules was confirmed by a Bruker D8-Advance X-ray powder diffractometer using Cu Kα radiation ($\lambda = 1.5406$ Å). Fig. 3.7 exhibits a typical XRD pattern of the synthesised calcium carbonate microspheres.
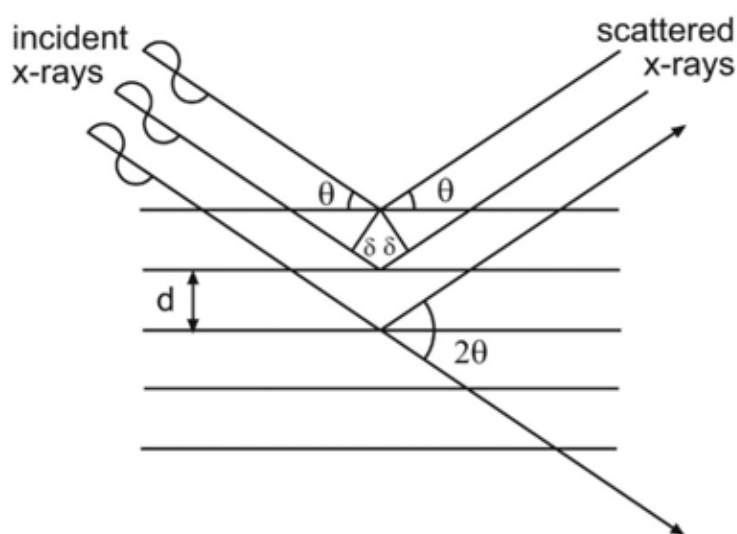
Scheme 3.8 Schematic demonstration of the relationship between waves and the atomic structure based on Bragg's Law.[190]
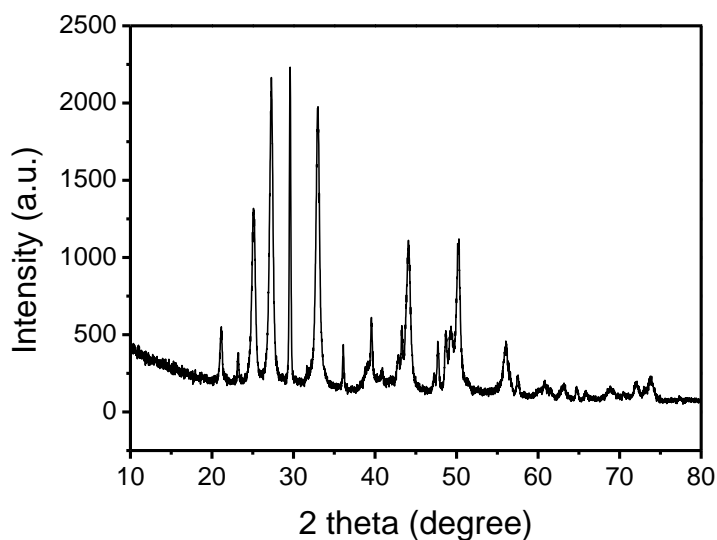
Fig. 3.7 A typical XRD pattern of the synthesised calcium carbonate microspheres including vaterite and calcite.

In many cases, XRD as a generally used characterisation method was combined with various techniques, such as EXAFS (Extended X-ray Absorption Fine Structure),[191] thermo-gravimetric analysis (TGA) and differential scanning calorimetry (DSC)[192].

3.4.4.2   Fourier-transform infrared (FT-IR) spectroscopy

FT-IR spectroscopy as a fast and non-destructive technique, utilises the infrared light to irradiate the sample, generating intensity changes of IR radiation received by the detector. The intensity differences are collected over a wide spectral range and then are converted into actual spectrum *via* a mathematical Fourier transform process by the synchronous motor. Scheme 3.6 demonstrates the mechanism of the FT-IR interferometer, the data acquisition and calculation.

The sample is illuminated by an infrared radiation source, which is modulated by the interferometer, consisting of a beam splitter and moving and fixed mirrors as shown in the upper left graphic in Scheme 3.6. The infrared light is split by an optical splitter into two

components, which are reflected by the moving and fixed mirrors (solid and dashed line of Scheme 3.6, upper left) and recombine at the optical splitter with constructive and destructive interference. Intensity differences of the infrared light passing through the sample are measured as a function of optical path length, and the intensity relies on the optical length caused by the two mirrors. As the moving velocity of the mirror is fixed, the measurement can simply record the time regime. The received signal (interferogram) is formulated as a function of frequency after the Fourier transformation process (Scheme 3.6, lower right). The IR spectrum is finally obtained by dividing the signal into the background and further mathematical manipulation (Scheme 3.6, lower left).
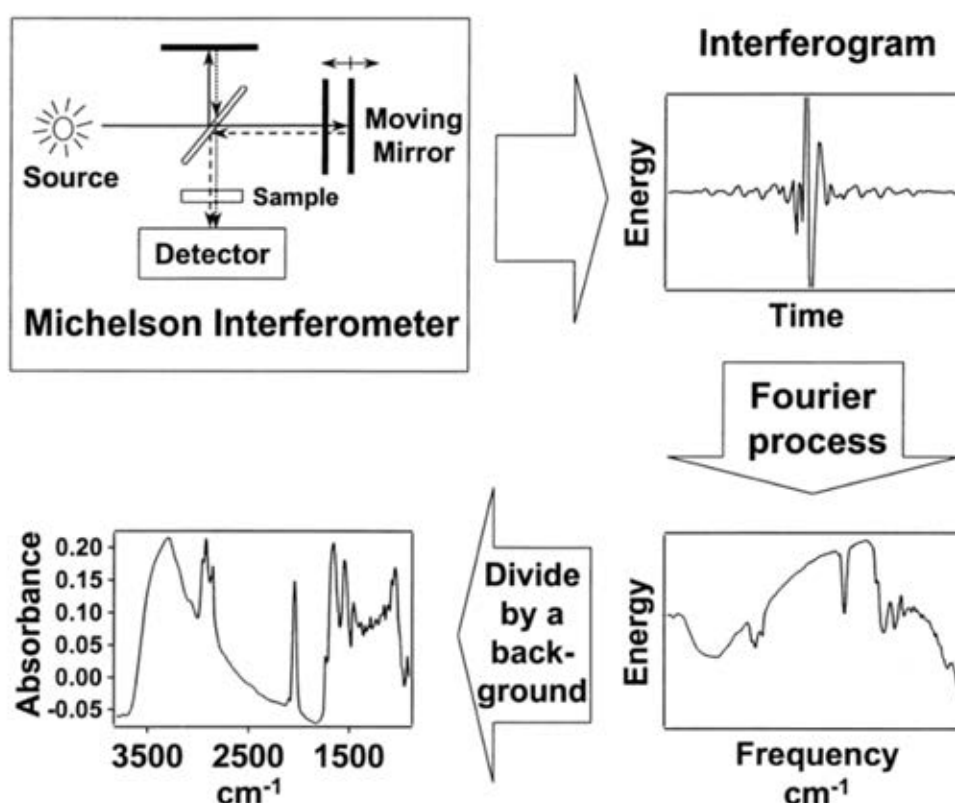
Scheme 3.9 Schematic demonstrating the mechanism of the FT-IR instrument, including the data generation, acquisition and manipulation.[193]

The FT-IR instrument consists of IR source, beam splitter, detector, attenuated total reflectance and Fourier transformation. The resulting FT-IR spectrum reflects the molecular structure and the molecular environment as the molecular fingerprint.[193,194] It can identify the unknown material qualitatively and quantitatively. The FT-IR spectra were performed on a Thermo Electron Nicolet 8700 spectrometer. A typical FT-IR spectrum of the shellac flakes is showed in Fig. 3.8.
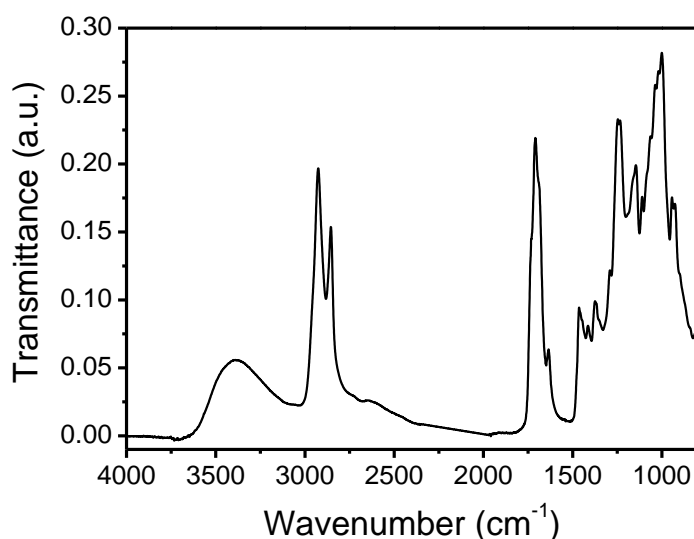
Fig. 3.8 A typical FT-IR spectrum of the shellac flakes.

3.4.5 Composition

The chemical composition of a material normally refers to the proportion of the different substances and/or the ratio of different elements existing in the composite materials. They can determine the properties and the end-uses of a composite material.[195] Thermogravimetric analysis (TGA), energy disperse X-ray (EDX) and X-ray photoelectron spectroscopy (XPS) are commonly used techniques for the composition determination in terms of the substance composition, elements distributions and surface elements, respectively.

3.4.5.1   Thermogravimetric analysis (TGA)

TGA is a technique to measure the sample weight continuously with the temperature changing over a period of time based on an instrument related to thermogravimetric analyser. The weight changes of different substances corresponding to the temperature variations are different, because different substances have different physical and chemical properties. The degradation temperature varies with different substances, and the weight loss can be thus recorded to identify the different proportions of the sample quantitatively as a function of time and temperature.[196]

Weight, temperature and time are considered to be the basic measurements for TGA. Regarding the TGA instrument, an electronic scale with high accuracy is used for the continuous measurements of the sample weight. The scale can be classified into vertical and horizontal types. In order to get the accurate data, calibration is necessary before the test, due to the interference caused by buoyancy effect or drag force during the measurement.[197] For some unstable materials easy to react with the air under heating conditions, purging inert gas such as N_2, He or Ar is essential to protect the samples.[198] In this project, the composition of the formed sample was recorded on a thermogravimetric analysis (STA 449 F3, NETZSCH). A typical TGA curve is showed in Fig. 3.9.
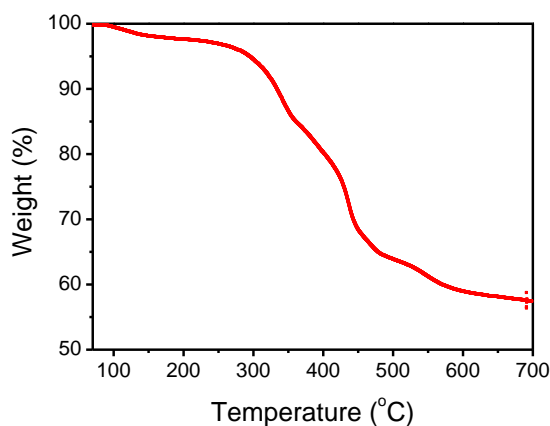
Fig. 3.9 A typical TGA curve of the formed polystyrene sulfonate-silica microsphere.

3.4.5.2 Energy disperse X-ray (EDX)

Energy dispersive X-ray (EDX), sometimes named energy dispersive X-ray analysis (EDXA), energy dispersive X-ray spectroscopy (EDS/EDXS) or energy dispersive X-ray microanalysis (EDXMA) is a widely used elemental measurement technique, utilising X-ray to irradiate the sample and the generated signals are received by a detector. The main principle of EDX is that each atom displays a unique electromagnetic emission spectrum due to its distinctive atomic structure. Some certain electrons in the inner shell of an atom may be excited by an incident X-ray beam, leaving an electron hole at its original position. The hole at the inner shell will be filled by an electron from the outer shell of the atom with higher energy, and the extra energy may be released from the inner shell with lower energy in the form of the X-ray emission, whose number and energy can be measured and determined by the EDX spectrum.[199,200]

The EDX setup consists of four main components, namely the excitation source (X-ray or electron beam), the X-ray detector, the pulse processor and the analysis meter. It normally combines with the SEM or TEM equipment, making the point acquisition, line scan or element mapping.[201] The point acquisition can be proceeded at a point corresponding to a SEM or TEM image, obtaining the elemental composition. For the line scan, it can be obtained by simply dragging a line on an electron micrograph, measuring the element distribution on this line, while the element mapping displays the element distribution of the whole micrograph. Herein, the EDX spectroscopy was carried out on an EDX detector (Oxford, Inca 300) in conjunction with SEM and an EDX detector (X-MAX 80 TLE, Oxford Instruments, Oxford, UK) connected with high resolution transmission electron microscope (HRTEM, Philips Tecnai F20). Typical EDX spectra obtained by point acquisition and line scan by SEM and element mapping by HRTEM are displayed in Fig. 3.10.
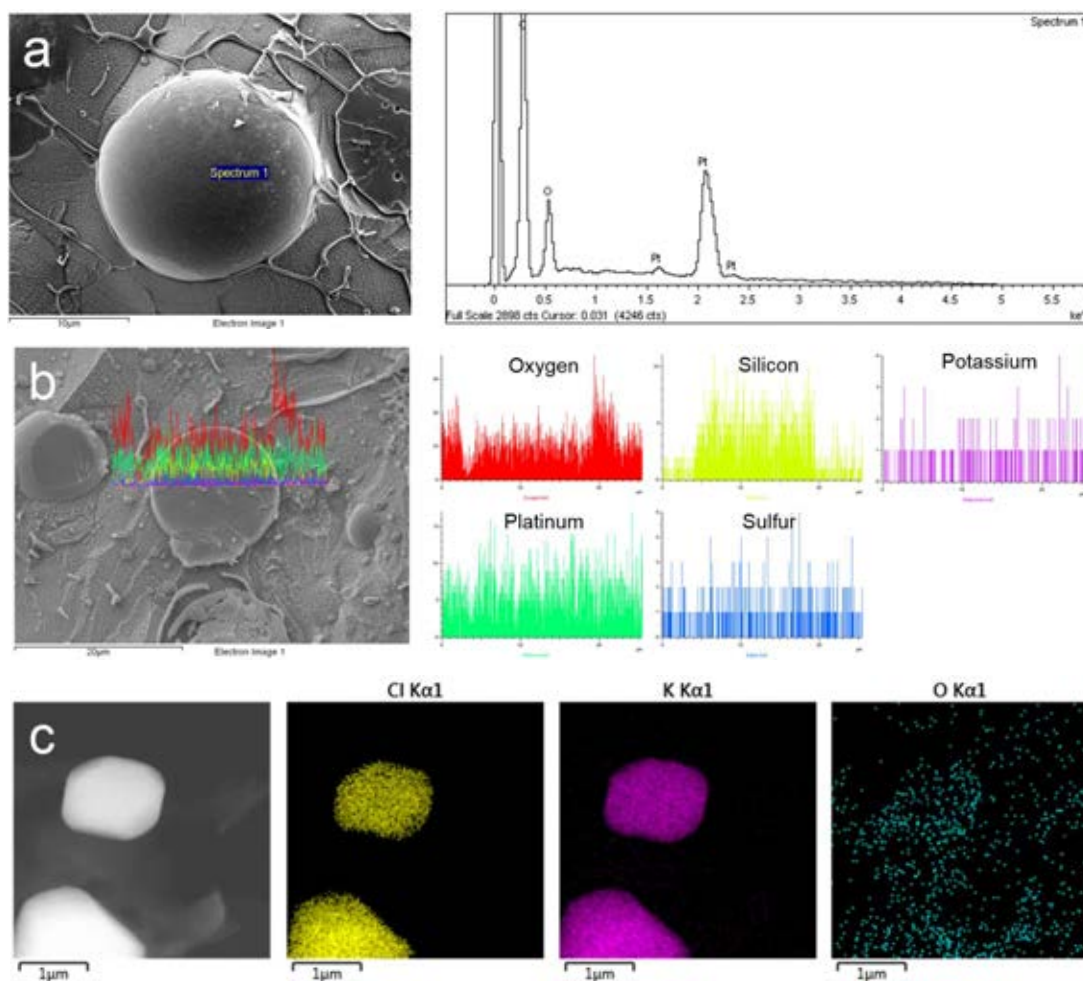
Fig. 3.10 A typical EDX spectra obtained by (a) point acquisition and (b) line scan of shellac microsphere and polystyrene sulfonate-silica microsphere, respectively by SEM, as well as (c) element mapping of potassium chloride microparticle.

3.4.5.3 X-ray photoelectron spectroscopy (XPS)

XPS referred as an old acronym Electron Spectroscopy for Chemical Analysis (ESCA) is the widely used in surface elemental analysis of the top 1-20 nm depth, providing quantitative and chemical state information of the surface of materials.[202-204] It uses the X-ray beam to irradiate the sample and collect the kinetic energy and number of electrons ejected from the sample simultaneously. This technique is applicable to all of the elements with atomic number ≥ 3 (lithium), namely except for hydrogen and helium. Plenty of materials including inorganic

materials[205], polymers[206] and hybrid materials[207] were analysed utilising XPS as surface characterisation method.

An X-ray photoelectron spectrometer consists of a radiation source, a sample stage, analyser and detector, which are all enclosed in a vacuum chamber as shown in Scheme 3.7. The light elements such as Al ($E_{K\alpha}$ = 1486.6 eV) or Mg ($E_{K\alpha}$ = 1256.6 eV) are usually selected as X-ray source to generate a narrow X-ray line. The resulting photoelectron spectrum received by the analyser and detector is normally expressed as frequency (counts/s) vs. binding energy. Herein, the XPS spectra were performed on an X-ray photoelectron spectrometer (ESCALab MKII) utilising Mg Kα radiation as an excitation source. A typical XPS spectrum is shown in Fig. 3.11.
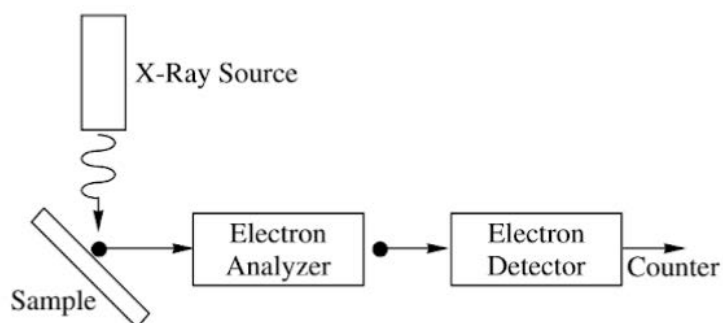
Scheme 3.10 Schematic demonstrating the mechanism of the X-ray photoelectron spectrometer.[208]
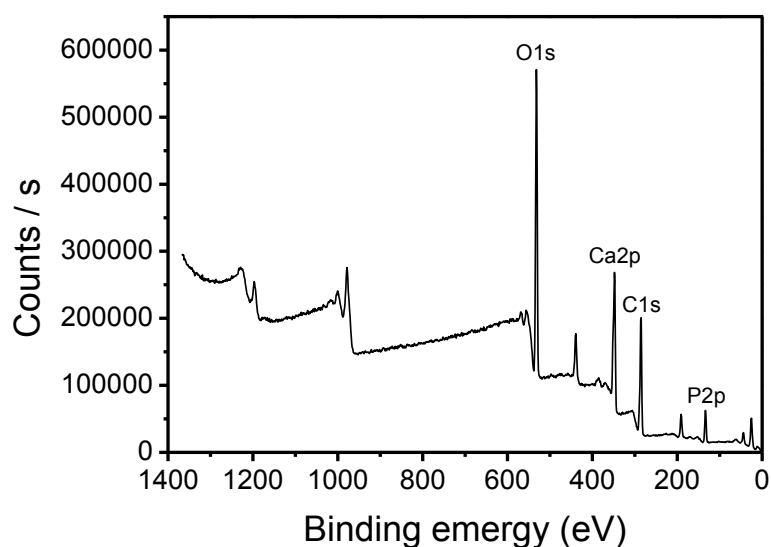
Fig. 3.11 A typical XPS spectrum of the prepared calcium phosphate microspheres.

3.4.6 Water contact angle measurements

Hydrophilicity and hydrophobicity are very important properties for the surface characterisations in many fields of research, e.g. the oil sorbents[209] and bionics[210]. The wettability of the surface of a solid material is dominated by two factors, namely the chemical composition and the topographical structure of the solid surface.[211,212] The wettability of the surface material is expressed as the water contact angle (θ) by Young's equation[213] (Scheme 3.8 & Equation 3.4).
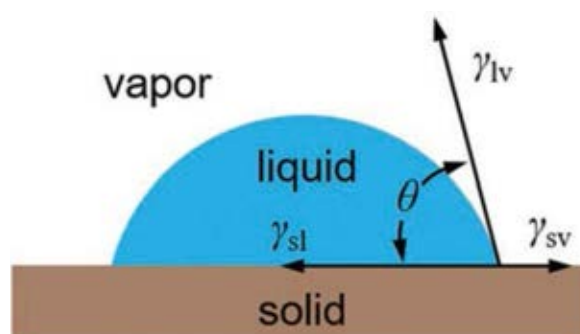
Scheme 3.11 Schematic illustration of the wettability of a water droplet resting on a solid surface expressed in the Young's model.[176]

68

$$\gamma_{sv} = \gamma_{sl} + \gamma_{lv} \cos\theta \qquad\qquad\qquad (Equation\ 3.4)$$

where γ_{sv}, γ_{sl}, and γ_{lv} represent the interfacial tensions of the solid-vapor, solid-liquid and liquid-vapor interfaces respectively, and θ is the contact angle.

Based on the work of Dupre and Girifalco-Good, the water contact angle can be expressed as Equation 3.5.[214] φ is a constant representing the characteristic of the system.

$$\cos\theta = 2\varphi\ (\gamma_{sv}/\gamma_{sl})^{1/2} - 1 \qquad\qquad\qquad (Equation\ 3.5)$$

When the water contact angle exhibits less than 90°, the material surface is determined to be hydrophilic, while for the one displaying more than 90° and more than 150° are assigned to be hydrophobic and superhydrophobic.[215]

In this project, the as-prepared sample powders were placed on a glass slide, slightly pressed by another slide, where a drop of water (3 μl) was placed gently on its surface. The water contact angle of each sample was measured by CAST 2.0 contact-angle-analysis system (Data-Physics, Germany).

3.4.7 Mechanical property (micromanipulation)

Micromanipulation was used to measure the rupture force of individual biological cells and artificial microcapsules.[163-167] Simply, a single microcapsule placed on a glass slide or in a chamber with liquid is compressed by a cylindrical probe glued onto the transducer (Aurora Scientific Inc., Canada) as displayed in Scheme 3.9a. The dry single microcapsule was observed by the side and bottom view cameras, and its size can be measured from its image on the monitor screen. The compression speed of the probe travelling down towards the microcapsule can be controlled. The electric signal generated by the force transducer and recorded by a data acquisition board in the computer indicates the force applied to the microcapsules by the transducer during the compression process. In this way, the mechanical

properties of the single capsule can be determined by the resulting force-displacement curve. The rupture force, displacement at rupture, nominal rupture stress, deformation at rupture and Young's modulus can be calculated from the obtained data. In addition, loading and unloading of compression at small deformations (such as 10 % of the particle size) to a single capsule is possible, obtaining the intrinsic material property of the capsule.[163]
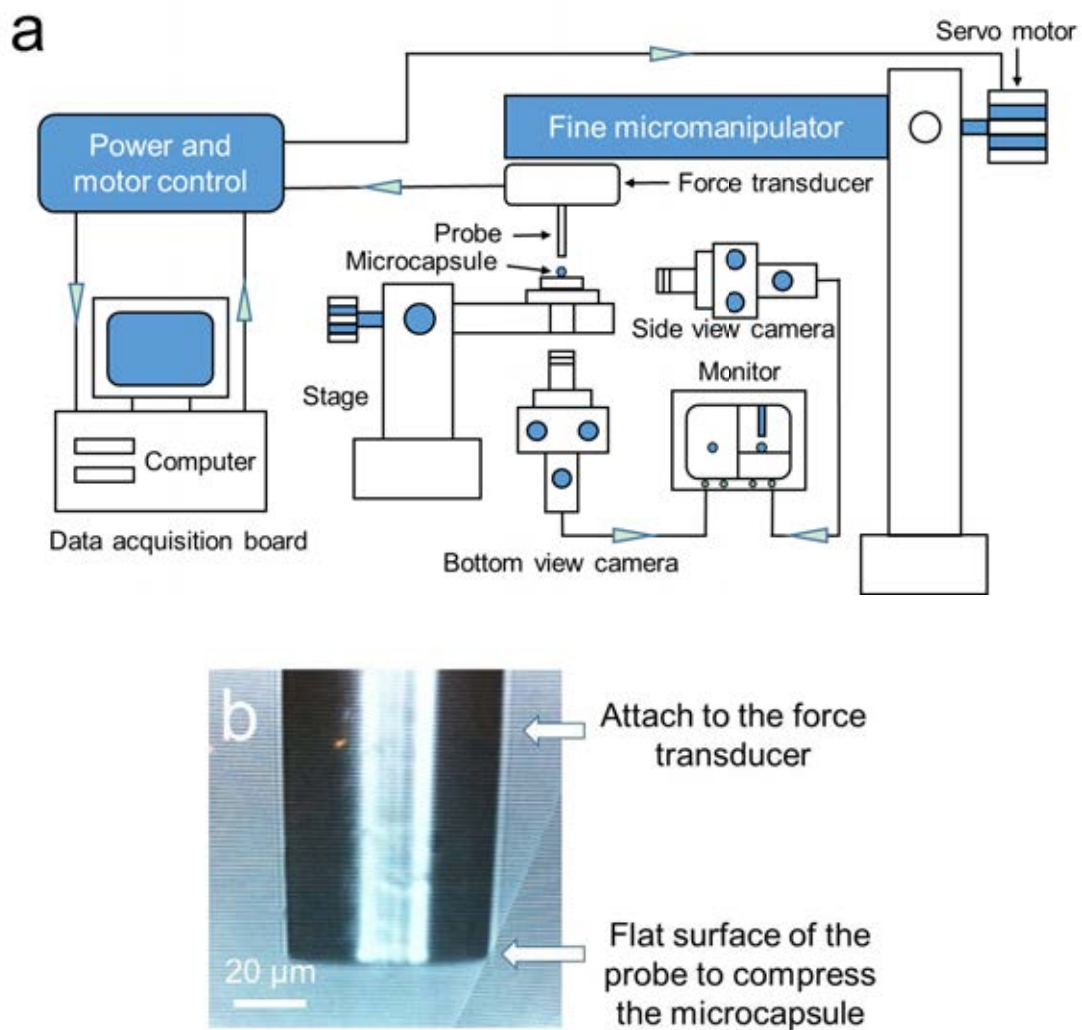
Scheme 3.12 (a) Schematic illustration of the micromanipulation rig and (b) the optical image of the glass probe attached to the transducer.

3.4.7.1 Probe preparation

A glass capillary (borosilicate, 1.0 mm O.D., 0.58 mm I. D.) fixed on a puller is heated to high temperature and the other end is then pulled to produce a tapered probe on a micropuller (Microforge, MF-900, Narishige, Japan). The obtained probe is further ground on an abrasive paper adhered to the surface of a grinding machine overnight (EG-40, Narishige, Japan). The flat-end probe is finally obtained and ready to be glued onto the force transducer (Scheme 2.8b). Generally, the diameter of the flat-end of the probe should be at least 1.5 times larger than the largest microcapsule, ensuring the microcapsules will not exceed the two parallel surfaces during the compression process.

3.4.7.2 Typical data obtained

The typical force-probe moving distance curve is plotted in Fig. 3.12. The probe moving distance between "0" and "a" corresponds to the stage of probe moving down before touching the microcapsule. During this stage, the detected force signal is calculated to be 0, while the force increased after a point, until the rupture point b. The force then drops down to c point, until the probe presses to the microcapsule debris on the glass slide (d point), afterwards the compression force increased rapidly.
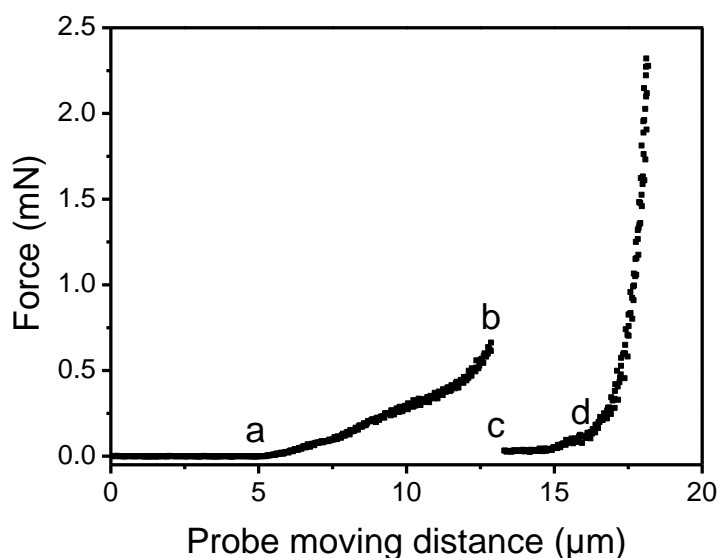
Fig. 3.12 The force-probe moving distance curve for compression of a single melamine formaldehyde microcapsule (diameter 19.4 μm).

3.4.8 Measurement of release profile

The release rates of the encapsulated active ingredients including K^+ and allura red were determined by flame photometry and UV spectrophotometry. They can measure the concentrations of the active ingredients in solutions and determine the release rates, payloads and encapsulation efficiencies of the active ingredients.

3.4.8.1 Flame photometry

Flame photometry, named flame atomic emission spectrometry is a widely used technique to measure the ion concentrations of some certain metallic elements. The principle of the technique is to quantify the flame intensity relying on the energy absorbed by atoms, which is detected by the monochromator, after the ion solution droplets are sprayed into the flame.[216] The droplets are dried into tiny solid salt particles, since the water evaporates rapidly under high temperature of the flame. The schematic process is displayed in Scheme 3.10.[169] The

photons can be generated and detected when the excited state atom transfers to the ground state atom under high temperature. The number of photons and the wavelength can be then measured, or the intensity of the light is detected by the operator instead.[169,216]
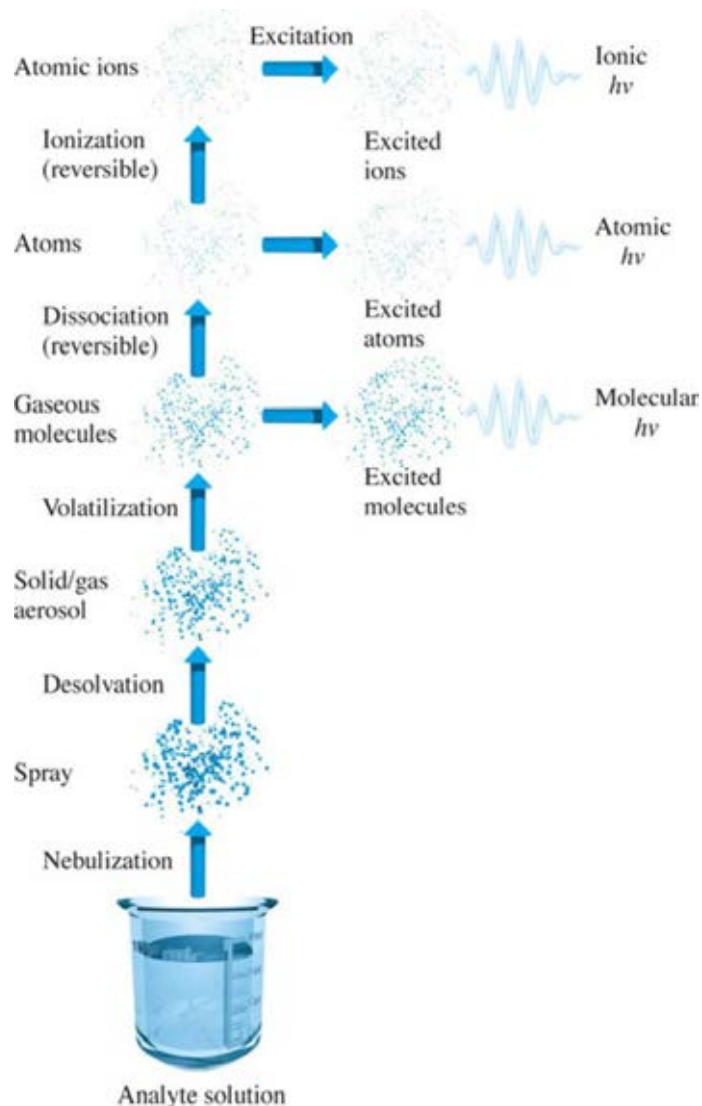
Scheme 3.13 Schematic illustration of the sample atomisation process in flame.[169]

Flame photometer equipment consist of four parts: burner, monochromators, detectors, recorder and display. The burner is used to generate the excited atoms, and the fuel and oxidants are necessary to create the flame, confirming excitation of the atoms as is shown in Scheme 3.11.[216]. Monochromators are used to separate the special wavelengths of the light from the

flame for the elements determinations. The emitted radiation being specific for each element is detected by the detector. Recorders and display are used to read out the recordings from the detector.
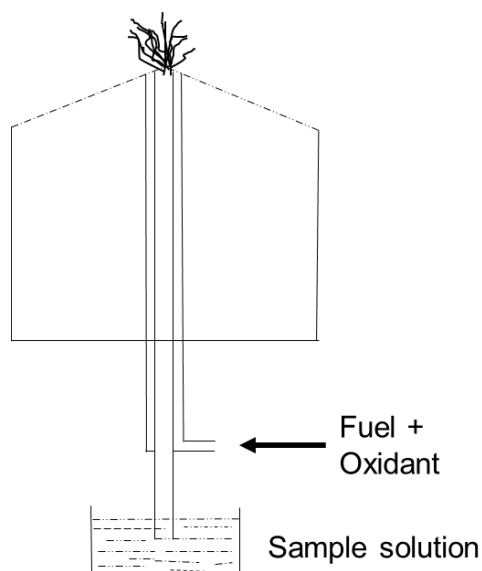
Scheme 3.11 Schematic illustration of the total consumption burner of the flame photometer instrument.

Herein, the releases of KCl and NaCl from the microspheres/microcapsules were performed in deionised water (100 ml) in a Gallenkamp orbital shaker with a 150 rpm rotation speed at 37 ºC. The released KCl and NaCl samples (5 ml) were obtained periodically at fixed time intervals between 5 min to 2 days, and replaced by fresh deionised water (5 ml). The concentration of K^+ and Na^+ ions were measured by the flame photometer (PFP-7, Jenway, UK).

A serial of standard concentrations of KCl solutions with a range of 0.1, 0.4, 0.6, 1, 2, 4, 6, 10 mg/L and DIW were prepared for the calibration of the equipment prior to the measurements of sample solutions. The standard solutions were pumped into the flame photometer and the intensity of each solution was recorded. A typical calibration curve was plotted with intensity *v.s.* their corresponding concentration (Fig. 3.13). The sample was then pumped into the flame

photometer and the intensity was tested. The concentration of the measured sample solution was finally calculated based on the standard calibration curve.
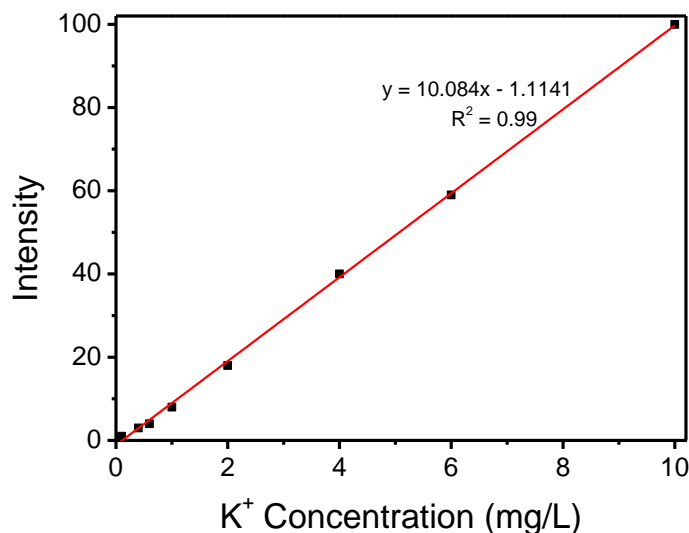
Fig. 3.13 A typical flame photometric standard calibration curve of the intensity-concentration profile for the K^+ ions solutions.

3.4.8.2 Ultraviolet-visible spectrophotometry

Molecular absorption spectroscopy in the ultraviolet or visible spectral region has been widely used for the determination of plenty of materials from spectra to quantitative measurements ranging from inorganic, organic, hybrid materials to biological species.[217] The UV spectroscopy is based on the interaction of light with atoms or molecules in the materials, resulting in a unique spectrum for a specific atom or molecule. The relationship among energy absorbed (ΔE), wavelength (λ), frequency (υ) and wave number ($\bar{\upsilon}$) of radiation can be described as Equation 3.5.[217]

$$\Delta E = h\upsilon = h\, c_l /\lambda = h\, \bar{\upsilon}\, c_l \qquad\qquad \text{(Equation 3.5)}$$

In the above equation, h is the Planck's constant, c_l represents the velocity of light and ΔE means energy absorbed in a molecule from ground state to excited state during the electronic transition process. The energy absorbed relies on the energy levels between ground state and excited state, which is inversely proportional to the wavelength of absorption. The position and intensity of the spectrum are the primary factors, and the band position is closely related to the wavelength of radiation. The energy of the radiation is equivalent to the requirements of the electronic transition between the low and high states of the electron.[217]

The principle of UV spectroscopy is based on the Beer-Lambert Law as displayed in Equation (3.6).

$$A = \varepsilon cl \hspace{5cm} \text{(Equation 3.6)}$$

A is the detected absorbance value from the UV-vis spectrophotometer; ε is the molar absorptivity; c refers to the concentration of the analyte and l is the path length of the cuvette in the Beer-Lambert equation. A beam of monochromatic light passes through a sample solution, and the decrease of the radiation intensity can be expressed as a function of the thickness of the absorbing solution, the concentration of the solution and the incident radiation. The function can thus be written as Equation (3.7):

$$A = \log (I_0/I) = \varepsilon cl \hspace{4cm} \text{(Equation 3.7)}$$

I_0 represents the intensity of the incident radiation; I refers to the intensity of the emergent radiation. In this way, the concentration of the analyte can be calculated by the detection of the light absorbance.

In this project, the releases of PSS and allura red molecules from the microspheres/microcapsules were performed in deionised water (100 ml) in a Gallenkamp orbital shaker with a 150 rpm rotation speed at 37 °C. The PSS and allura red samples (5 ml) were obtained periodically at fixed time intervals between 5 min to 2 days/10 days, and

replaced by fresh deionised water (5 ml). The PSS and allura red solutions were detected by a UV spectrophotometer (Cecil 2021 UV spectrophotometer) at 254 nm and 504 nm, respectively.

A serial of standard concentrations of PSS and allura red solutions were prepared for the calibration of the UV spectrophotometer prior to the measurements of sample solutions. The standard solutions were prepared in cuvettes and detected by the UV spectrophotometer. The absorbance of each solution was recorded corresponding to its concentrations. A typical calibration curve was plotted with absorbance *v.s.* their corresponding concentration as shown in Fig. 3.13. The sample was then contained in cuvettes and measured by the UV spectrophotometer. The concentration of the measured sample solution was finally calculated based on the standard calibration curve. PSS and allura red solutions were detected by a UV spectrophotometer (Cecil 2021 UV spectrophotometer) at 254 nm and 504 nm, respectively.

$y = 0.0488x + 0.0072$
$R^2 = 0.99$
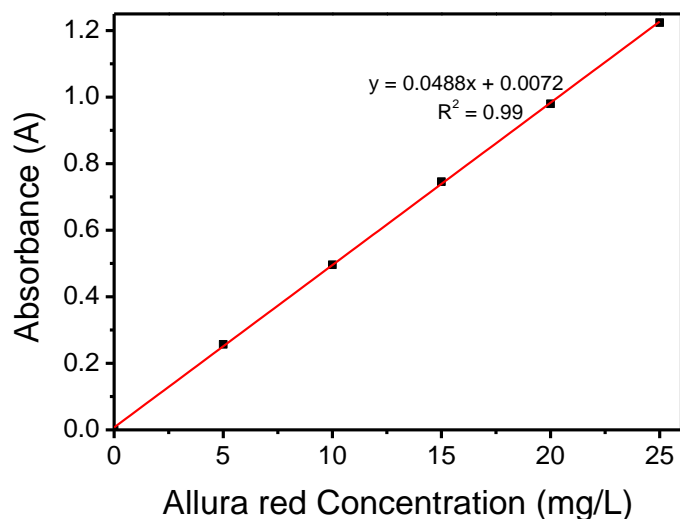
Fig. 3.14 A typical UV-Vis spectrophotometric standard calibration curve of allura red solutions at 504 nm.

3.4.9 Calculations of payload and encapsulation efficiency of active ingredients, including KCl, NaCl and allura red

Payloads and encapsulation efficiencies of K^+, Na^+ ions and allura red molecules were measured by a flame photometer (PFP-7, Jenway, UK) and a UV spectrophotometer at 504 nm (Cecil 2021 UV spectrophotometer), respectively. The prepared microspheres/microcapsules sample powder were ground using mortar and pestle to a fine powder, which were dissolved in aqua regia (HCl : HNO_3 = 3:1) overnight. The sample debris was separated via centrifugation, and the supernatant solution was diluted with DIW by a factor of 20. The concentrations of K^+ and Na^+ solution were detected by the flame photometer, while the one of allura red was measured by the UV spectrophotometer. The payloads and encapsulation efficiencies of KCl, NaCl and allura red were calculated using Equations (3.8) and (3.9), respectively as follows:

$$\text{Payload} = \frac{\text{Mass of active ingredients recovered from the obtained microspheres/microcapsules}}{\text{Mass of the obtained microspheres/microcapsules}}$$

(Equation 3.8)

$$\text{Encapsulation efficiency} = \frac{\text{Mass of active ingredients recovered from the obtained microspheres/microcapsules}}{\text{Mass of active ingredients input}}$$

(Equation 3.9)

Chapter 4 Novel Polystyrene Sulfonate-Silica Microspheres as a Carrier of a Water Soluble Inorganic Salt (KCl) for Its Sustained Release, via a Dual-Release Mechanism

Abstract: A novel type of organic-inorganic composite solid microsphere is developed here, comprised of polystyrene sulfonate and silica ($PSS-SiO_2$), which has been synthesised from polystyrene sulfonic acid and tetraethyl ortrhosilicate. The microsphere can (i) encapsulate a low molar mass (<100 Da) inorganic salt (KCl), and (ii) provide sustained release (>48 hours) of the salt to an aqueous dispersion of the microspheres, which has hitherto not been possible. The $PSS-SiO_2$ microspheres were prepared *via* two methods, including manually pipette dropwise and syringe pump dropwise (100 μl/min) additions of TEOS. In addition, a novel dual-release mechanism of the salt from the microspheres, which leads to the sustained release, is proposed and this delivery system may therefore have potential applicability for the controlled and prolonged release of other actives.

4.1 Introduction

Microencapsulation is an important technology providing a means to stabilise active ingredients, and/or control their release for a range of industrial sectors including printing, household care, beauty care, agrochemicals, and pharmaceuticals.[15,218,219] Various techniques have been developed, including interfacial polymerisation, *in situ* polymerisation, solvent evaporation and coacervation, to encapsulate different types of active ingredients, which can be oil-soluble, water-soluble, liquids or powders.[220-224] Encapsulation of water-soluble active ingredients is usually achieved by creating a water/oil emulsion followed by chemical reaction and physical self-assembly at the interface of the two liquids.[15,225] Water soluble molecules ranging from large biomolecules (such as proteins, polysaccharides, enzymes) to small molecules (such as doxorubicin, carbamide peroxide, polyphenols), and inorganic salts have

been encapsulated in microcapsules.[58,63,225-229] The significances of encapsulation of water soluble inorganic salt include not only applications in making functional food products and controlling phase change for energy storage, but also in oral care and increasing the osmotic pressure inside capsules to control the release of organic molecule.[230-233] However, soluble inorganic salt in microcapsules tends to release to aqueous environment quickly, e.g. all potassium chloride (KCl) encapsulated in ethylcellulose and Eudragit microspheres of 250 to 595 μm in diameter was released within 6 hours[234-236]. To the author's best knowledge, it has not been possible to achieve sustained release of inorganic salt longer than 6 hours in terms of microencapsulation.

Herein, a facile method to synthesise a novel type of microsphere from polystyrene sulphonic acid and tetraethyl orthosilicate (TEOS) was developed, which affords a polystyrene sulphonate-silica organic-inorganic composite (PSS-SiO$_2$) with encapsulated KCl, as a model of low molar mass water soluble inorganic salt, and the KCl release upon dispersion of the microspheres in water was studied. Silica was selected as the matrix materials due to its excellent biocompatibility, while the PSS as a negatively charged ion exchange resin was incorporated in the matrix for the interactions between positively charged ions and PSS resin, aiming to delay the release of the encapsulated ions. The characterisations and mechanisms of the fabrication of PSS-SiO$_2$ microspheres are presented in this chapter.

4.2   Experimental sections

4.2.1 Synthesis of PSS-SiO$_2$ microparticles with KCl/NaCl encapsulated

The synthesis of PSS-SiO$_2$ microparticles were carried out in a stirred vessel, whose details were described in Section 3.3.1. The one formed with less content of TEOS was named as PSS-0.7SiO$_2$ microsphere (Section 3.3.2).

4.2.2 Characterisations of the synthesised PSS-SiO₂ microparticles with KCl/NaCl encapsulated

The morphologies and cross-sections of the prepared microparticles were observed with an optical microscope (301-371.011, Leica, Germany) and SEM (Philips XL-30 FEG ESEM). Their size distribution, SPAN and the mean volumetric size (D_{43}) were measured by a laser light scattering technique (Mastersizer 2000, Malvern Instruments, UK). The phase of the sample was confirmed by a Bruker D8-Advance X-ray powder diffractometer using Cu Kα radiation ($\lambda = 1.5406$ Å), and the FT-IR spectra was performed on a Thermo Electron Nicolet 8700 spectrometer. The composition was recorded on a thermogravimetric analysis (STA 449 F3, NETZSCH). The chemical composition of the sample was evaluated by an energy disperse X-ray microanalysis (EDX) (Oxford, Inca 300) in conjunction with SEM.

4.3 Results and discussions

4.3.1 Pipette dropwise addition of TEOS
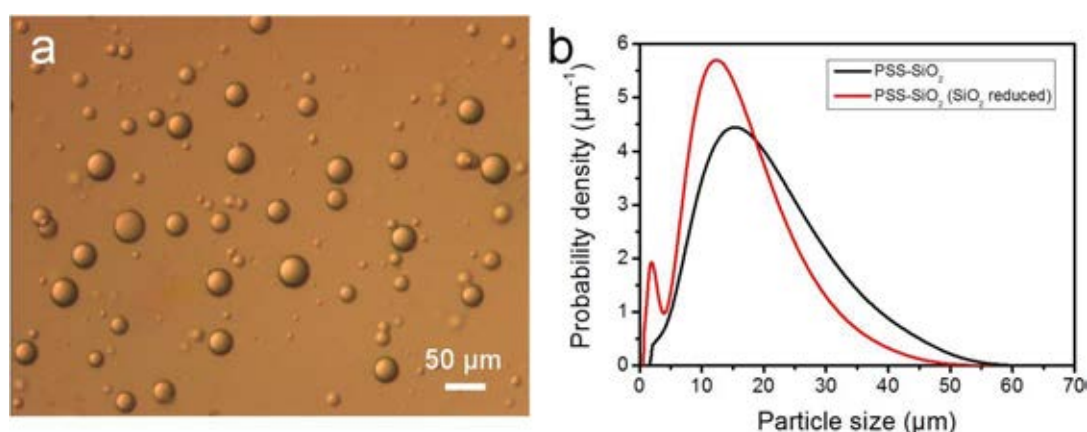
Fig. 4.1 (a) Optical micrograph of the obtained PSS-SiO₂ microparticles, and (b) size distribution of the prepared PSS-SiO₂ microparticles and PSS-SiO₂ microparticles with a reduced amount of SiO₂.

The synthesized PSS-SiO$_2$ microparticles showed spherical shapes, and the size distributions of the two as-prepared samples with different amounts of SiO$_2$ demonstrate that they were on the microscale, less than 100 μm in diameter as shown in Fig. 4.1. The SPAN values were 1.34 and 1.38 for PSS-SiO$_2$ and PSS-SiO$_2$ (SiO$_2$ reduced to 70 % content), respectively, whilst the volume weighted mean (D_{43}) diameter were 22.2 μm and 17.6 μm, which indicates that the less amount of SiO$_2$ led to the slightly decreased size of the microparticles. This might be due to the excessive amount of SiO$_2$ produced in the former case, which accumulated on the surface of the emulsion droplets. A cryo-SEM image in Fig. 4.2a displays the rough surface of the obtained PSS-SiO$_2$ microparticles and Fig. 4.2b shows the cross-section of the formed microparticles. It seems that the core of PSS-SiO$_2$ microparticle was solid.
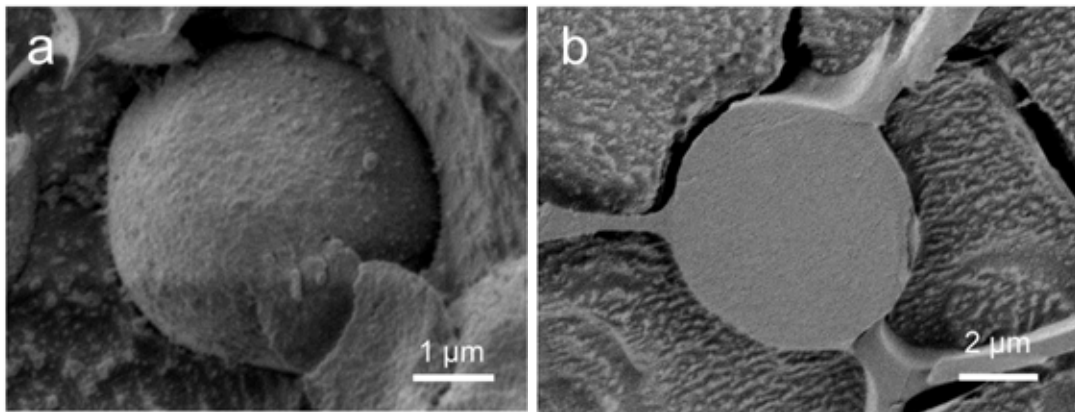
Fig. 4.2 Cryo-SEM images of (a) the formed PSS-SiO$_2$ microparticles and (b) the cross-sections of PSS-SiO$_2$ microparticles.
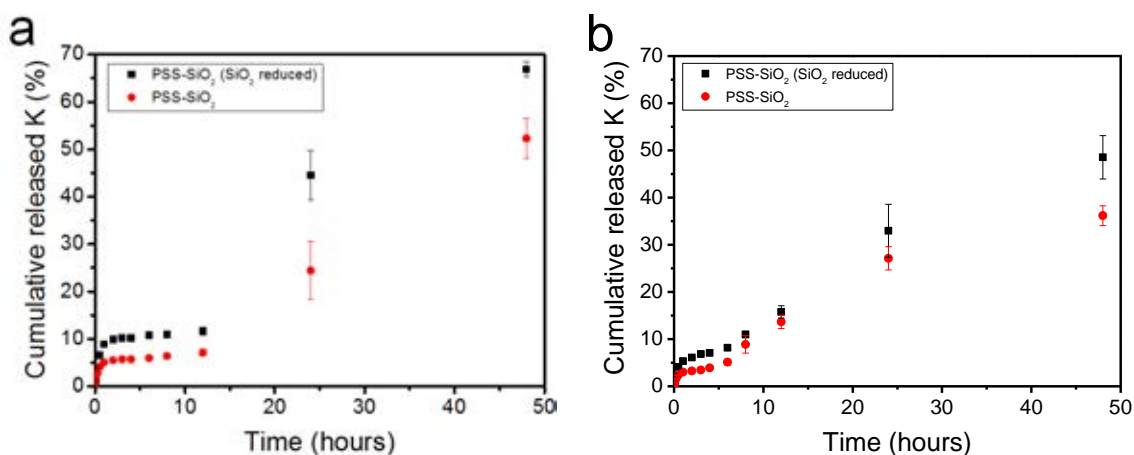
Fig. 4.3 In vitro release profiles of K^+ from PSS-SiO$_2$ microparticles with different amounts of SiO$_2$ in aqueous environment at 37 ^{o}C by (a) shaking (shaking speed 150 rpm) and (b) unshaking. (Each experiment was conducted at least 3 times and the error bars represent the standard error of the mean)

The encapsulation efficiency of KCl in PSS-SiO$_2$ microparticles was calculated using Equation 3.9 in Chapter 3, and it reached 98 % and 97 % (+/- 1%) for PSS-SiO$_2$ and PSS-SiO$_2$ (SiO$_2$ reduced), respectively, which was significantly higher for encapsulation of the small water soluble ions than the other methods[234,235]. The high encapsulation efficiency was attributed to the advantages of the method developed, namely, low solubility of polymer (PSS) in oil, high concentration of polymer in water, low solubility of the active ingredient (KCl) in oil phase and the ion exchange between the polymer (PSS) and ingredient (KCl).[221] Low solubility of PSS in the oil and highly concentrated PSS solution prevented the active ingredient from diffusion into the continuous phase, which probably resulted in fast solidification of microparticles. Moreover, low solubility of KCl in the oil phase and the ion exchange, limited the K^+ ions release from the microspheres during encapsulation, which was another reason to achieve high encapsulation efficiency.[221]

The obtained microparticles revealed a sustainable release of KCl up to 2 days, which was much longer than the one (approximately 360 min) for ethylcellulose microspheres, Eudragit microspheres with several hundred micron in diameter and saturated polyglycolyed glycerides matrices based on previous researches[234-236]. The significantly prolonged release time of K^+ was due to the interaction between the oppositely charged polymers and K^+ ions. In addition, the release rates of K^+ could be controlled by changing the structure of the microparticles. As is shown in Fig. 4.3, the microparticles formed with a reduced amount of SiO_2 showed a higher release rate than the original one, which was mainly due to the decreased compactness of the obtained microparticles since the reduction in size from 22.2 µm to 17.6 µm leading to an increase in the specific area by 26% cannot fully account for the increase in the release rate. Both the samples exhibited a burst release of K^+ (Fig 4.3a and 4.3b), which might result from that the K^+ ions attached on the surface of the microparticles. Interestingly, the release rates of the two samples slowed down when the time prolonged to 2 h, whilst they jumped to 21% and 42% respectively when the samples released in water for 24 hours. The released K^+ amount kept increasing to 52% and 67% after shaking for 48 hours in water. The sharp increase of the release rates and the comparatively large standard error bars after 24 hours were attributed to the cracks and break-ups of the microparticles, which are shown in Fig. 4.4c, 4.4d. In comparison, the release of K^+ showed a comparatively lower rate under the unshaken condition (Fig. 4.3b). The optical micrographs shown in Fig. 4.4a, 4.4b demonstrate that the PSS-SiO_2 microparticles remained intact after being in water unshaken for 2 days. In this way, the release rate of K^+ was accelerated slightly by shaking.
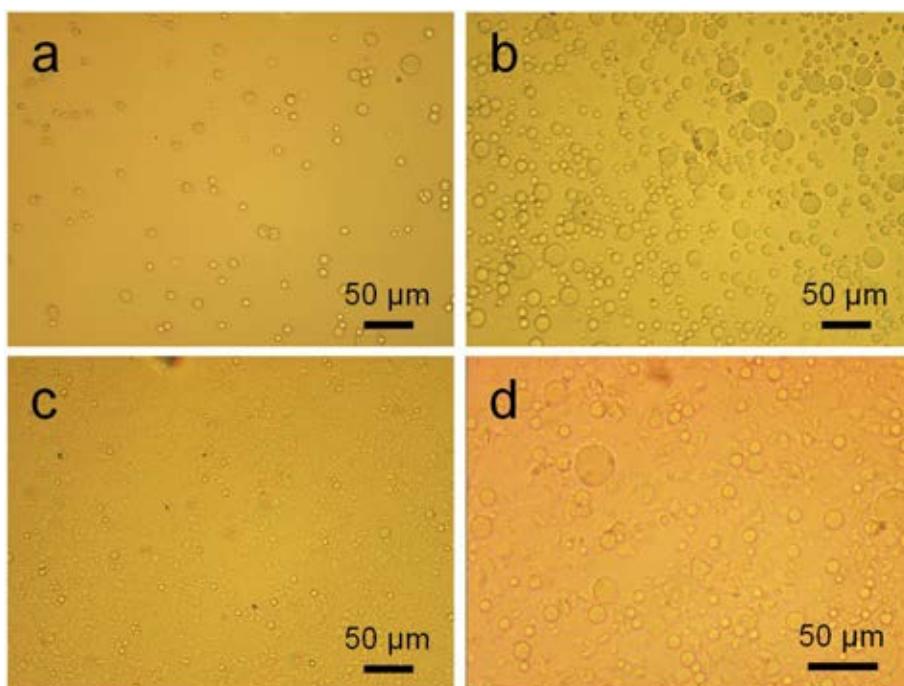
Fig. 4.4 Optical micrographs of PSS-SiO$_2$ microparticles treated in water unshaken for (a) 0 second, (b) 2 days, and shaken for (c) 1 day and (d) 2 days, respectively.
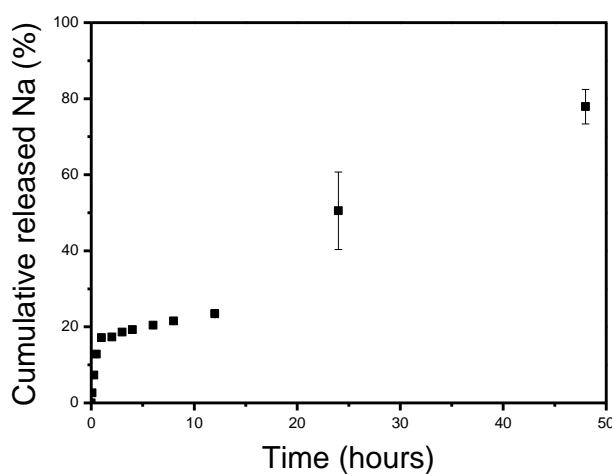
Fig. 4.5 In vitro release profile of Na$^+$ from PSS-SiO$_2$ microparticles in aqueous environment at 37 $^{\circ}$C by shaking (shaking speed 150 rpm). (The data was generated from at least triplicate experiments)

The system developed here was suitable for K$^+$ to achieve a sustained release, and it might also be adapted to other kinds of positively charged ions. Here, Na$^+$ was selected as an example of such ions and the encapsulation efficiency achieved 97% (+/- 1%) calculated by Equation 3.9

in Chapter 3. As is shown in Fig. 4.5, the PSS-SiO$_2$ microparticles demonstrate a sustained release of Na$^+$ for 2 days, and it reveals a higher release rate than the one for KCl. This might be due to the smaller radius of Na$^+$ compared with K$^+$, which led to the lower interaction force between PSS and Na$^+$.[237]

4.3.2 Syringe pump dropwise addition of TEOS
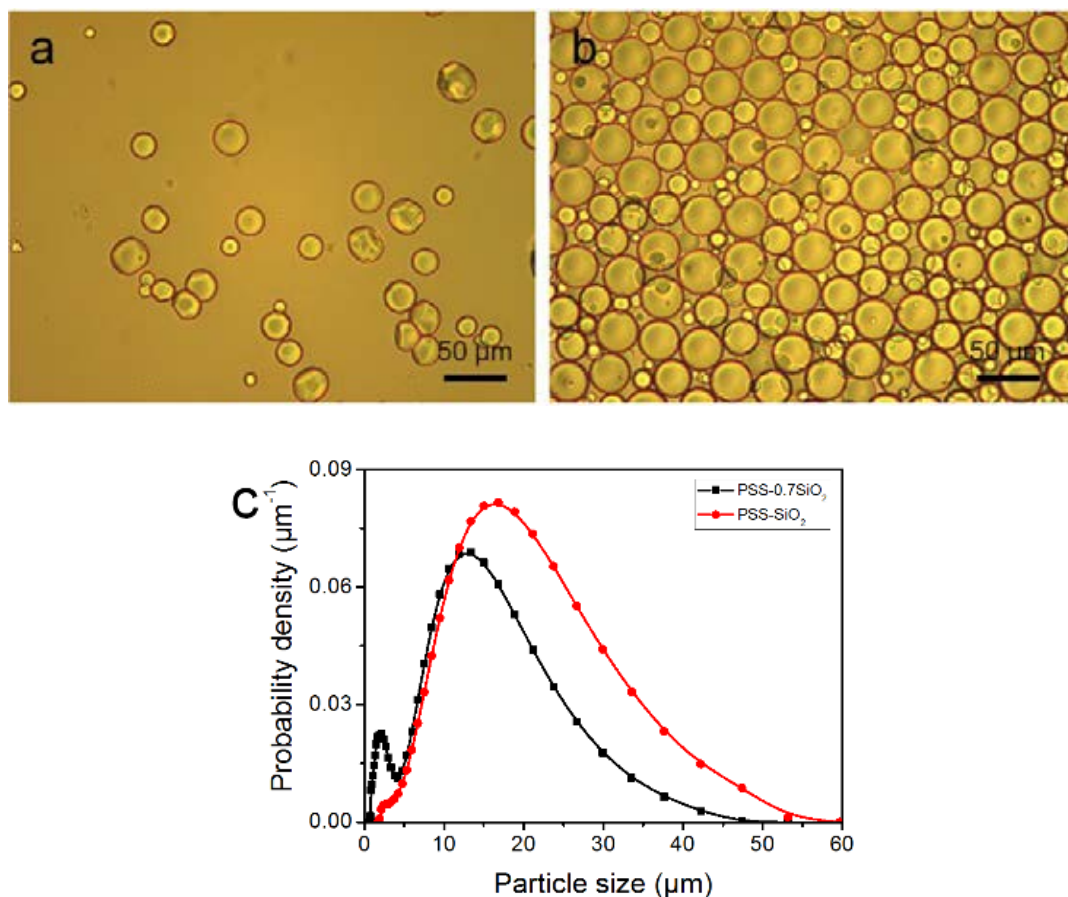
Fig. 4.6 Optical micrographs of the (a) PSS-0.7SiO$_2$ and (b) PSS-SiO$_2$ microparticles. (c) The size distributions (DLS) of PSS-0.7SiO$_2$ and PSS-SiO$_2$ microparticles.

The PSS-SiO$_2$ microparticles were synthesized in the emulsion droplets, formed from an aqueous phase (3 mL) containing polystyrene sulfonic acid (0.6 g) and KCl (100 mg) and an oil phase (100 ml) (3: 100 v/v) containing polyglycerol polyriconoleate (0.8 g), to which TEOS (0.7 mL or 1 mL) was added dropwise (4 hours). Thus, two samples of PSS-SiO$_2$ microparticles were synthesized, PSS-0.7SiO$_2$ and PSS-SiO$_2$, respectively. The optical micrographs and size

distributions of both particles types are shown in Fig. 4.6a & 4.6b and Fig. 4.6c, respectively. The PSS-0.7SiO$_2$ microparticles revealed a non-spherical shape (Fig. 6a), whilst PSS-SiO$_2$ were essentially spherical (Fig. 4.6b). The size distributions illustrate that the volume weighted mean diameter (D_{32}) were 11.41 $\pm$ 0.03 µm (SPAN 1.35 $\pm$ 0.02) and 17.15 $\pm$ 0.04 µm (SPAN 1.284 $\pm$ 0.001) for PSS-0.7SiO$_2$ and PSS-SiO$_2$, respectively. The microparticle size distributions look wide, which was attributed to the fed-batch (aqueous phase in oil emulsification followed by dropwise addition of TEOS) process to prepare them, and was typical for similar processes.[238] Clearly, the amount of the tetraethyl orthosilicate in the synthesis influenced the morphology and size of the resulting particles. The SEM characterizations (Fig. 4.7) suggest that these morphological and size differences may be due to the insufficient amount of silica accumulated into the emulsion droplets for PSS-0.7SiO$_2$.
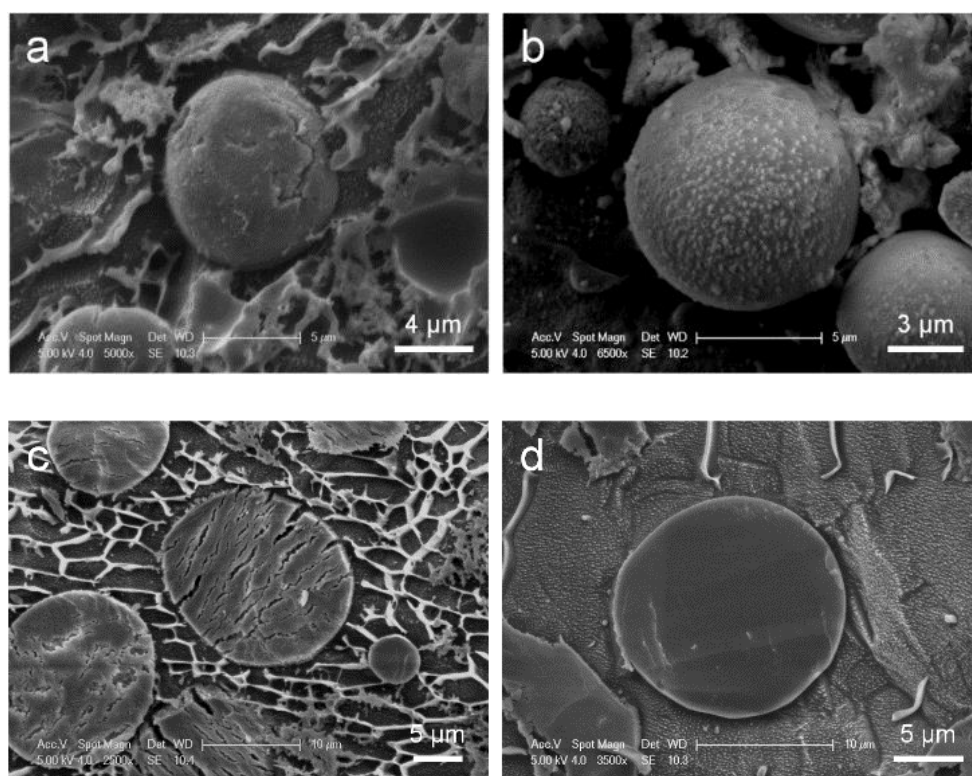
Fig. 4.7 Cryo-SEM images of the intact (a) PSS-0.7SiO$_2$, and (b) PSS-SiO$_2$ microspheres, and the cross-section (freeze-fracture) (c) PSS-0.7SiO$_2$, and (d) PSS-SiO$_2$ microspheres.

The PSS-0.7SiO$_2$ microspheres revealed a fractured surface (Fig. 4.7a), whilst PSS-SiO$_2$ microspheres were relatively smooth and more spherical (Fig. 4.7b). The cross-section of the PSS-0.7SiO$_2$ microspheres revealed the fracturing was not limited to the surface (Fig. 4.7c); in contrast, the PSS-SiO$_2$ microspheres were solid throughout (Fig. 4.7d). Clearly, the concentration of initial silicon monomer (TEOS) affected the size, shape and morphology of the particles.
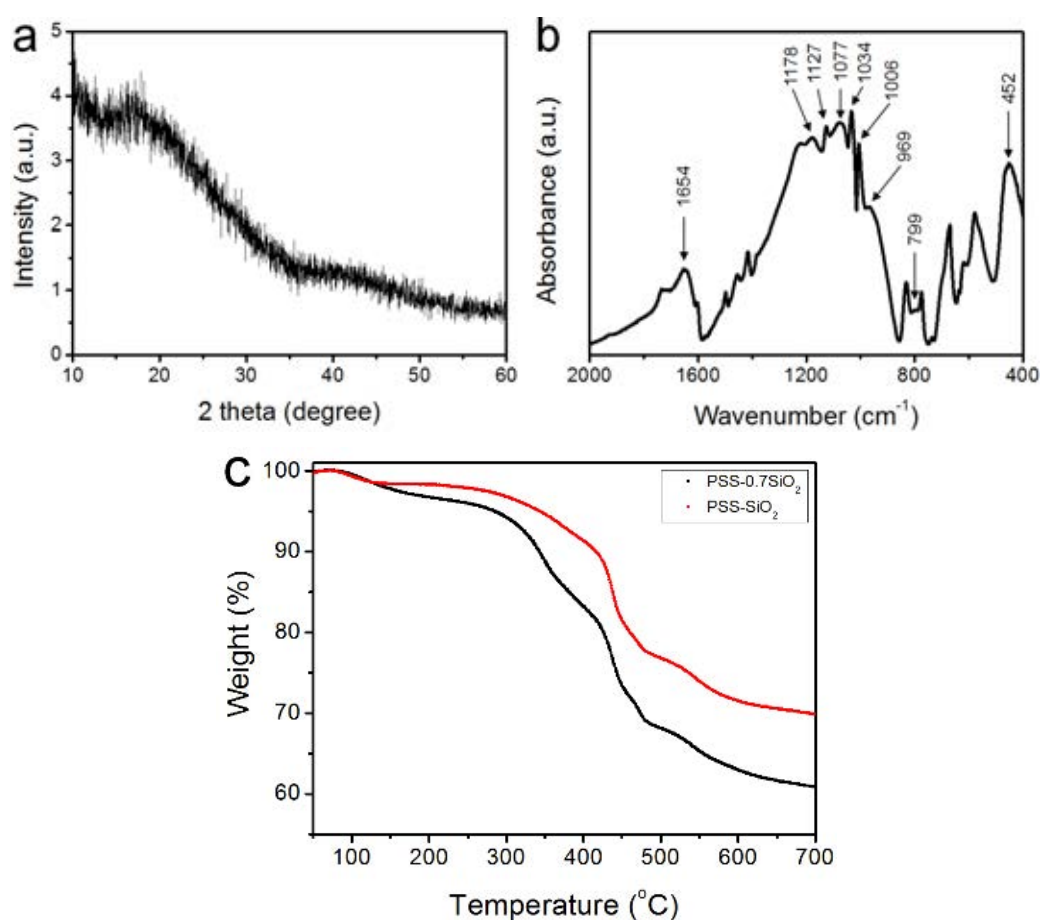
Fig. 4.8 (a) X-ray diffraction (XRD) pattern and (b) FT-IR spectra of PSS-SiO$_2$ microspheres. (c) Thermogravimetric analysis (TGA) curves of the PSS-0.7SiO$_2$ and PSS-SiO$_2$ microparticles.

The phase of the PSS-SiO$_2$ microspheres was confirmed by XRD, which indicates an amorphous SiO$_2$ phase through the absence of diffraction peaks (Fig. 4.8a).[239] The Fourier-transform infrared (FT-IR) spectra of PSS-SiO$_2$ microspheres are shown in Fig. 4.8b. The absorption peaks at around 1077, 799 and 452 cm^{-1} were attributed to the antisymmetric stretching, symmetric stretching and bending vibrations of Si-O-Si bonds, and the peak at around 940-960 cm^{-1} corresponded to Si-OH stretching vibrations, respectively.[240-243] The absorbance values at 1178 (1184), 1127 (1130), 1034 (1042) and 1006 (1011) cm^{-1} were assigned to the spectrum of PSS component in the PSS-SiO$_2$ composite (the values in brackets are neat PSS[244]). The shift to lower wavenumber compared to the spectrum of the neat PSS is presumably due to the conformationally more restrictive composite matrix and/or the sulphonic acid groups having undergone ion exchange with K$^+$.[245,246]

Fig. 4.8c presents the TGA thermograms of PSS-0.7SiO$_2$ and PSS-SiO$_2$, both revealing multistep weight loss. The first weight loss at ~100 $^{\circ}$C was attributed to the loss of 'weakly' bound water, and the second loss (100-200 $^{\circ}$C) was due to water which hydrates the $-$SO$_3^-$K$^+$ groups.[247] The third loss starting at ~320 $^{\circ}$C was assigned to the degradation of sulfonate moiety in the PSS,[247] followed by the final decomposition of the 'polystyrene' from 420 to 490 $^{\circ}$C.[247] It can be concluded from the thermograms that PSS-0.7SiO$_2$ microspheres contained a higher amount of water and PSS. The residual mass of the two samples were 61% and 70% for PSS-0.7SiO$_2$ and PSS-SiO$_2$, respectively, which confirms that the silica content was higher for the PSS-SiO$_2$ microspheres, suggesting that this is the reason for the greater structural integrity of the PSS-SiO$_2$ microspheres, relative to PSS-0.7SiO$_2$ microspheres (Fig. 4.7).
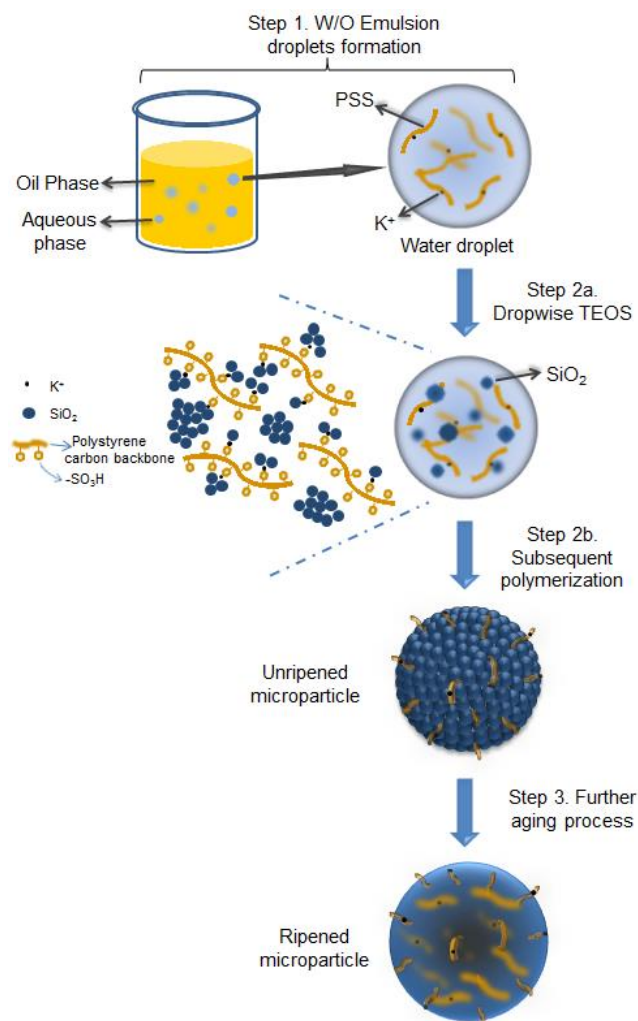
Scheme 4.1 Illustration of PSS-SiO$_2$ microspheres synthesis with KCl encapsulated via acid catalysed reaction.

The proposed formation mechanism of the PSS-SiO$_2$ microspheres is shown in Scheme 4.1. Initial ion exchange of the sulfonic acid protons for K$^+$ occurred during the water in oil emulsification step (Step 1, Scheme 4.1).[237,248] To this emulsion TEOS was added dropwise, leading to its hydrolysis (Step 2a, Scheme 4.1) and subsequent polymerization (Step 2b, Scheme 4.1) forming initially discrete SiO$_2$ particles intercalated into the PSS-K complex by ionic bonds in the aqueous microsphere,[249] which might be similar to the process of forming PSS-silica hybrids utilizing the ionic interactions between the amino groups and silica.[250] The SiO$_2$ particles ripened and grew (Step 3, Scheme 4.1) within the aqueous microsphere trapping the PSS/K$^+$ and free KCl. The reduced TEOS monomer synthesis affording PSS-0.7SiO$_2$

microspheres, which revealed defects within the structure (Fig. 4.7a & 4.7c), presumably could not ripen fully, and hence afforded the fractured SiO_2 texture.

The energy dispersive X-ray (EDX) analysis of a PSS-0.7SiO_2 microsphere revealed the elemental composition of both the surface (Fig. 4.9a) and inner core (Fig. 4.9b) contained Si, C, and S in similar ratios, which supports the proposed inclusion of PSS in the formation process. There was no evidence of K^+ in the EDX analysis, presumably because the concentration of K^+ (less than 0.3 mmol/L) was lower than the limit of detection (1.2 mmol/L) in the EDX experiment.[251] However, K^+ was observed in the release studies described below.
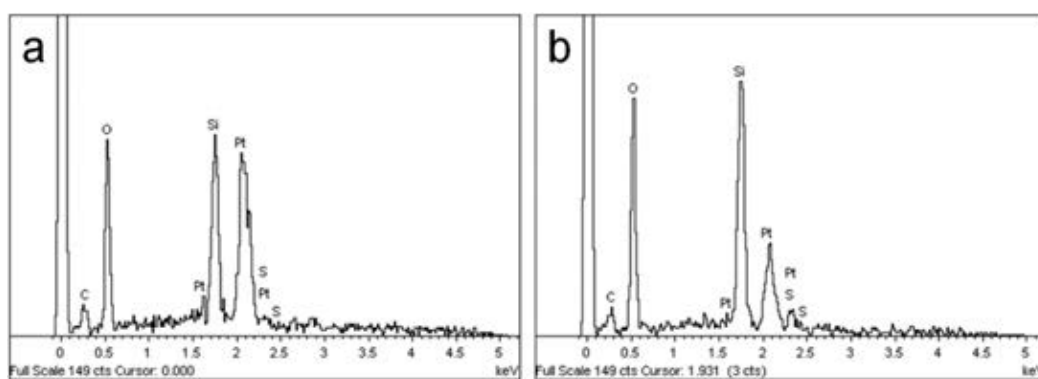
Fig. 4.9 EDX analysis of (a) the microsphere surface and (b) the inner core of PSS-0.7SiO_2 microspheres.

The microspheres were dispersed in water and the release of both K^+ and PSS from the microspheres was monitored, via removal of aliquots at extended time intervals over 48 hours, and analysis with flame photometry (K^+) and UV/Vis spectroscopy (PSS). Interestingly, not only did PSS-0.7SiO_2 release more K^+ (Fig. 4.10a) and PSS (Fig. 4.10b) than PSS-SiO_2, but also had a prolonged release of K^+ (Fig. 4.10a): >48 hours relative to 1 hour for PSS-SiO_2. For PSS-0.7SiO_2 microspheres the K^+ was initially released rapidly over 1 hour in a similar fashion to PSS-SiO_2 (Step 1, Scheme 4.2). This initial stage of K^+ release was coincident with the PSS release, suggesting the anion exchanged (H^+ for K^+) PSS was the initial source of K^+ (Step 1,

Scheme 4.2). However, unlike PSS-SiO$_2$ that showed a continuous plateau up to 48 hours with cumulative K$^+$ release <20 %, the PSS-0.7SiO$_2$ initial plateau was somewhere between 12 and 24 hours, during which a second release of K$^+$ began over the timeframe up to and exceeding 48 hours (plateau not reached at 48 hours) with ~75% of the K$^+$ released, and no additional release of PSS. Given for both PSS-0.7SiO$_2$ and PSS-SiO$_2$ all the PSS release was finished with 1 hour (Fig. 4.10b), the second stage of K$^+$ release must be from the microspheres. Presumably the higher content of SiO$_2$ in PSS-SiO$_2$ and the consequent defect free structure (Fig. 4.7b and 4.7d) prevented K$^+$ (and PSS) release from these microspheres, whilst the more open 'fractured' PSS-0.7SiO$_2$ microsphere structure (Fig. 4.7a and 4.7c) allowed the K$^+$ to be released directly from these microspheres on a longer timescale than the first release (Step 2, Scheme 4.2).
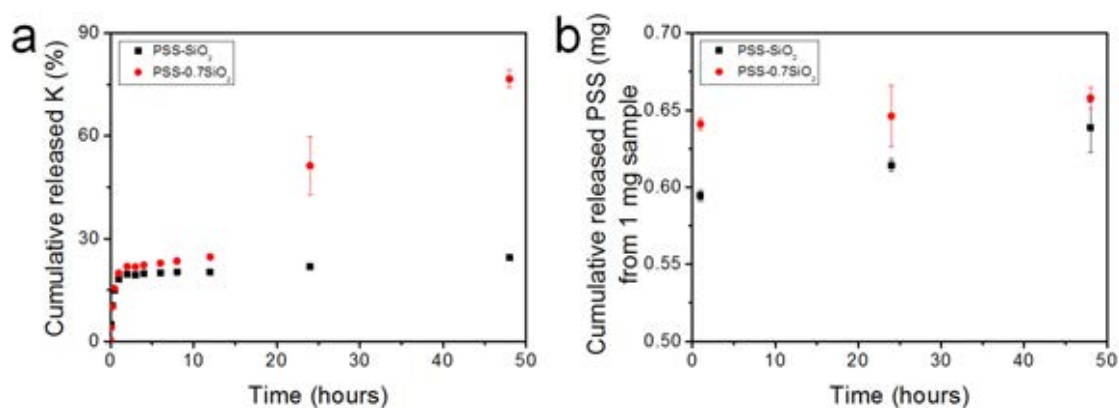
Fig. 4.10 Release profiles of (a) K$^+$ and (b) PSS from PSS-0.7SiO$_2$ and PSS-SiO$_2$ microspheres dispersed in water at 37 ^{o}C with shaking at a speed of 150 rpm. (Each experiment was conducted at least 3 times and the error bars represent the standard error of the mean)
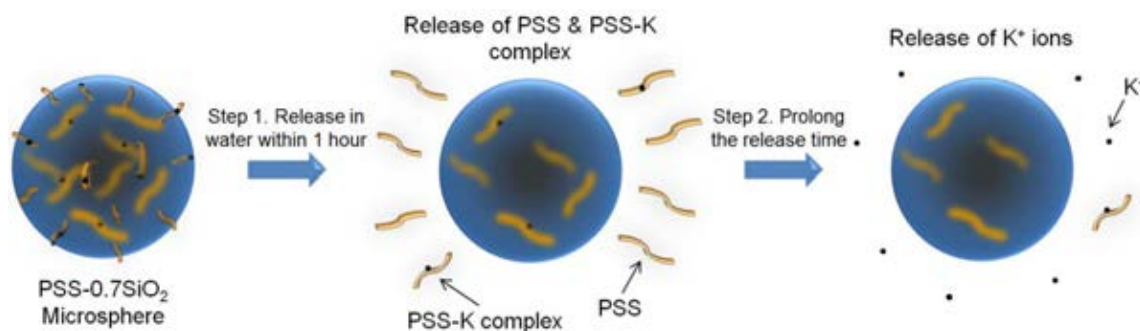
Scheme 4.2 Schematic of the PSS-0.7SiO$_2$ microspheres dual-release process in an aqueous environment.

The payload of KCl in the microspheres was calculated using Equation 3.8 in Chapter 3 and it reached $10.8 \pm 1\%$ and $9.5 \pm 1\%$, and the encapsulation efficiency reached $93 \pm 1\%$ and $95 \pm 1\%$ for PSS-0.7SiO$_2$ and PSS-SiO$_2$, respectively, based on Equation 3.9 in Chapter. The reasons leading to the high encapsulation efficiencies were discussed in Section 4.2.1 in Chapter 4.

4.4   Mechanical properties

The mechanical properties of the PSS-SiO$_2$ microspheres fabricated by the pipette and syringe pump dropwise additions of TEOS may be related to the release profiles of encapsulated ingredients in water. The mechanical properties of the two batches of PSS-SiO$_2$ microspheres were determined by the micromanipulation technique developed by Zhang et al.[252] A single PSS-SiO$_2$ microsphere was compressed by two parallel flat surfaces (Fig. 4.11a, 4.11b), and a force versus displacement curve for compression of the single PSS-SiO$_2$ microsphere was obtained as shown in Fig. 4.11c. 30 PSS-SiO$_2$ microspheres were selected to be measured by the micromanipulation technique for the two batch samples. The mechanical properties containing the nominal rupture stress vs. diameter, displacement at rupture vs. diameter and rupture force vs. diameter were calculated for the two batch PSS-SiO$_2$ microsphere samples as

93

shown in Fig. 4.12, which demonstrates that the microspheres synthesised by the syringe pump dropwise addition of TEOS exhibits higher nominal rupture stress, displacement at rupture and rupture force for a give diameter compared with the ones formed by pipette dropwise addition, which indicates the microspheres generated by the former method were stronger. The nominal rupture stress of PSS-SiO$_2$ microspheres (syringe pump dropwise) shows similar rupture stress range (mostly <60 MPa) with the other microspheres.[113] The microspheres fabricated by the pipette dropwise addition of TEOS did not survive after 1 day shaken (150 rpm) as shown in Fig. 4.4c & 4.4d, which are well interpreted by the mechanical data in Fig. 4.12. In this way, the PSS-SiO$_2$ microspheres fabricated *via* the syringe pump dropwise addition of TEOS displays better mechanical stability and lower release rates of encapsulated active ingredients than the ones formed *via* the pipette dropwise addition as summarised in Fig. 4.13.
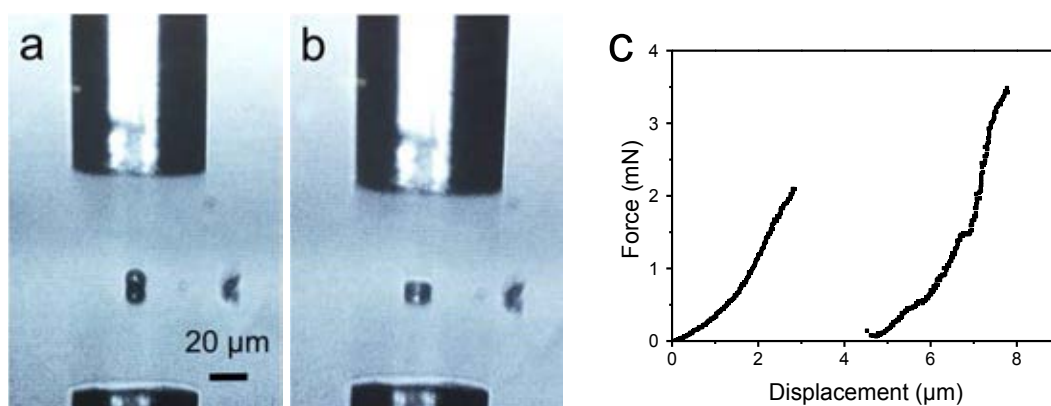
Fig. 4.11 Optical images obtained from the screen (a) before and (b) after compressing a single PSS-SiO$_2$ microsphere to rupture. (c) Typical force vs. displacement curve for compressing a single PSS-SiO$_2$ microsphere (diameter 10.8 μm) to rupture. The compression speed was 2 μm/s.
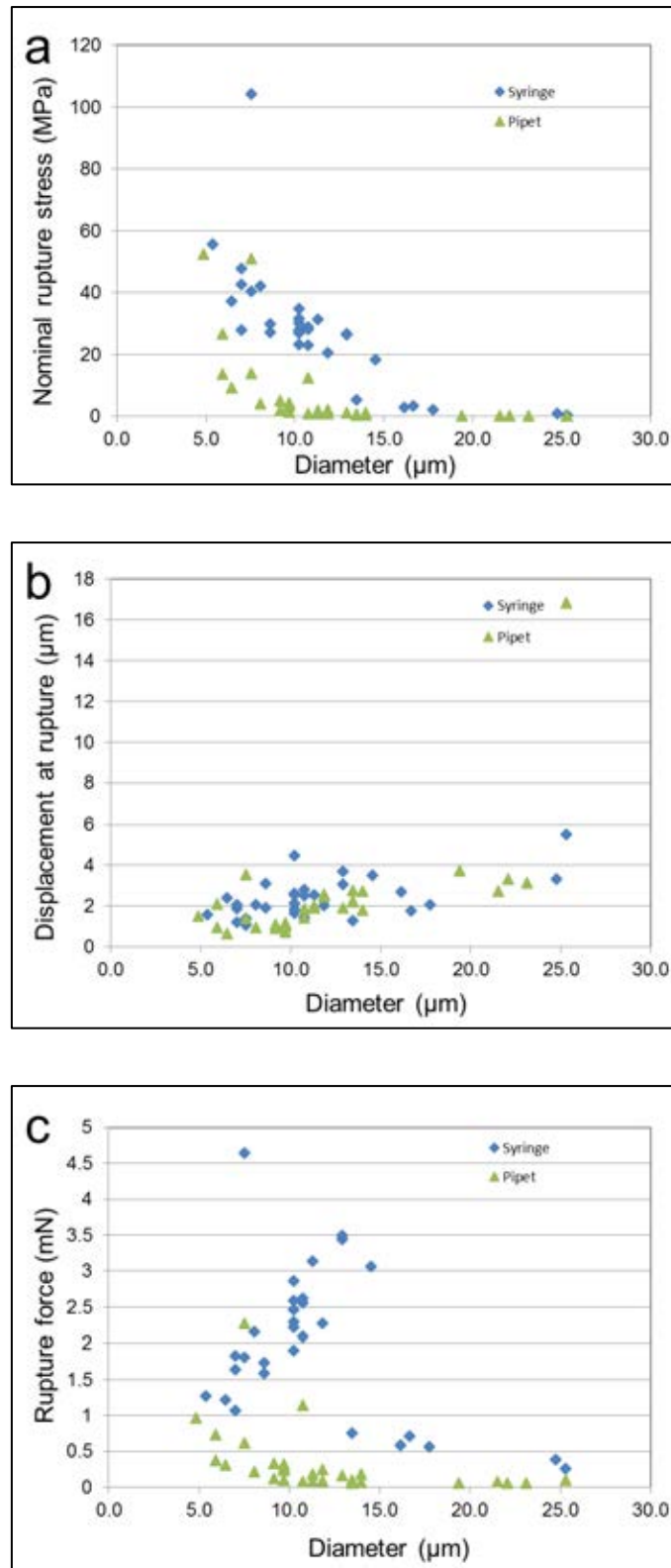
Fig. 4.12 (a) Nominal rupture stress vs. diameter (b) displacement at rupture vs. diameter and (c) rupture force vs. diameter for PSS-SiO$_2$ microspheres fabricated by the syringe pump and pipette dropwise additions of TEOS.
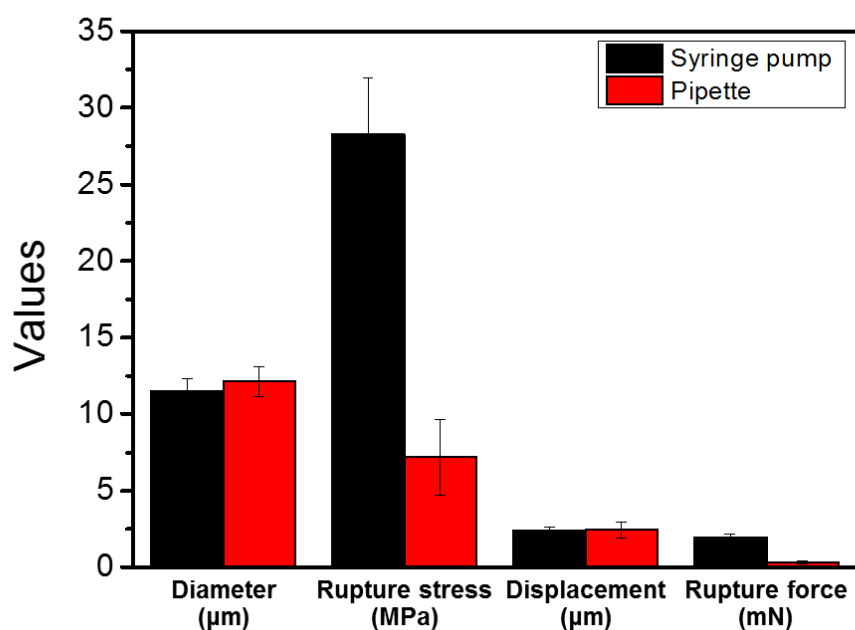
Fig. 4.13 The mean values of the diameter, rupture stress, displacement and rupture force for the PSS-SiO$_2$ microspheres synthesised via syringe pump and pipette.

4.5 Conclusions

In summary, a novel and simple method was developed here to form inorganic-organic composite microspheres which encapsulated a water soluble inorganic salt (KCl), with an encapsulation efficiency of 93 ± 1%. Notably, chemical modification of the microparticles enabled a sustained release of K$^+$ ions exceeding 48 hours, when dispersed in an aqueous phase, which is >8 times greater than what has been achieved previously.[25-27] The PSS-SiO$_2$ microspheres fabricated *via* the syringe pump dropwise method displays higher mechanical stability and lower release rates of encapsulated active ingredient than the ones formed *via* the pipette dropwise method. The proposed novel dual-release mechanism offers an opportunity for the prolonged release of other inorganic salts, and may lead to new applications in the agrochemical, pharmaceutical, food and household/personal care industrial sectors.

Chapter 5 Novel Encapsulation of Water Soluble Inorganic or Organic Ingredients in Melamine Formaldehyde Based Microspheres to Achieve Their Sustained Release in Aqueous Environment

Abstract: Melamine formaldehyde (MF) as a versatile chemical cross-linking agent has been broadly used in the encapsulation of oil phase, but it has not been possible to form MF microcapsules with water soluble ingredients encapsulated, which can achieve a sustained release in water. Herein, a novel type of melamine formaldehyde microcapsules with a desirable barrier property has been made to encapsulate water soluble ingredients, including potassium chloride (KCl) and allura red (dye) as models of inorganic salt and organic molecule, respectively, via an *in situ* polymerisation method. In addition, the melamine formaldehyde based microcapsules were designed to be fabricated in combination with biocompatible shellac or oppositely charged ion exchange resin (polystyrene sulfonate, PSS). They all showed a sustained release of KCl and allura red for 12 h and >10 days in aqueous environment, respectively. The encapsulation efficiency of the formed MF based microcapsules reached 74.2 ($\pm$ 3.8) % and 94.7 ($\pm$ 1.6) % for KCl and allura red, respectively.

5.1 Introduction

Microencapsulation is an important technology to stabilise active ingredients and/or control their release for a range of industrial sectors including healthcare, household care, cosmetics and agrochemicals.[1-3] Various techniques including interfacial polymerisation, *in situ* polymerisation, solvent evaporation and coacervation, have been developed to encapsulate different types of active ingredients, such as oil-soluble, water-soluble, amphiphilic, powders or cells.[221,253-256] Encapsulation of water-soluble active ingredients is usually achieved by forming a water in oil (W/O) emulsion, initially stabilised by the self-assembly of molecular and/or polymolecular surfactants at the liquid/liquid interface, followed by further

consolidation through chemical cross-linking of the surfactants at the interface, leading to robust isolatable capsules.[2,16] The actives that have been encapsulated range from biomacromolecules, such as proteins,[3] polysaccharides,[227] and enzymes[225,257] to small molecules, such as doxorubicin,[227,228] peroxide,[258] polyphenols,[226] and inorganic salts[259,260].

Shellac as a resin secreted from a kind of female insect (lac bug), is a polymer with excellent biocompatibility and low water permeability, which has received plenty of attentions recently[63,261-264]. The carboxyl groups of shellac can interact with calcium ions[112,113] and amino groups[265] and further enhance the biocompatibility of the materials.

Melamine formaldehyde (MF) is a versatile chemical cross-linking agent and has been broadly used in a number of encapsulation applications, due to its polycondensates providing tight seal, thermal and mechanical stability and acid/alkaline resistance.[266-268] MF polycondensates have been used as shell material to encapsulate oils in applications in the area of carbonless copy paper,[269] fragrant oil[270,271] and herbicide/insecticide delivery[272]. Vast examples can be found utilising MF as shell materials to encapsulate oil phase/hydrophobic ingredients.[36,270,271] It is comparatively easy to disperse the MF precondensate shell materials in the aqueous continuous phase forming the MF shell on interface of the O/W emulsion *via in situ* polymerisation process. However, there are very few examples utilising MF to form microparticles to encapsulate water soluble ingredients and achieve a sustained release, since the continuous phase is oil. It is still a challenge to encapsulate small water soluble ingredients exhibiting a long-term release in aqueous environment. Herein, a novel way to synthesise MF microspheres was developed as well as the one fabricated in combination with biocompatible shellac or oppositely charged ion exchange resin (polystyrene sulfonate, PSS) to encapsulate water soluble ingredients, including potassium chloride (KCl) and allura red (dye) as models of inorganic salt and organic molecule, respectively, via an *in situ* polymerisation method, and they have showed sustained releases of KCl and allura red for 12 h and >10 days in aqueous

environment, respectively. The sustained release of active ingredients were attributed to the proper barrier provided by the MF based matrix, rather than incorporation of the ion exchange resin.

5.2 Experimental sections

5.2.1 Synthesis of MF based microcapsules with KCl/allura red encapsulated

The synthesis of MF based microcapsules were carried out in a stirred vessel with standard configuration including 4 baffles, whose details were described in Section 3.3.3. The experimental details of the fabrications of MF^{wtc} & MF microcapsules, MF-shellac microcapsules and MF-PSS microspheres were presented in Section 3.3.3, Section 3.3.4 and Section 3.3.5, respectively.

5.2.2 Characterisations of the synthesised MF based microcapsules with KCl/NaCl encapsulated

The morphologies and cross-sections of the prepared microcapsules were observed with an optical microscope (301-371.011, Leica, Germany) and a Scanning Electron Microscope (SEM) (Philips XL-30 FEG ESEM). The cross-sections of the microcapsules were cut by a microtome (Reichert-Jung). The size distribution, SPAN and the mean volumetric size (D_{43}) of the microcapsules were measured by a laser light scattering technique (Mastersizer 2000, Malvern Instruments, UK). The FT-IR spectra were obtained using a Thermo Electron Nicolet 8700 spectrometer. The chemical composition of the sample was evaluated by an energy disperse X-ray microanalysis (EDX) (Oxford, Inca 300) in conjunction with SEM. The concentrations of KCl and allura red were measured by a flame photometer (PFP-7, Jenway, UK) and a UV spectrophotometer at 504 nm (Cecil 2021 UV spectrophotometer), respectively.

The mechanical properties of microcapsules were determined by a micromanipulation technique.

5.3   Results and discussions

The novel MF microcapsules were designed to be fabricated via two methods, including with and without copolymer (poly(acrylamide-acrylic acid)). An aqueous phase containing the MF precondensate solution, formaldehyde, with or without poly(acrylamide-acrylic acid) copolymer and the active (KCl or allura red) with the pH adjusted to 4.3, was emulsified within an oil (sunflower oil) phase at a stirring speed of 600 rpm (Scheme 5.1, Step 1) to form a Pickering emulsion (unripened (low-level cross-linking) microcapsules), with the cross-linking MF or MF and copolymer acting as the stabilising surfactants at the liquid/liquid interface.[222,273] The unripened MF microcapsules were then heated at 55 $^{\circ}$C for 30 min, which partially solidified as the outer shell,[274] and the stirring speed was then increased to 1200 rpm, which was maintained for further 30 min, to prevent aggregation between the unripened microcapsules (Step 2). The fully ripened MF microcapsules were finally formed by heating at 75 $^{\circ}$C for further 5 h (Step 3). The MF microcapsules (ripened) formed with or without the copolymer were named as MF microcapsules and MF[wtc] microcapsules, respectively. The MF microcapsules (ripened) formed with different volumes of formaldehyde solution (200 μl and 600 μl, 37% (aq.) w/w) were named as MF (200 F) and MF (600 F) microcapsules, respectively. All of the experimental details are displayed in section 3.3.3 in Chapter 3.
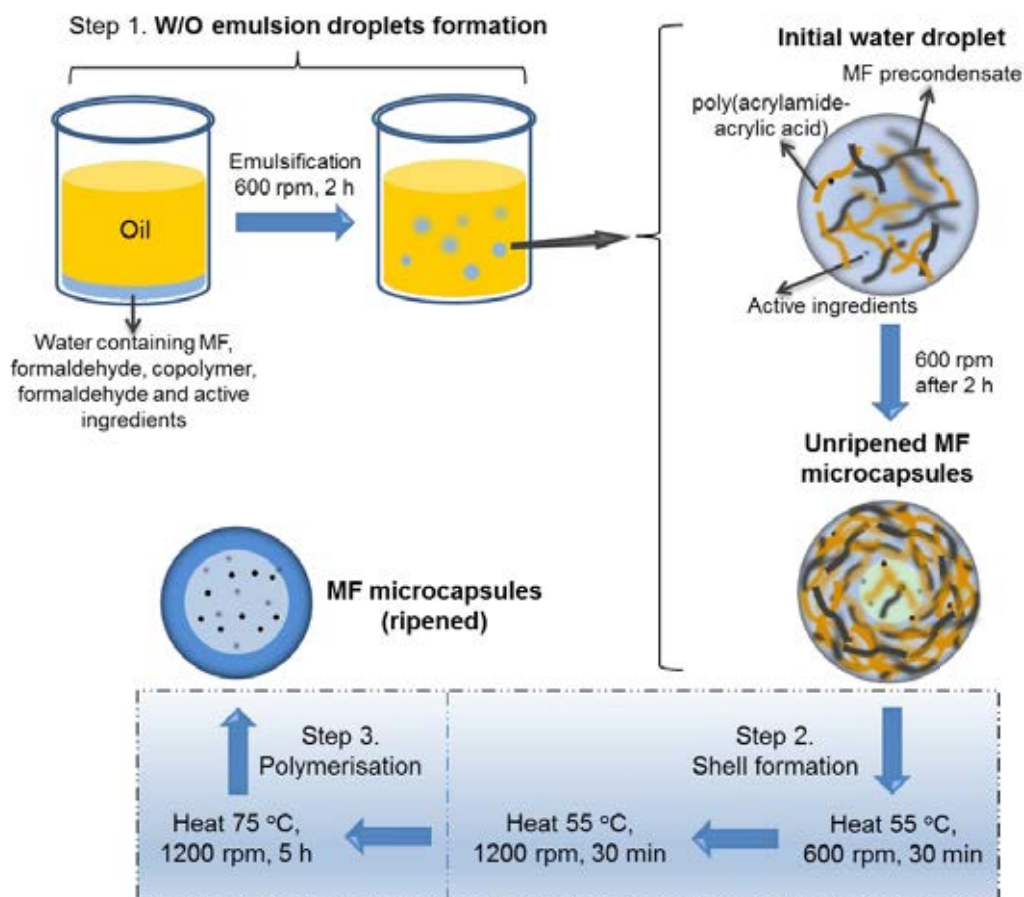
Scheme 5.1 Illustration of MF microcapsules synthesised *via* an *in situ* polymerisation process with water soluble ingredients (KCl salt/allura red molecules) encapsulated.

5.3.1 Synthesis and characterisation of MF microcapsules without copolymer

The synthesised MF^{wtc}-KCl microcapsules showed spherical shapes with a smooth surface on the microscale as shown in Fig. 5.1a & 5.1b. The size distribution exhibited in Fig. 5.1c shows the volume weighted mean diameter (D_{43}) was 9.3 ($\pm$ 0.1) μm (SPAN 1.45 $\pm$ 0.05). Unfortunately, the release profile in Fig. 5.1d demonstrates a very fast release rate with 77.5 $\pm$ 1 % of K$^+$ ions leaking out within the initial 15 min, indicating the poor barrier provided by the neat MF material. The payload and encapsulation efficiency of KCl in the MF^{wtc}-KCl microcapsules were calculated using Equations 3.8 & 3.9 in Chapter 3, and the payload reached 2.8 ($\pm$ 0.1) %, and the encapsulation efficiency showed 39.0 ($\pm$ 1.4) % for KCl encapsulation.
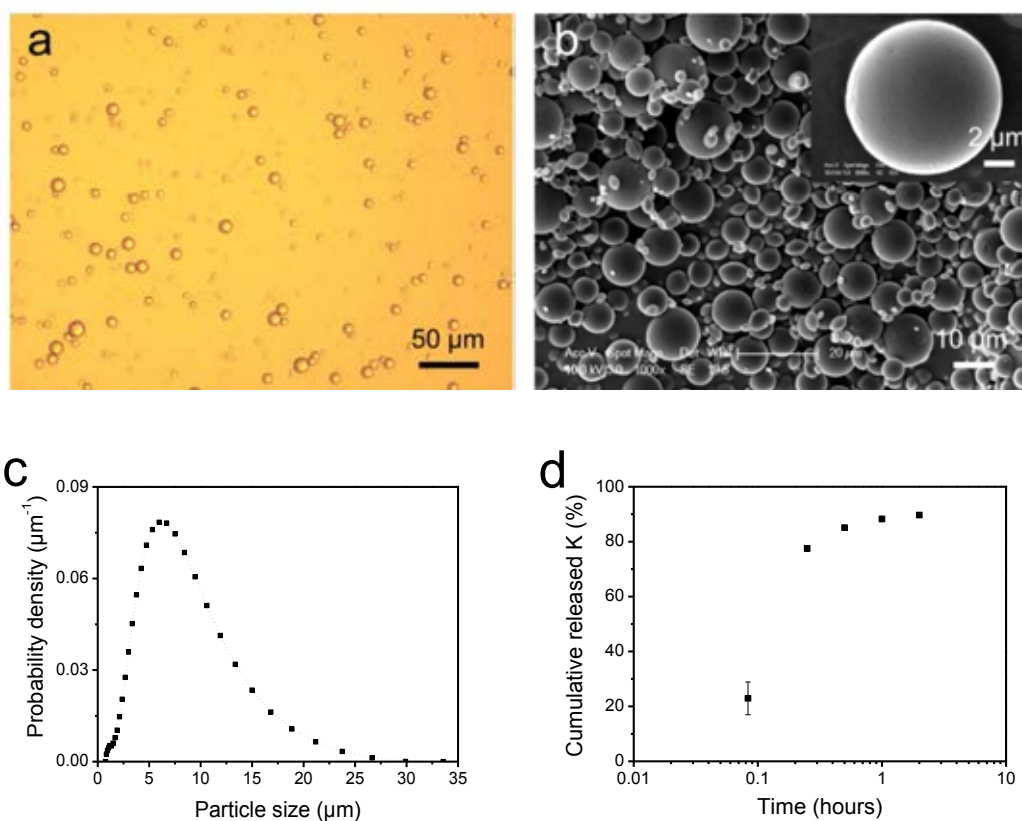
Fig. 5.1 (a) Optical micrograph, (b) SEM image and (c) size distribution of the formed MF^{wtc}-KCl microcapsules dispersed in DIW. The inset in panel (b) shows its SEM image in high magnification. (d) Cumulative release profile of K$^+$ ions from MF^{wtc}-KCl microcapsules dispersed in DIW at 37 °C with shaking at a speed of 150 rpm. (Each experiment was conducted at least 3 times).

5.3.2 Synthesis and characterisation of MF microcapsules with copolymer
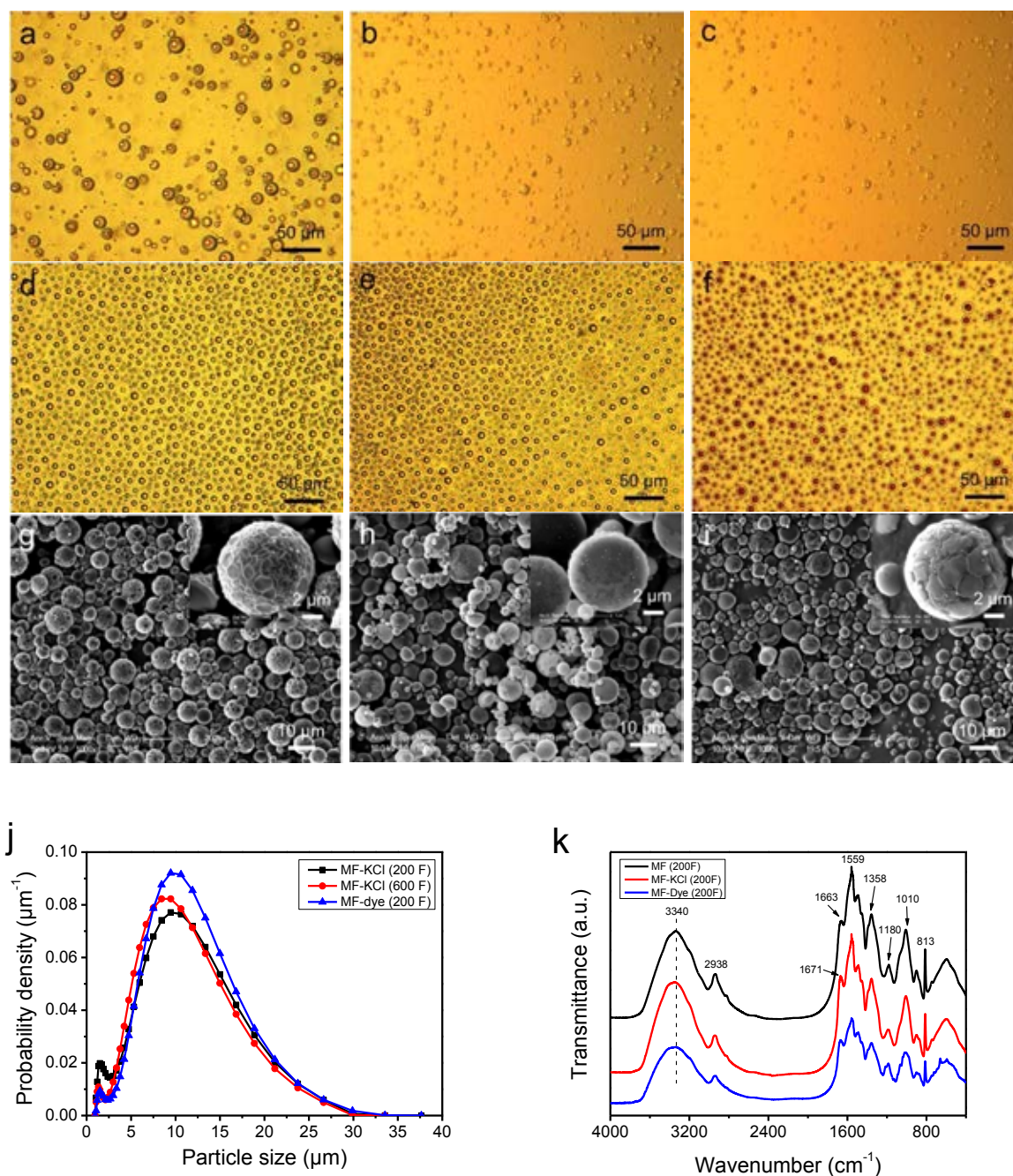
Fig. 5.2 Optical micrographs of unripened MF-KCl (200 F) microcapsules produced (a) at 600 rpm for 2 h, (b) before and (c) after 1200 rpm, 55 °C for 30 min; (d) MF-KCl (200 F) microcapsules, (e) MF-KCl (600 F) microcapsules and (f) MF-dye (200 F) microcapsules dispersed in water. SEM images of (g) MF-KCl (200 F), (h) MF-KCl (600 F) microcapsules, and (i) MF-dye (200 F) microcapsules. The inset in panel (g), (h) and (i) shows their SEM

images in high magnifications, respectively. (j) The size distributions of MF-KCl (200 F), MF-KCl (600 F) and MF-dye (200 F) microcapsules, and (k) FT-IR spectra of MF (200 F), MF-KCl (200 F) and MF-dye (200 F) microcapsules.

In order to improve the barrier property provided by the MF material, the copolymer (poly(acrylamide-acrylic acid)) as a commonly used cross-linking agent was introduced to integrate with MF precondensate forming the shell material to encapsulate active ingredients.[30,36] The W/O emulsion droplets were stabilised by the pre-cross-linked MF precondensate and copolymer at pH 4.3, which adsorbed at the interface of the emulsion as shown in the optical micrograph (Fig. 5.2a), forming the unripened MF microcapsules with a core-shell structure. After preheated at 55 ^{o}C for 30 min, the unripened MF microcapsules partly solidified and they were strong enough to survive when the stirring speed was increased to 1200 rpm, to avoid aggregation between microcapsules (Fig. 5.2b, 5.2c). The unripened microcapsules maintained their shapes and sizes after the stirring speed was increased as shown in Fig. 5.2c. The formed ripened MF-KCl (200 F), MF-KCl (600 F) and MF-dye (200 F) microcapsules showed spherical shapes on the microscale, and the MF-dye revealed a red core under the optical microscope, indicating the encapsulated dye in the MF microcapsules (Fig. 5.2d, 5.2e, 5.2f). The MF-KCl (600 F) revealed a smoother surface than the MF-KCl (200 F) one, which resulted from the increasing amount of formaldehyde integrated into the MF polymerisation process (Fig. 5.2g, 5.2h). The surface of MF-dye (200 F) microcapsules exhibiting some small clusters might be attributed to the dye molecules integrated into the cross-linking of MF precondensate and copolymer (Fig. 5.2i).

Table 5.1 The SPAN value, mean size D_{43} and viscosity data of initially mixed aqueous solution (before emulsification) for each batch of MF samples. The figure after ± represents the standard error of the mean.

Sample	Mean size D_{43} (µm)	SPAN	Viscosity (Pas)
MF-KCl (200 F)	13 (± 1)	1.26 (± 0.01)	0.0187 (± 7 x 10^{-4})
MF-KCl (600 F)	12 (± 1)	1.3 (± 0.02)	0.0169 (± 7 x 10^{-4})
MF-dye (200 F)	13 (± 1)	1.21 (± 0.05)	0.0188 (± 8 x 10^{-4})

The size distributions exhibited in Fig. 5.2j show similar mean size D_{43}, SPAN and viscosity of solution as displayed in Table 5.1. The formed MF microcapsules were characterised by the Fourier-transform infrared (FT-IR) spectrometry. The absorption peaks of N-H stretching vibration at around 3340, 1559 and 813 cm^{-1}, the C-N stretching at around 1358 cm^{-1}, the C-H stretching at around 2938 and 1180 cm^{-1} and the methylol at roughly 1010 cm^{-1}, are the characteristics of MF and copolymer (Fig. 5.2k).[275-277] The slight shifts of carboxyl group at 1671 cm^{-1} for MF-KCl, might be due to the interactions between the carboxyl groups of copolymer and K$^+$ ions, relative to the peak at 1663 cm^{-1} for the neat MF.[278]
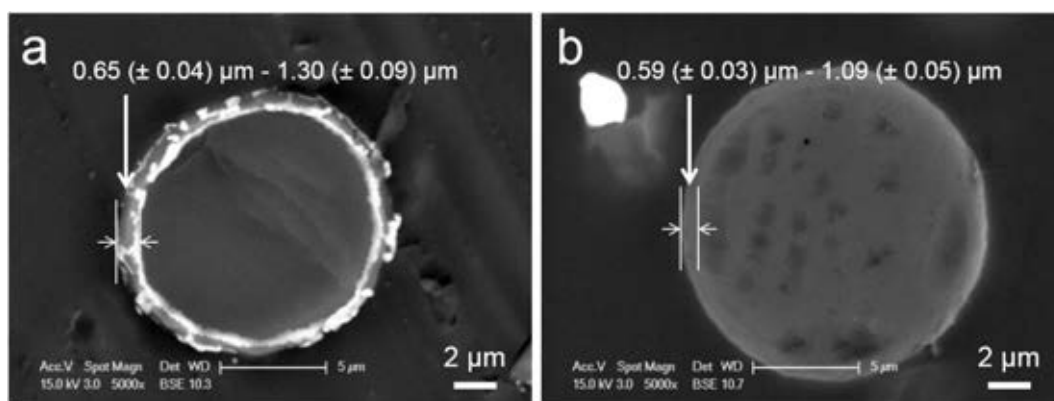
Fig. 5.3 TEM images of the cross-section of (a) MF-KCl (200 F) and (b) MF-KCl (600 F) microcapsules embedded in epon/araldite resin. (Each data was calculated from at least 30 microcapsules)

The cross-sections of MF-KCl (200 F) and MF-KCl (600 F) microcapsules are shown in Fig. 5.3, indicating clear shell structures. The MF-KCl (200 F) microcapsules displayed a thicker shell (0.65 ($\pm$ 0.04) μm - 1.30 ($\pm$ 0.09) μm) with a uniformly distributed core than MF-KCl (600 F) microcapsules (0.59 ($\pm$ 0.03) μm - 1.09 ($\pm$ 0.05) μm) with an inhomogeneously distributed core. The high concentration of formaldehyde in MF-KCl (600 F) led to the excess amount of formaldehyde in the water phase and might increase the polymerisation rate between MF precondensate and free formaldehyde, forming the unevenly distributed self-assembled solid MF core. Meanwhile, it led to higher local concentrations of formaldehyde, forming a smoother and more compact surface (Fig. 5.2h). The shell thicknesses of MF-KCl (600 F) microcapsules were thus thinner than the one of MF-KCl (200 F) microcapsules due to the less amount of MF assembled in the shell. The elemental compositions of shell and core of MF-KCl (200 F) microcapsules confirmed by the energy dispersive X-ray (EDX) analysis, demonstrate that both of the shell and core contained C, N, Na and Cl, revealing the existence of assembled MF precondensate and copolymer (Fig. 5.4). Meanwhile, the detectable K element in the core indicates that the K^+ ions were encapsulated in the MF microcapsules.
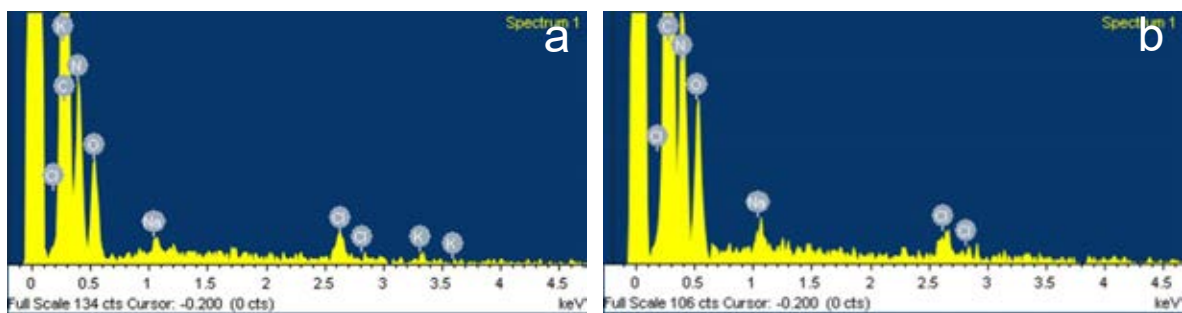
Fig. 5.4 EDX analysis of (a) the core and (b) the shell of MF-KCl (200 F) microcapsule.
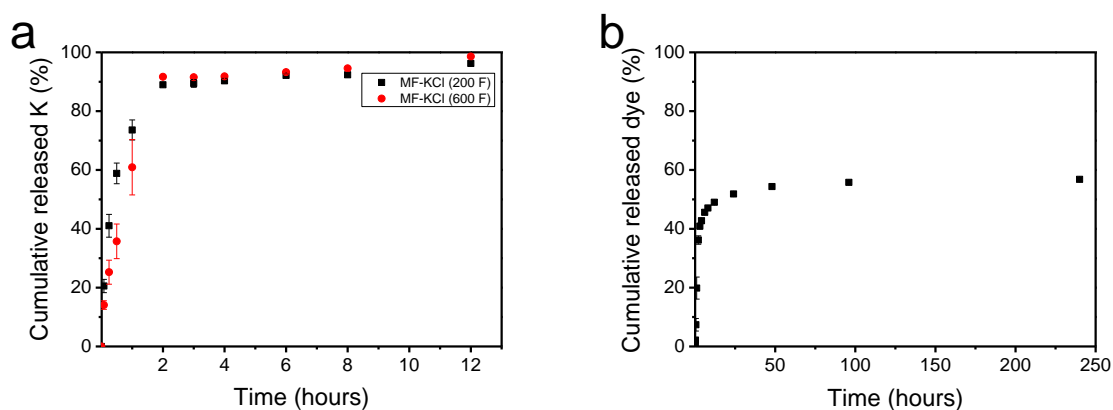
Fig. 5.5 Cumulative release profiles of (a) K^+ ions from MF-KCl (200 F) microcapsules, MF-KCl (600 F) microcapsules and (b) dye molecules from MF-dye (200 F) microcapsules dispersed in water at 37 °C with shaking at a speed of 150 rpm.

Table 5.2 The F/M (molar ratio), payload, encapsulation efficiency and Young`s modulus of each batch of MF samples.

Sample	F/M Molar	Payload (%)	Encapsulation Efficiency (%)	Young`s Modulus (GPa)
MF-KCl (200 F)	0.7	7.7 (± 0.3)	69.8 (± 2)	3.3 (± 0.2)
MF-KCl (600 F)	1.7	7.2 (± 0.1)	68.6 (± 1.5)	2.8 (± 0.2)
MF-dye (200 F)	0.7	8.4 (± 0.1)	81.9 (± 1)	4.9 (± 0.2)

The microcapsules were dispersed in water and the release of K^+ ions or dye molecules from the microcapsules was monitored, via removal of aliquots at extended time intervals over 12 hours and 10 days, and analysed with flame photometry (K^+) and UV/Vis spectroscopy (dye), respectively. The cumulative release data of K^+ ions in Fig. 5.5a from two batches of MF-KCl microcapsules demonstrates a sustained release within 2 hours, releasing out roughly 90 % of the encapsulated ions, and then followed by a slow release up to 12 h, which might be due to the interaction between K^+ and carboxyl groups of copolymer as indicated by FT-IR (Fig. 5.2k). Interestingly, the release of K^+ ions from MF-KCl (600 F) with more content of formaldehyde revealed a slower release rate, which may be attributed to the formed more compact MF, providing a better barrier to the encapsulated ions, compared to MF-KCl (200 F). The release rate of allura red (dye) molecules from MF (200 F) displays a sustained release, revealing a fast release leaking 36.2 ± 1.4 % within 2 h and then slowed down, leaking 56.8 ± 0.4 % for 10 days (Fig. 5.5b). The payloads and encapsulation efficiencies of KCl and dye in the MF microcapsules were calculated and the results are shown in Table 5.2. Clearly, the ones for dye in MF microcapsules were higher than for KCl ions, which probably resulted from the larger molar mass of allura red, and its functional groups might interact with MF and the copolymer.
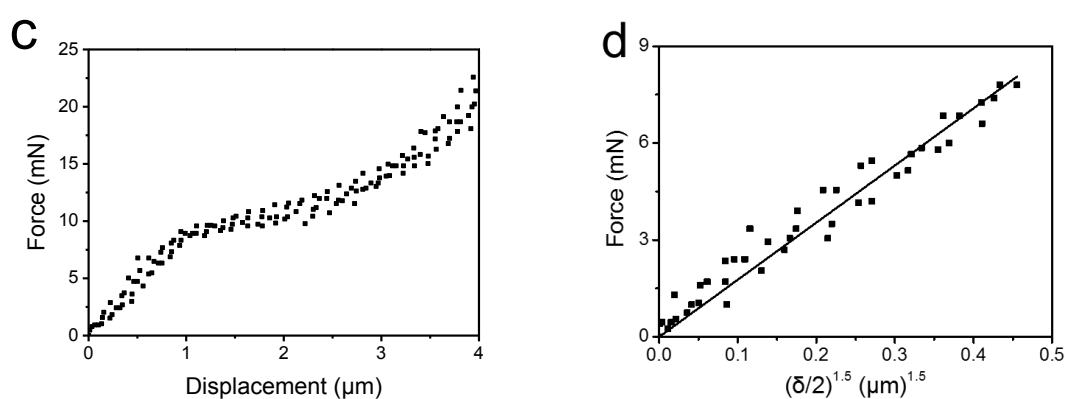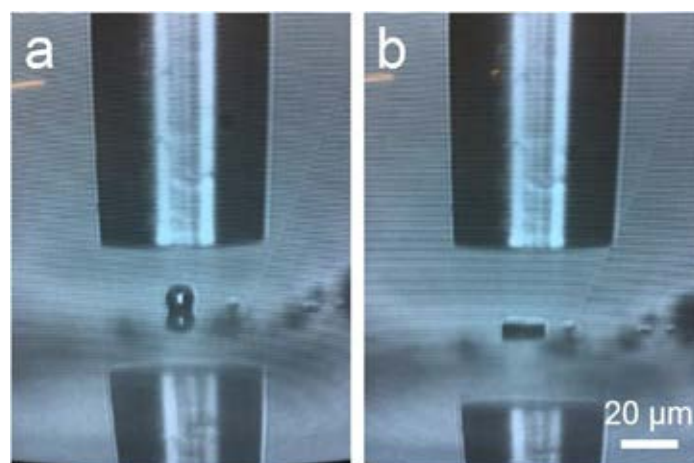
Fig. 5.6 Optical images obtained from screen (a) before and (b) after compressing a single MF microcapsule to large deformation. (c) The linear fit of the Hertz model to the data from compression of a single MF-KCl (200 F) microcapsule to 10% nominal deformation. The compression speed was 2 μm/s.

The mechanical properties of MF microcapsules were measured by a micromanipulation technique.[252] A single MF microcapsule was compressed by two parallel flat surfaces (Fig. 5.6a, 5.6b), and a force versus displacement curve for compression of the single MF-KCl (200 F) microcapsule was obtained as shown in Fig. 5.6c. The relationship of force (F) versus displacement (δ) is assumed to represent the elastic behaviour, when the nominal deformation calculated by Equation 5.1 is $\leq$ 10%, described by the Hertz model as given in Equation 5.2.[163] R is the diameter of the microcapsule; E is the Young's modulus of the microcapsules and v is the Poisson's ratio.

$$\text{Nominal deformation (\%)} = \frac{\delta}{R} \times 100$$

(Equation 5.1)

$$F = \frac{4}{3}\frac{E}{(1-\nu^2)} R^{1/2}\left(\frac{\delta}{2}\right)^{3/2}$$

(Equation 5.2)

In this way, a force vs. $(\delta/2)^{3/2}$ curve was fitted with the Hertz model (Equation 5.2), see Fig. 5.6d, and they are in good agreements with a correlation coefficient of 0.99, which justifies the assumption of the elastic behavior when the nominal deformation is ≤ 10 %. The precise Poisson's ratio is unknown for various mixtures, but here it is assumed to be incompressible (ν = 0.5).[279] The Young's modulus values of the three batches of MF microcapsules are shown in Table 5.2, and the MF-KCl (200 F) microcapsules formed with the less amount of formaldehyde indicates a higher Young`s value due to the thicker shells and uniform cores, relative to the MF-KCl (600 F) microcapsules with an interstitial hollow core. In general, the Young`s modulus of the formed MF microcapsules with a range of 2.8-3.3 GPa displayed a similar value to the previous publications about MF microcapsules, and the larger shell thickness could enhance the stiffness of the microcapsule.[280,281]

5.3.3 Synthesis and characterisation of MF-shellac microspheres

The novel MF-shellac microspheres were designed to be fabricated via an *in situ* polymerisation process in combination with biocompatible shellac. The procedure is similar to the Scheme 5.1, except for the dropwise addition of shellac solution (2 g/ml in ethanol, 1 ml) into the above emulsion, stirring at 600 rpm for 3 h before the polymerisation process. The MF-shellac microspheres (ripened) formed with different volumes of formaldehyde solution (200 μl and 600 μl, 37% (aq.) w/w) were named as MF-shellac (200 F) and MF-shellac (600 F) microspheres, respectively. All of the experimental details are displayed in section 3.3.4 in Chapter 3.
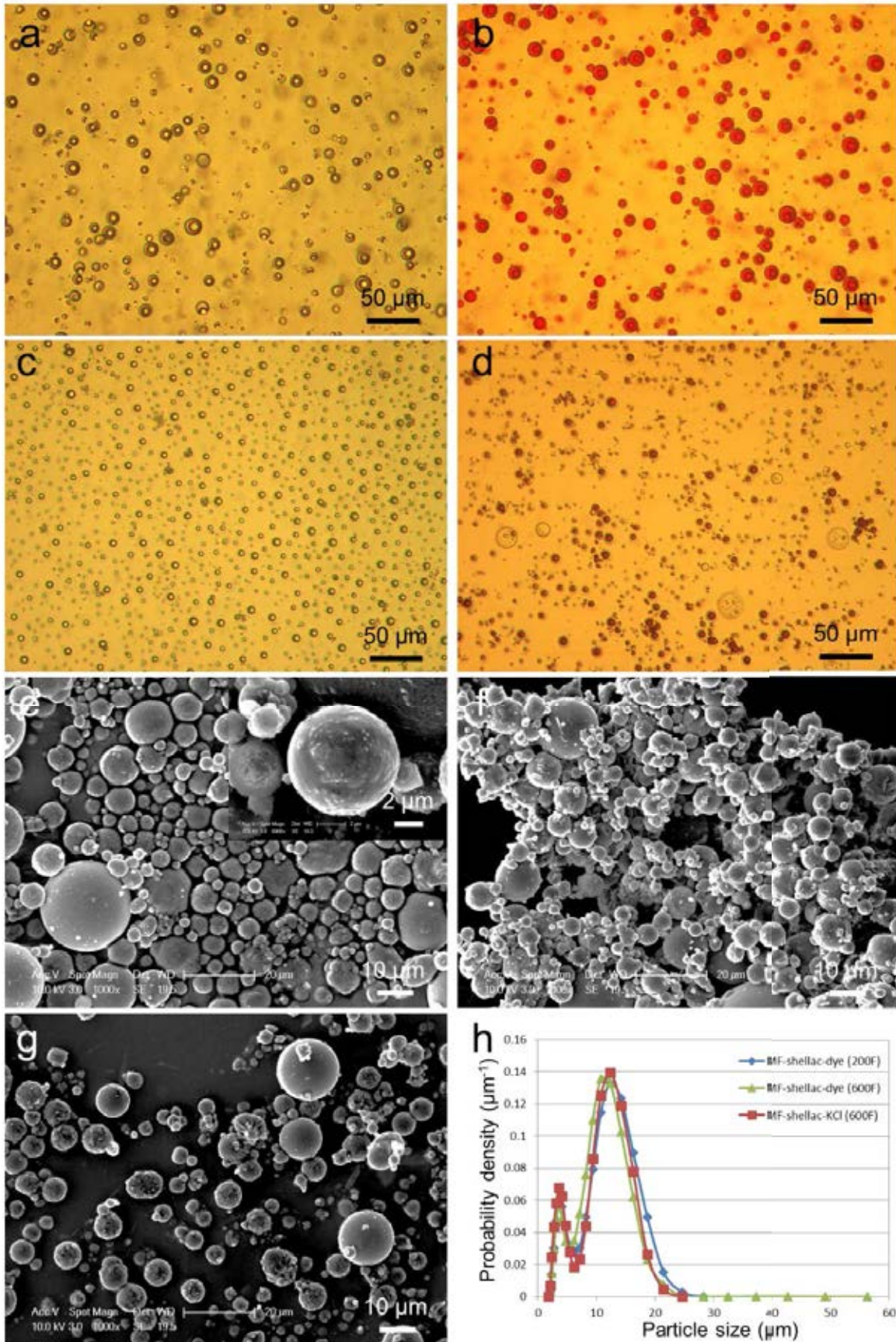
Fig. 5.7 Optical micrographs of (a) unripened MF-shellac-KCl (600 F), (b) unripened MF-shellac-dye (600 F) microspheres produced at 600 rpm for 2 h, (c) MF-shellac-KCl (600 F) and (d) MF-shellac-dye (600 F) microspheres dispersed in water. SEM images of (e) MF-shellac-KCl (600 F), (f) MF-shellac-dye (200 F) and (g) MF-shellac-dye (600 F) microspheres. The inset in panel (e) shows its SEM image in high magnification. (h) The size distributions of (e) MF-shellac-KCl (600 F), (f) MF-shellac-dye (200 F) and (g) MF-shellac-dye (600 F) microspheres dispersed in water.

Table 5.3 The SPAN and mean size D_{43} for each batch of MF-shellac microsphere samples. The figure after ± represents the standard error of the mean.

Sample	SPAN	D_{43} (µm)
MF-shellac-KCl (600 F)	0.95 (± 0.02)	11.45 (± 0.03)
MF-shellac-dye (200 F)	0.95 (± 0.01)	11.95 (± 0.01)
MF-shellac-dye (600 F)	1.00 (± 0.01)	12.46 (± 0.02)

The W/O emulsion droplets were stabilised by the pre-cross-linked MF precondensate and copolymer at pH 4.3, which adsorbed at the interface of the emulsion as shown in the optical micrograph (Fig. 5.7a, 5.7b), forming the unripened MF microcapsules with a core-shell structure. After the dropwise addition of shellac solvent and further polymerisations, the optical micrographs of the MF-shellac-KCl (600 F) (ripened) and (d) MF-shellac-dye (600 F) (ripened) microspheres dispersed in water are exhibited in Fig. 5.7c & 5.7d, respectively. The formed MF-shellac-KCl (600 F) and MF-shellac-dye (600 F) microspheres showed spherical shapes on the microscale, and the MF-shellac-dye (600 F) microspheres revealed a red core under the optical microscope, indicating the encapsulated dye in the MF-shellac microspheres (Fig. 5.7c, 5.7d). The SEM images in Fig. 5.7e, 5.7f and 5.7g show a smooth surface of the formed MF-

shellac microspheres with KCl and allura red encapsulated. The size distributions exhibited in Fig. 5.7h show similar SPAN and mean size D_{43}, which were around 12 μm (Table 5.3).
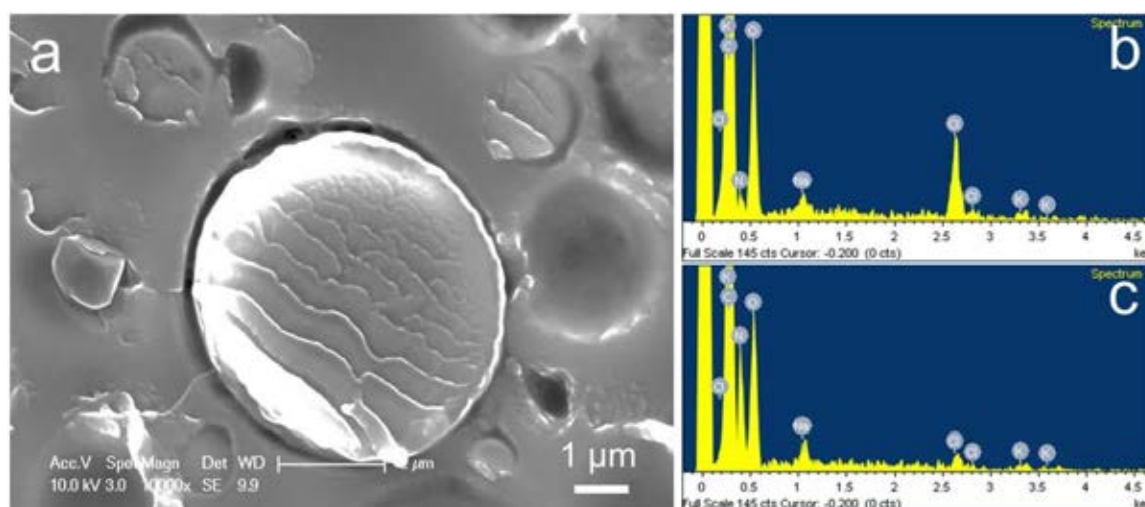
Fig. 5.8 TEM images of the cross-section of (a) MF-shellac-KCl (600 F) microspheres embedded in epon/araldite resin and EDX analysis of (b) the near-edge part and (c) core of the (a) cross-section of MF-shellac-KCl (600 F) microspheres.

The cross-sections of MF-shellac-KCl (600 F) microspheres are shown in Fig. 5.8a, indicating a solid structure throughout. The elemental compositions of the near-edge part and core of MF-shellac-KCl (600 F) microspheres confirmed by the energy dispersive X-ray (EDX) analysis, demonstrate that both of the shell and core contained C, N, O, Na, K and Cl, revealing the existence of assembled MF precondensate and copolymer (Fig. 5.8b & 5.8c). Interestingly, the intensity of N peaks are different between the near-edge and core of the microsphere. The lower intensity of N peak of the near-edge indicates its lower content of MF compared with the core. This should be attributed to the accumulation of dropwise added shellac onto the surface of unripened MF microspheres. Meanwhile, the detectable K element indicates that the K$^+$ ions were encapsulated in the MF microspheres. The formed MF microcapsules were characterised by the Fourier-transform infrared (FT-IR) spectroscopy. The absorption peaks of N-H stretching vibration at around 3340, 1559 and 813 cm^{-1}, the C-N stretching at around 1358 cm$^-$

[1], the C-H stretching at around 2938 and 1180 cm^{-1} and the methylol at roughly 1010 cm^{-1}, are the characteristics of MF and copolymer (Fig. 5.8).[275-277] The red shift of the peak at around 3400 cm^{-1} in the MF-shellac-KCl (600 F) microspheres is attributed to the OH groups of the shellac. The emerging peak at 2856 cm^{-1} is assigned to the methyl and methylene groups of shellac.[282] In this case, the FT-IR spectrum of MF-shellac-KCl (600 F) indicates the existence of shellac and MF (Fig. 5.9).
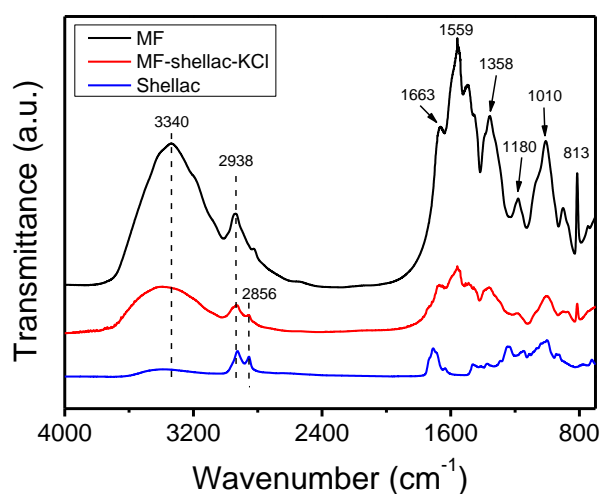
Fig. 5.9 FT-IR spectra of MF, MF-shellac-KCl (600 F) microspheres and neat shellac.

The microspheres were dispersed in water and the release of K$^+$ ions or dye molecules from the microcapsules was monitored, via removal of aliquots at extended time intervals over 12 hours and 10 days, and analysed with flame photometry (K$^+$) and UV/Vis spectroscopy (dye), respectively. The cumulative release data of K$^+$ ions in Fig. 5.10a from the MF-shellac-KCl (600 F) microspheres demonstrates a sustained release within 2 hours, releasing out roughly 90% of the encapsulated ions, and then followed by a slow release up to 12 h, which might be due to the interaction between K$^+$ and carboxyl groups of copolymer as discussed in FT-IR spectra in Fig. 5.2k. The release rates of allura red (dye) molecules from both two batches of MF-shellac-dye (200 F) and MF-shellac-dye (600 F) microspheres display a sustained release, revealing a fast release leaking of 36.6 ± 1.3 % and 27.6 ± 1.3 % within 2 h and then slowed

down, leaking 60.3 ± 0.6 % and 45.0 ± 0.8 % for 10 days, respectively (Fig. 5.10b). The payloads and encapsulation efficiencies of KCl and dye in the MF-shellac microspheres were calculated using the Equations 3.8 & 3.9 in Chapter 3, and the payloads reached around 7 %, and the encapsulation efficiencies showed 74.2 ($\pm$ 3.8) % for KCl and >80 % for dye encapsulation, respectively (Table 5.4). Clearly, the encapsulation efficiency for dye in MF-shellac microspheres was higher than for KCl ions, which probably resulted from the larger molar mass of allura red, and its functional groups might interact with MF and the copolymer.
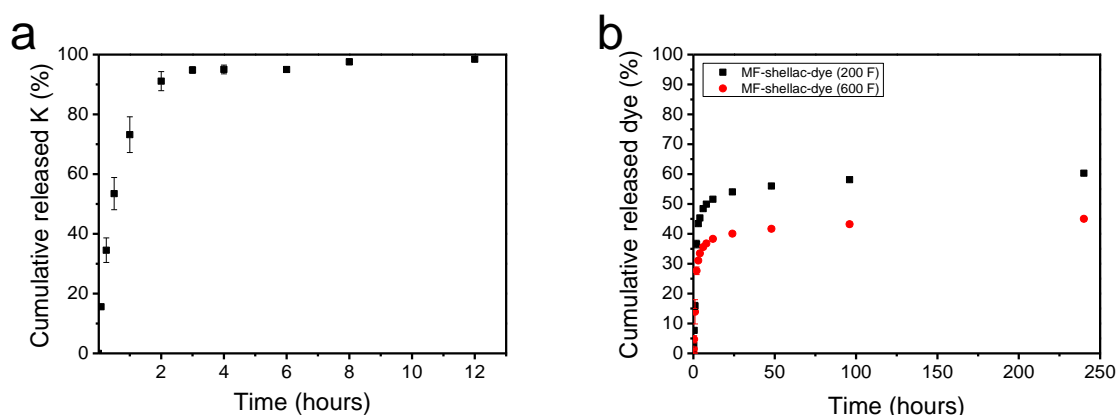

Fig. 5.10 Cumulative release profiles of (a) K^+ ions from MF-shellac-KCl (600 F) microspheres and (b) dye molecules from MF-shellac-dye (200 F) and MF-shellac-dye (600 F) microspheres dispersed in water at 37 °C with shaking at a speed of 150 rpm.

Table 5.4 The F/M (molar ratio), payload and encapsulation efficiency of each batch of MF-shellac microspheres.

Sample	F/M Molar ratio	Payload (%)	Encapsulation Efficiency (%)
MF-shellac-KCl (600 F)	1.7	6.9 ($\pm$ 0.8)	74.2 ($\pm$ 3.8)
MF-shellac-dye (200 F)	0.7	7.2 ($\pm$ 0.6)	94.7 ($\pm$ 1.6)
MF-shellac-dye (600 F)	1.7	7.0 ($\pm$ 0.1)	85.5 ($\pm$ 3.8)

5.3.4 Synthesis and characterisation of MF^{wtc}-PSS microspheres

The novel MF^{wtc}-PSS microspheres were designed to be fabricated via an *in situ* polymerisation process in combination with oppositely charged ion exchange resin (polystyrene sulfonate, PSS) similar to the previous MF microcapsules fabrication (Scheme 5.1). An aqueous phase containing the MF precondensate solution, PSS and the active (KCl) was emulsified within an oil (sunflower oil) phase at a stirring speed of 600 rpm for 2 h. The unripened MF^{wtc}-PSS microspheres were then further polymerised via the same procedure with Scheme 5.1. Briefly, the unripened microspheres were heated at 55 °C at 600 rpm for 30 min and then increased to 1200 rpm, which was maintained for further 30 min. The fully ripened MF^{wtc}-PSS microspheres were finally formed by heating at 75 °C for further 5 h.
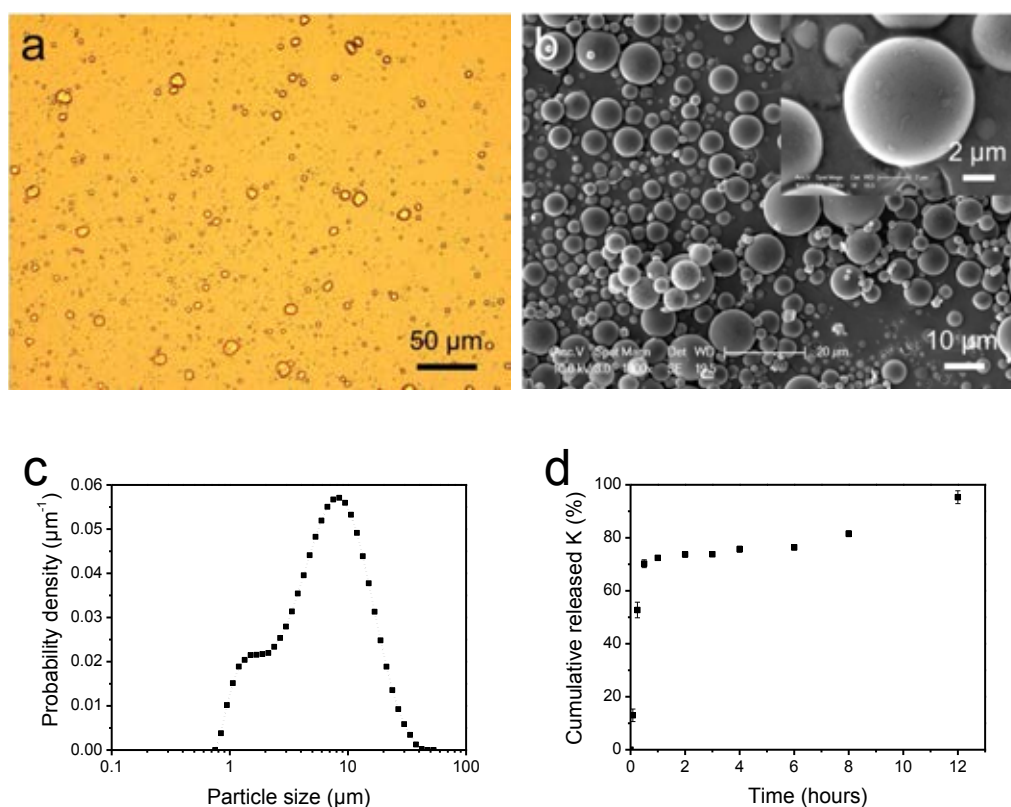
Fig. 5.11 (a) Optical micrograph, (b) SEM image and (c) size distribution of the formed MF^{wtc}-PSS-KCl microspheres dispersed in DIW. The inset in panel (b) shows its SEM image in high magnification. (d) Cumulative release profile of K$^+$ ions from MF^{wtc}-PSS-KCl microspheres

dispersed in DIW at 37 °C with shaking at a speed of 150 rpm. (Each experiment was conducted at least 3 times).

The synthesised MF^{wtc}-PSS-KCl microspheres showed spherical shapes with a smooth surface on the microscale as shown in Fig. 5.11a & 5.11b. The size distribution exhibited in Fig. 5.11c shows the volume weighted mean diameter (D_{43}) was 12.7 (± 0.3) μm (SPAN 1.67 ± 0.02). Notably, the release profile in Fig. 5.11d demonstrates a very fast release rate with 70.2 (± 1.5) % of K$^+$ ions leaking out within the initial 30 min, followed by a sustained release until 12 h, reaching 95.3 (± 2.4) % release of K$^+$ ions. The initial fast release might be attributed to the release of free K$^+$ ions encapsulated in the MF microspheres, while the following sustained release might be interpreted by the interaction between K$^+$ ions and PSS resin. The payload and encapsulation efficiency of KCl in the MF^{wtc}-PSS-KCl microspheres reached 4.0 (± 0.1) % and 42.3 (± 1.6) %, respectively.

5.4   Conclusions

In conclusion, novel melamine formaldehyde based microcapsules/microspheres with aqueous phase encapsulated were developed in this study, and the water soluble ingredients, including ion (K$^+$) and small molecule (allura red) were encapsulated, indicating a sustained release in water environment for 12 h and >10 days, respectively. The microencapsulation technique offered a novel way to synthesise MF based microcapsules/microspheres with water soluble ingredients encapsulated, achieving their sustained release in water.

The encapsulation efficiency of the MF based microcapsules/microspheres fabricated with copolymer displayed > 65 %, whilst the one of the MF^{wtc} microcapsules and MF^{wtc}-PSS microspheres fabricated without copolymer just exhibited 42.3 (± 1.6) % for KCl encapsulation. The lower encapsulation efficiency of the MF^{wtc} microcapsules might be due to

the poor MF shell barrier fabricated without using the copolymer. In this case, the MF^{wtc}-PSS microspheres formed without copolymer displayed a fast release rate of K$^+$ ions within 30 min, but the sustained release achieved up to 12 h was attributed to the interaction between PSS resin and K$^+$ ions. The higher encapsulation efficiency of the MF-shellac microspheres may be ascribed to the coating of shellac and the integration of copolymer in the MF materials. In addition, the formed MF microcapsules displayed Young`s modulus values in the order of GPa, revealing a strong stiffness of the material. Therefore, the developed MF formation method has provided a new way to deliver different kinds of water soluble ingredients, which may have applications in various areas of scientific research and industry.

Chapter 6 Novel Microencapsulation of Small Water Soluble Ingredients to Achieve No Release in Aqueous Environment

Abstract: Encapsulation technology has been widely researched, and applied to different industry sectors, but it has not been possible to prevent the release of small water-soluble ingredients from microcapsules in aqueous environment. Herein, a novel approach to encapsulate small water-soluble ingredients including K^+ ions and allura red (dye, M_w = 496.42 g·mol^{-1}) molecules has been developed based on the formation of melamine formaldehyde-octadecyltrichlorosilane-melamine formaldehyde (MOM) microcapsules, which prevent their release in aqueous environment for 1 month. The key for the microcapsules to provide the excellent barrier property to entrap the active ingredients is profited from the sandwich of the hydrophobic material between the two melamine formaldehyde shells. The novel encapsulation approach can have vast applications in developing functional products such as fast moving consumer goods (FMCGs), agrochemical, printing and energy storage.

6.1   Introduction

Encapsulation technology provides a means to entrap active ingredients and deliver them to the target place at the right time, applied in a variety of industries.[283-285] It can be advantageous to enhance the stability or shelf life of the active ingredients, mask their undesirable odor/taste and control their release in different environments.[286] The microencapsulation technology has found vast applications in many industrial sectors, e.g. the pharmaceutical industries for the drug delivery systems,[287-289] fast moving consumer goods (FMCGs) for the controlled release of active ingredients (such as fragrances, bleaches and dyes),[290,291] and food industries for the controlled release of flavors.[283,286,292]

In terms of the controlled release of the encapsulated ingredients, it can normally be classified as immediate release, prolonged release, modified release and delayed release.[293] There are

vast successful examples to encapsulate active ingredients including the hydrophilic and hydrophobic ingredients with controlled release.[173,294-297] However, the encapsulation of hydrophilic ingredients, specifically the ones with low molar masses exhibiting no release in aqueous phase remains a challenge, although its realisation is of great significance for their long-term storage until they are delivered to a target place via triggered release in many applications. Herein, a novel encapsulation strategy was developed taking advantage of the embedded hydrophobic intervening layer between two melamine formaldehyde layers to provide a proper barrier. The key to offer the proper barrier is the utilisation of hydrophobic material, which has been vastly applied in oil sorbents[176,209,298], but has not been used for encapsulation. Notably, the potassium chloride (KCl) salt and allura red as small water soluble ion and molecule model, respectively, were successfully encapsulated via the novel encapsulation method and they displayed no release in pure water for 1 month.

6.2 Experimental sections

6.2.1 Synthesis of M_1, M_2, M_1O, M_2O and M_2OM microcapsules with KCl/allura red encapsulated

The synthesis of M_1, M_2, M_1O, M_2O and M_2OM microcapsules were performed in a stirred vessel with standard configuration including 4 baffles. Section 3.3.6 presents the experimental details of synthesis of M_1 and M_2 microcapsules, and Section 3.3.7 and Section 3.3.8 demonstrate the fabrications of M_1O, M_2O and M_2OM microcapsules, respectively.

6.2.2 Characterisations of the synthesised M_1, M_2, M_1O, M_2O and M_2OM microcapsules with KCl/allura red encapsulated

The morphologies of the as-prepared samples were observed by optical microscopes (IX71, Olympus and 301-371.011, Leica, Germany), SEM (JSM-6700F) and TEM (JEOL-1400). The

size distributions including the mean size (D_{32}) and SPAN were tested by a laser scattering Mastersizer 2000 (Malvern Instruments, UK). The EDX mapping was performed on a high resolution transmission electron microscope (HRTEM, Philips Tecnai F20) with an EDX detector (X-MAX 80 TLE, Oxford Instruments, Oxford, UK). XPS was obtained by an X-ray photoelectron spectrometer (ESCALab MKII) utilising Mg Kα radiation as an excitation source. FTIR spectra were detected from 4000 to 400 cm^{-1} at room temperature by a FTIR spectrometer (Bruker Vector-22). TGA was recorded on a TG thermal analyser (Perkin Elmer Diamond) from room temperature to 800 °C with a heating rate of 10 °C min^{-1} under N$_2$ ambience. Water contact angle measurements were carried out on a CAST 2.0 contact-angle-analysis system (Data-Physics, Germany). The concentrations of K$^+$ ions and allura red solutions were determined by ICP-EMS (optima 7300 DV, PerkinElmer) and UV spectrophotometer at 504 nm (Cecil 2021), respectively.

6.3 Results and discussions

6.3.1 Synthesis of MOM microcapsules

The MOM microcapsules were designed to comprise two melamine formaldehyde (MF) layers (inner shell and outer shell) with an intervening hydrolysed octadecyltrichlorosilane (OTS) layer located between them, synthesised by two in-situ polymerisation steps and a simple dropwise coating step (Scheme 1). The water-in-oil (W/O) emulsion was initially formed with an active ingredient and melamine formaldehyde precondensate (MFP) dispersed homogeneously in the aqueous core in a beaker (Φ 65 mm $\times$ 95 mm with standard configuration including 4 baffles) at a stirring speed of 800 rpm by a Rushton turbine (Φ 31 mm), whose pH was adjusted to 4.3. (Step 1, Scheme 6.1). The self-assembled MFP gradually formed in aqueous phase and migrated to the interface of water and oil, producing an unripened MF inner

layer of microcapsules named as unripened M microcapsules, whose morphologies were affected by the content of a surfactant (polyglycerol polyricinoleate, PGPR). The aqueous core was located near the edge of water and oil interface at the condition of a low amount of PGPR (0.05 g), forming the microcapsule with "acorn" morphology named as M_1 microcapsule (ripened) after polymerisation, while the one was in the centre for the high content of PGPR (0.2 g), obtaining a microcapsule with core-shell structure named as M_2 microcapsule (ripened) (Step 2, Scheme 6.1). All of the microcapsules without mentioned ripened or unripened default to ripened as an abbreviation. OTS was then added dropwise into the emulsion, and hydrolysed after meeting the moisture of the M microcapsule surface, creating a hydrophobic alkylsilane self-assembled monolayer (SAM) onto the surface of M microcapsule via the interaction between alkylsilane compounds of OTS and amine groups of MF (Step 3, Scheme 6.1). The formed M_2-OTS microcapsules, named M_2O microcapsules were harvested by centrifugation and were finally coated with an outer layer of MF, whose procedure was based on the previous research[299] (Step 4, Scheme 6.1). Briefly, MFP and poly(acrylamide-acrylic acid) copolymer were firstly dissolved in deionised water (DIW), where they pre-cross-linked at pH 4.3 overnight (around 15 h) (Step 4.1, Scheme 6.1). Half amount of the slurry of preformed M_2O microcapsules in vegetable oil was then poured into the above aqueous solution, which were stirred to form an oil-in-water emulsion (Step 4.2, Scheme 6.1). The pre-cross-linked polymers finally deposited onto the surface of M_2O microcapsules, forming the M_2OM microcapsules after polymerisation via heating and controlling the acidity (Step 4.3, Scheme 6.1).
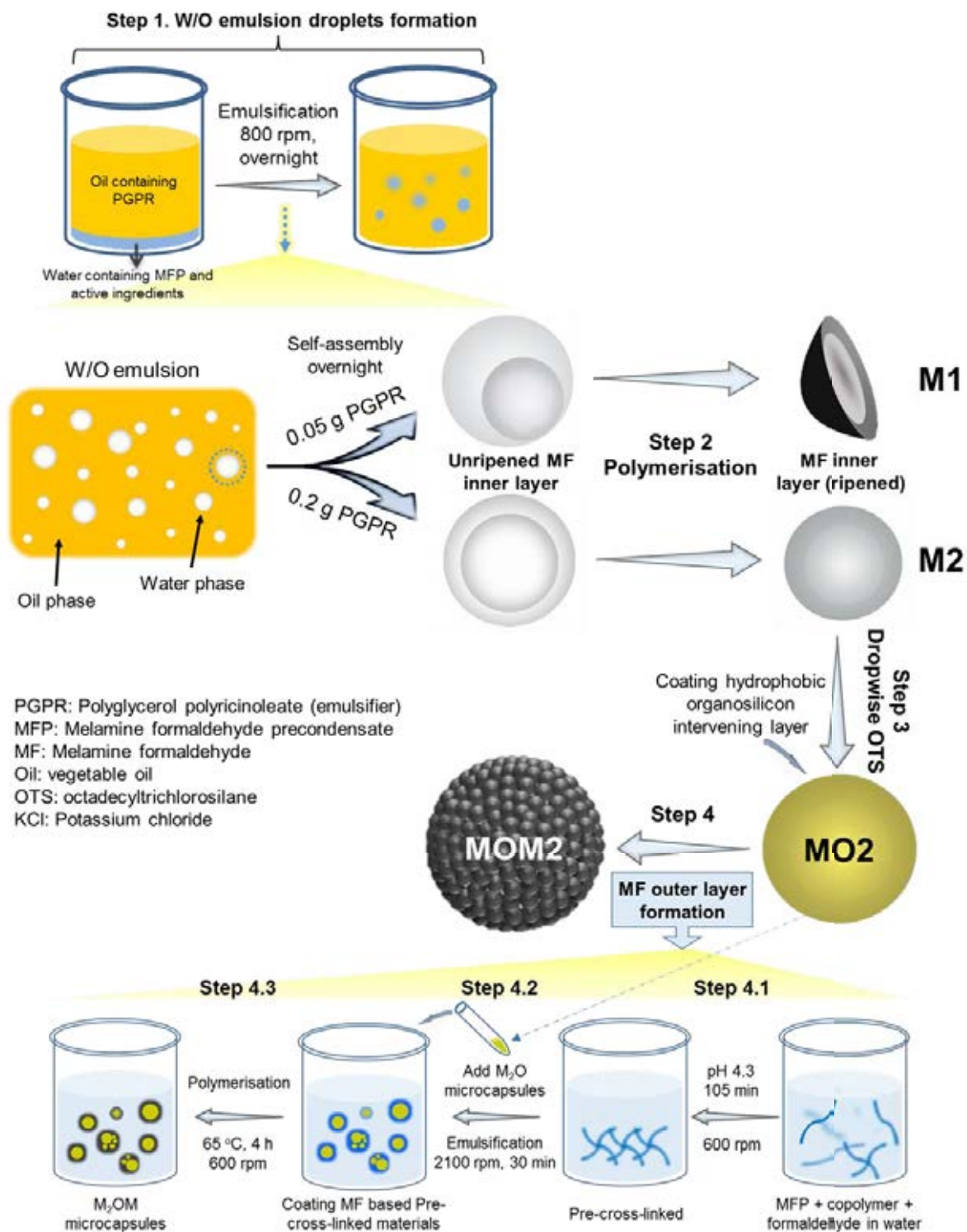
Scheme 6.1 Simple fabrication scheme of the M₂OM microcapsules with an active ingredient encapsulated via two in-situ polymerisation steps and one dropwise coating step.

6.3.2 Characterisations of M, MO and MOM microcapsules

The unripened M-KCl microcapsules were initially formed after emulsification overnight as shown in Fig. 6.1a and 6.1d. The ones obtained with less PGPR showed an off-centred core-shell structure (Fig. 6.1a) with larger mean diameter, while for the ones formed with more PGPR, they mostly displayed the aqueous cores in the centre with smaller mean size. The different sizes of the unripened M-KCl microcapsules were due to the different interfacial tensions caused by different contents of surfactant.[300] Both of the two types of the above unripened M-KCl microcapsules were ripened after the polymerisation. The M_1-KCl microcapsules with less PGPR displayed "acorn"-like morphologies (Fig. 6.1b), while the M_2-KCl microcapsules with more PGPR revealed spherical shapes (Fig. 6.1e). Both of the M_1-KCl and M_2-KCl microcapsules showed the smooth surfaces. The dropwise added OTS was then hydrolysed and further interacted with the surface of M-KCl microcapsules, when it met the absorbed surface water or the entrapped water in the inner side of the M-KCl microcapsules. Interestingly, the M_1-KCl microcapsules were comparatively weak during the coating process of alkylsilane SAM due to their weak shell, forming the broken M_1-OTS-KCl microcapsules, named M_1O-KCl microcapsules as shown in Fig. 6.1c. The M_1O-KCl sample powder displayed a water contact angle of 129.2 ± 0.2^o, revealing a hydrophobic property after silanisation. On the contrary, an intact spherical structure is shown in Fig. 6.1f with a water contact angle of 144.1 ± 0.5^o after the silanisation process of M_2-KCl microcapsules for the M_2-OTS-KCl microcapsules (named M_2O-KCl microcapsules). The M_2-KCl microcapsules with more surfactant demonstrated stronger mechanical strength due to their uniformly distributed shell, relative to M_1-KCl microcapsules. The weak point of the unevenly distributed shell might tend to be broken up under strong shear force.
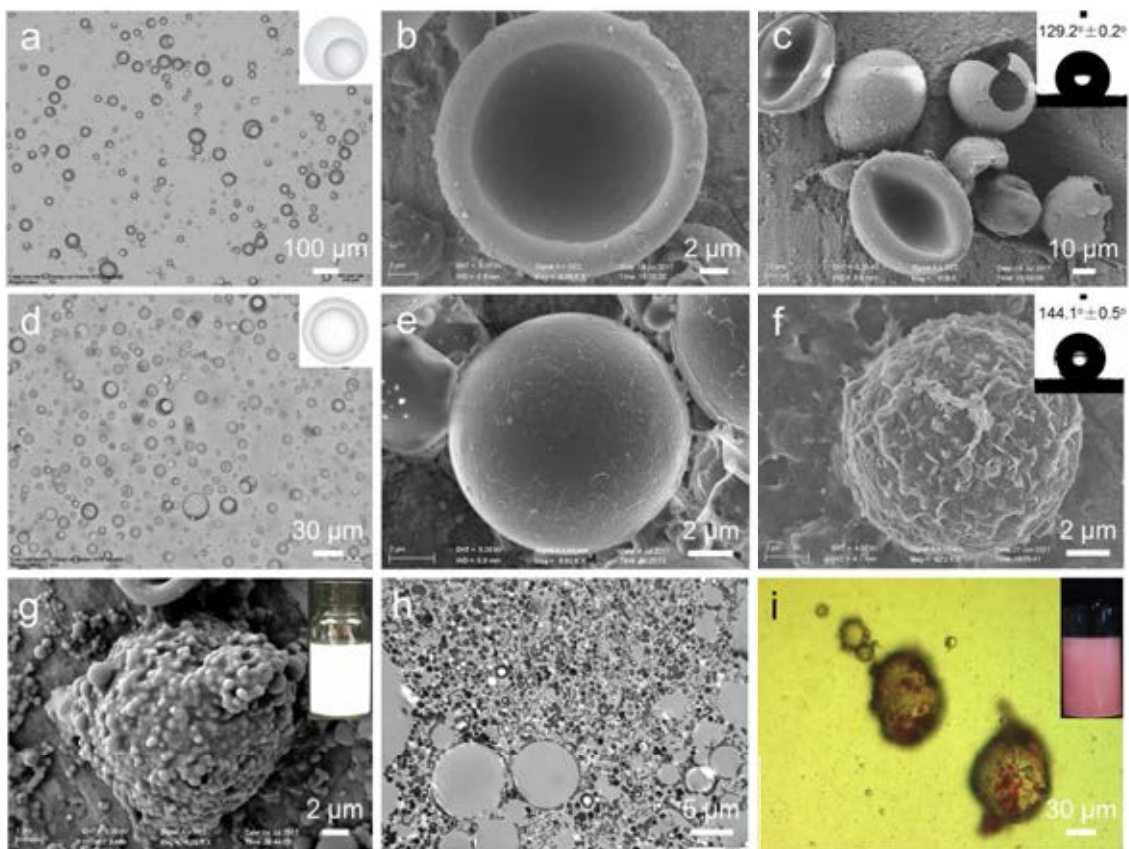
Fig. 6.1 Optical micrographs of (a) unripened M_1-KCl, (d) unripened M_2-KCl and (i) M_2OM-dye microcapsules; SEM images of (b) M_1-KCl, (c) M_1O-KCl, (e) M_2-KCl, (f) M_2O-KCl and (g) M_2OM-KCl microcapsules; (h) TEM image of the ultra-thin cross-section of M_2OM-KCl microcapsules embedded in epon/araldite resin. The insets in panel c and f display the water contact angles of M_1O-KCl and M_2O-KCl microcapsules in sample powder, respectively, and the ones in panel g and i show the digital image of M_2OM-KCl and M_2OM-dye microcapsules dispersed in DIW (1 mg/ml).

After the outer layer of MF was deposited onto the oil slurry droplets containing M_2O-KCl microcapsules, the M_2OM-KCl microcapsules were finally formed with good water dispersibility (Fig. 6.1g). The TEM image of the cross-section of M_2OM-KCl microcapsules embedded in resin revealed the core-shell structure (Fig. 6.1h). The small nanoparticles might be attributed to the off-centred slice of the M_2OM-KCl microcapsules or some tiny silanised M nanocapsules gathered together. For the encapsulation of dye, the optical image of the M_2OM-dye microcapsules displays clearly the structures of the microcapsules with multi-cores (Fig. 6.1i). The composition of the M_2OM-KCl microcapsules is confirmed by the EDX mapping in Fig. 6.2. The C, N, O elements illustrate the shell is composed of MF and the Cl element embedded in the shell indicates the Cl^- ions hydrolysed from OTS were entrapped in the hydrophobic layer in the shell materials. Some of the M_2OM-KCl microcapsules showed multi-cores of M microcapsules coated with alkylsilane SAM dispersed in oil with a coating of cross-linked MF and copolymer outside (Fig. 6.2). The C elements represent the encapsulated oil and epon/araldite resin.
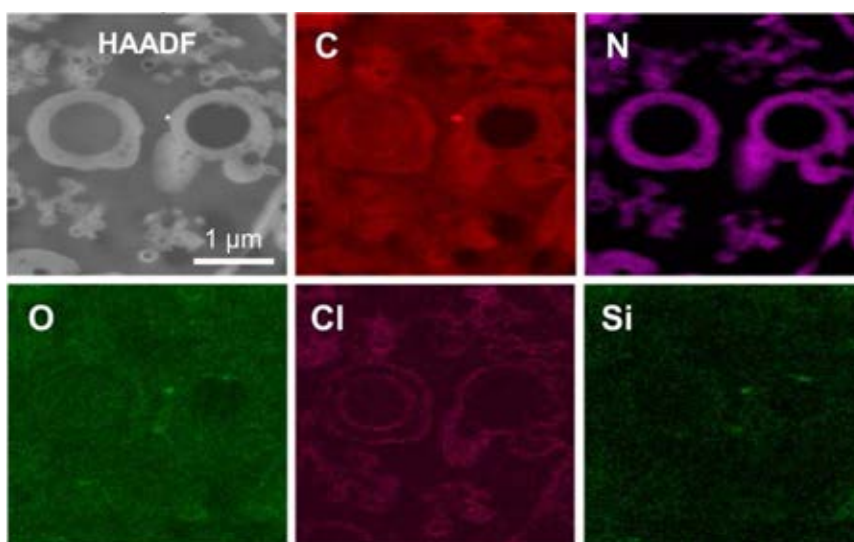
Fig. 6.2 EDX mapping of the cross-section of M_2OM microcapsules embedded in epon/araldite resin.

a

b

c

127
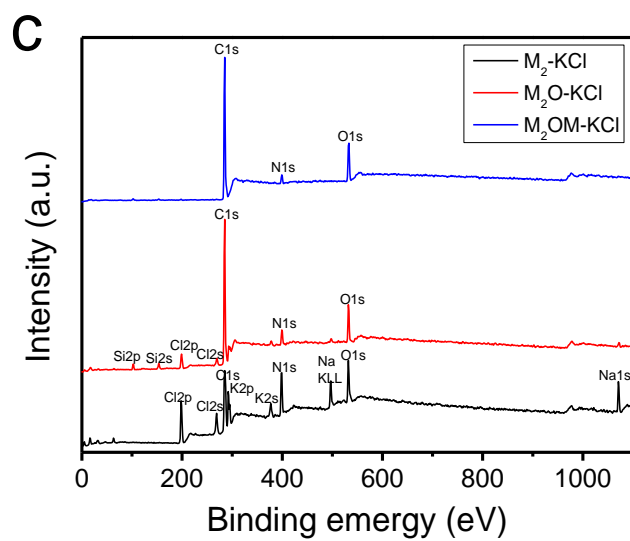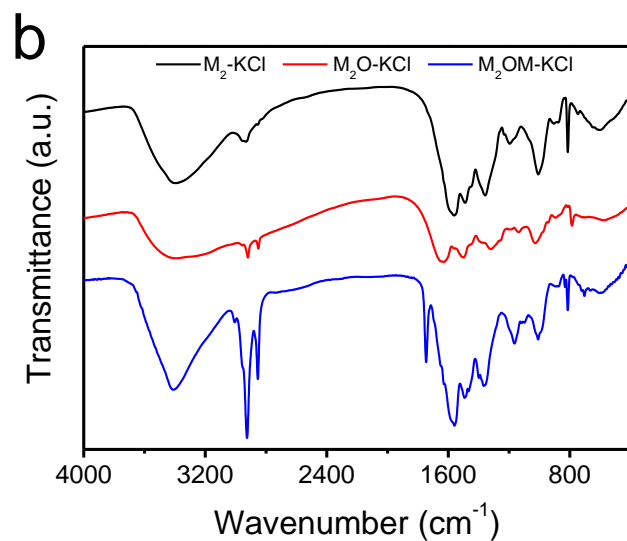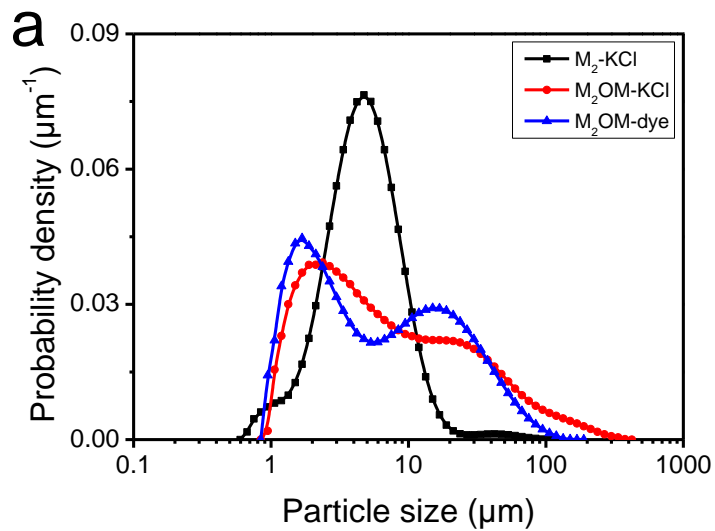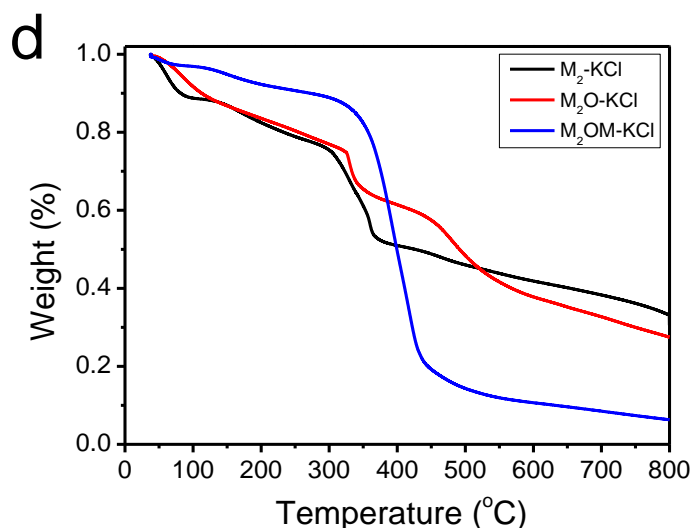
Fig. 6.3 (a) The size distributions of M_2-KCl, M_2OM-KCl and M_2OM-dye microcapsules; (b) The FT-IR, (c) XPS spectra and (d) TGA curves of the M_2-KCl, M_2O-KCl and M_2OM-KCl microcapsules.

The size distributions of the M_2-KCl, M_2OM-KCl and M_2OM-dye microcapsules are shown in Fig. 6.3a. The volume weighted mean sizes (D_{32}) of M_2OM-KCl and M_2OM-dye microcapsules displayed 18.2 ± 0.7 μm (SPAN 3.6 ± 0.3) and 12.26 ± 0.05 μm (SPAN 2.38 ± 0.01), respectively, which were higher than 5.7 ± 0.1 μm (SPAN 2.3 ± 0.7) for the M_2-KCl microcapsules. This might be due to the encapsulation of multiple M_2 microcapsules with oil phase in the outer layer of MF shell. The FT-IR spectrum of M_2-KCl microcapsules in Fig. 6.3b displays the N-H absorption bands at around 813, 1560, and 3400 cm^{-1}, the C-N absorption band at 1358 cm^{-1}, the C-H stretching bands at approximate 1196 and 2933 cm^{-1} and the methylol at roughly 1008 cm^{-1} as the characteristics of MF.[301,302] After the deposition of alkylsilane SAM onto the surface of M_2-KCl microcapsules, the N-H absorption bands disappeared and the new bands emerged at around 1630, 2851 and 2919 cm^{-1} corresponding to the C-H symmetric and antisymmetric stretching of -CH$_2$ group in OTS. The band at 2957 cm^{-1} was attributed to the C-H stretching mode of terminal -CH$_3$ group, indicating the

128

formation of densely assembled monolayer of alkylsilane for the M$_2$O-KCl microcapsules.[303] The peaks at roughly 787, 1028 and 1138 cm^{-1} corresponded to the formation of Si-O-Si bond, and the decreased broad peak of water at 3400 cm^{-1} revealed the transition from hydrophilic to hydrophobic surface.[304] After the formation of the outer layer of MF, the reappearances of N-H, C-N, methylol bands in Fig. 6.3b illustrated the formation of MF, and the strong peaks at 2854 and 2925 cm^{-1} corresponded to the carbon backbone of copolymer.[277]

The chemical compositions of the microcapsule samples were determined by XPS. The XPS spectrum of M$_2$-KCl displays the elements of C, N, O, K and Cl, while the M$_2$O-KCl shows nearly total disappearance of K peaks, the appearance of another Si element and a stronger C peak, indicating the coating of alkylsilane layer onto the surface of M$_2$-KCl microcapsules (Fig. 6.3c). The M$_2$OM-KCl microcapsules displayed C, N and O elements, which illustrated the M$_2$O-KCl microcapsules were encapsulated by the MF outer layer. The thermal properties of the formed microcapsules were determined by TGA as shown in Fig. 6.3d. In case of M$_2$-KCl microcapsules, the weight loss before 100 $^{\circ}$C was attributed to the evaporation of the absorbed water on the microcapsules. The main weight loss starting from 100 $^{\circ}$C was due to the slow release of the encapsulated aqueous core, followed by the mass loss from 300 to 370 $^{\circ}$C, which should be ascribed to the release out of the encapsulated aqueous core by the breakage of microcapsule shell. The mass losses in the region of 370-405 $^{\circ}$C and after 405 $^{\circ}$C were assigned to the decompositions of methylene bridges and triazine ring, respectively.[302] Whereas, the M$_2$O-KCl and M$_2$OM-KCl microcapsules displayed delayed significant weight losses starting from 325 $^{\circ}$C, which can be explained by the breakage of the strengthened microcapsule shell, via the coating of alkylsilane SAM onto the surface of MF shells. Clearly, the larger weight loss in the temperature region of 450-550 $^{\circ}$C can be interpreted as the decomposition of alkylsilane for M$_2$O-KCl and M$_2$OM-KCl microcapsules compared with M$_2$-KCl microcapsules, and the sharp mass loss from 325 $^{\circ}$C may be explained by the decomposition

of the encapsulated oil and water phases via the breakages of the outer and inner layers of MF shells for the M$_2$OM-KCl microcapsules.

6.3.3 Release from MOM microcapsules

Regarding the release profile of K$^+$ ions from M$_2$-KCl microcapsules in Fig. 6.4, it demonstrates a 92 ± 2 % release of payload in water within 30 min, while the M$_2$OM microcapsules displayed no release of K$^+$ ions and allura red (dye) molecules in aqueous environment for 1 month. The payloads and encapsulation efficiencies of the M$_2$ and M$_2$OM microcapsules were calculated by Equation 3.8 & 3.9, as summarised in Table 6.1. Both of M$_2$OM-KCl and M$_2$OM-dye microcapsules exhibited more than 80 % in terms of the encapsulation efficiencies, which were higher than the one for M$_2$-KCl microcapsules, due to some tiny M$_2$O-KCl nanocapsules integrated together in the oil slurry and recovered after their further coating by the outer layer of MF.
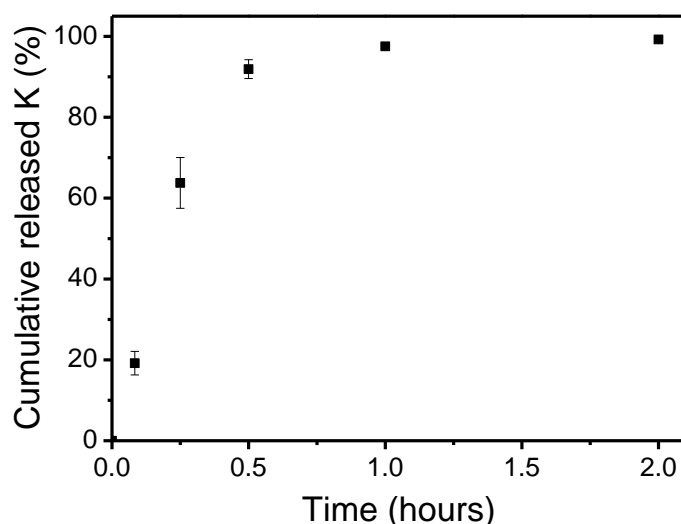
Fig. 6.4 Release profile of K$^+$ ions from M$_2$-KCl microcapsules dispersed in DIW (100 ml) at room temperature at a shaking speed of 150 rpm. (Each experiment was conducted at least 3 times, and the error bars represent s.e.m. (standard error of the mean)).

Table 6.1 The payloads and encapsulation efficiencies of the M_2 and M_2OM microcapsules. The mean value was calculated based on at least triplicate experiments. The error bars represent s.e.m.

Sample	Payload (%)	Encapsulation Efficiency (%)
M_2-KCl	15.0 (± 0.3)	79.3 (± 2)
M_2OM-KCl	4.8 (± 0.4)	86 (± 5)
M_2OM-dye	2.6 (± 0.2)	90 (± 3)

6.4   Conclusions

The morphologies of M_1 and M_2 microcapsules were significantly affected by the amount of PGPR added in the oil phase. A layer of PGPR was initially formed at the interface of water and oil and further interacted with MFP by hydrogen bonds between carboxyl groups of PGPR and amidogen of MF. Regarding the M_2 microcapsules, more surfactant migrated to the interface of water and oil, and their interactions with the self-assembled MFP reinforced the interfacial MF inner shell, leading to the formation of the cores located in the centre of the unripened M_2 microcapsules (Fig. 6.1d) and the core-shell structure after polymerisation. Whereas, the less content of PGPR in the oil fails to cover the interface completely, resulting in the off-centred core-shell structure for the unripened M_1 microcapsules and the "acorn"-shaped microcapsules after polymerisation.

The mechanism for the deposition of alkylsilane SAM on the surface of M microcapsules is attributed to the interactions between alkylsilane compounds of OTS and amine groups of MF. The OTS was firstly hydrolysed, condensed via the formation of silanol groups, when it met the absorbed water on the surface of the M microcapsules. The formed oligomers of OTS by the condensation of OTS monomers further interacted with MF via hydrogen or covalent bonds (Scheme 6.2). The hydrophobic layer of alkylsilane SAM was thus deposited onto the surface

of M microcapsules, which was consistent with the EDX mapping in Fig. 6.2 showing a layer of Cl elements assembling around the outlines of the M$_2$ microcapsules. The EDX mapping also revealed that the Cl⁻ ions hydrolysed from OTS were entrapped in the hydrophobic layer of alkylsilane, which provided a proper barrier to the encapsulated ingredients, achieving no release of inorganic ions and organic dye molecules. Previously, the encapsulation of KCl in saturated polyglycolyed glycerides matrices[121], Eudragit[120] and ethylcellulose[119] microspheres displayed 6-hour sustained release in water, and the organic-inorganic composite microspheres just achieved a 48-hour sustained release of KCl, utilising the interactions between K ions and polymer[305]. To the best of the author's knowledge, it has not been possible to prevent the release of small water soluble ingredients from microcapsules in aqueous environment. Therefore, the novel method presented here offers a way to encapsulate small water soluble ions and molecules with no release in aqueous environment, providing vast applications in FMCGs, agrochemical, printing, energy storage etc.
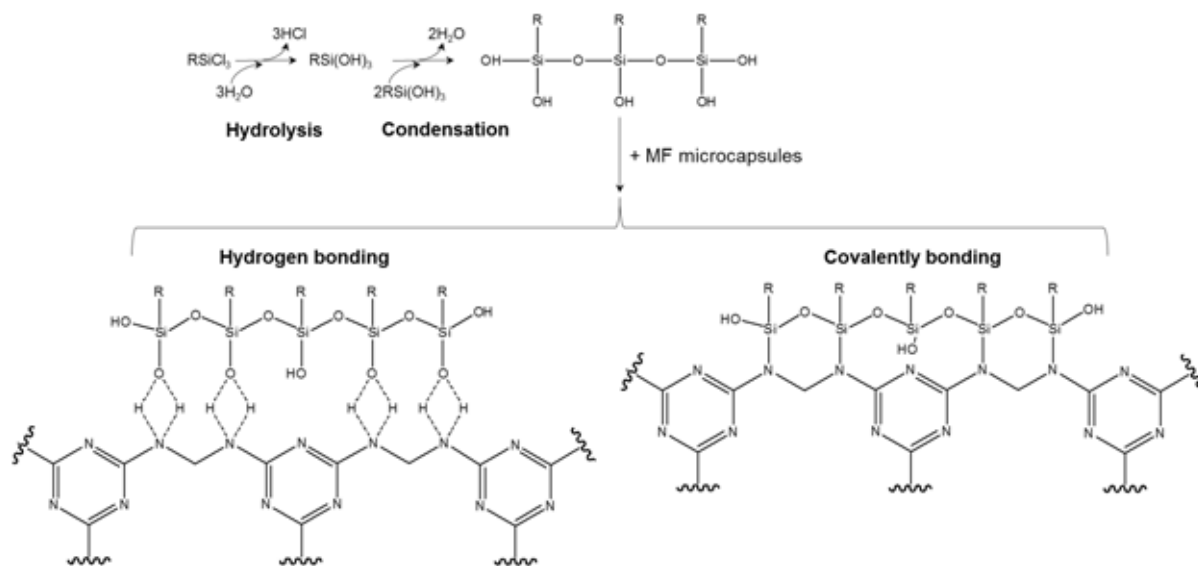
Scheme 6.2 Mechanism of silanisation process of M microcapsules.

Chapter 7 Overall Conclusions and Recommendations for Future Works

7.1 Overall conclusions

There are vast examples of encapsulation for controlled release of hydrophilic or hydrophobic ingredients to the target place at the right time. Whereas, it has not been possible to encapsulate the small water soluble salts or molecules, which can achieve long-term sustained release up to weeks or even no release in water phase. The main objective of the project is to encapsulate small water soluble salts or molecules exhibiting long-term sustained release or no release in the aqueous environment. Three methods were developed here taking KCl and allura red as models of small water soluble ions and molecules respectively, as summarised below in Scheme 7.1:
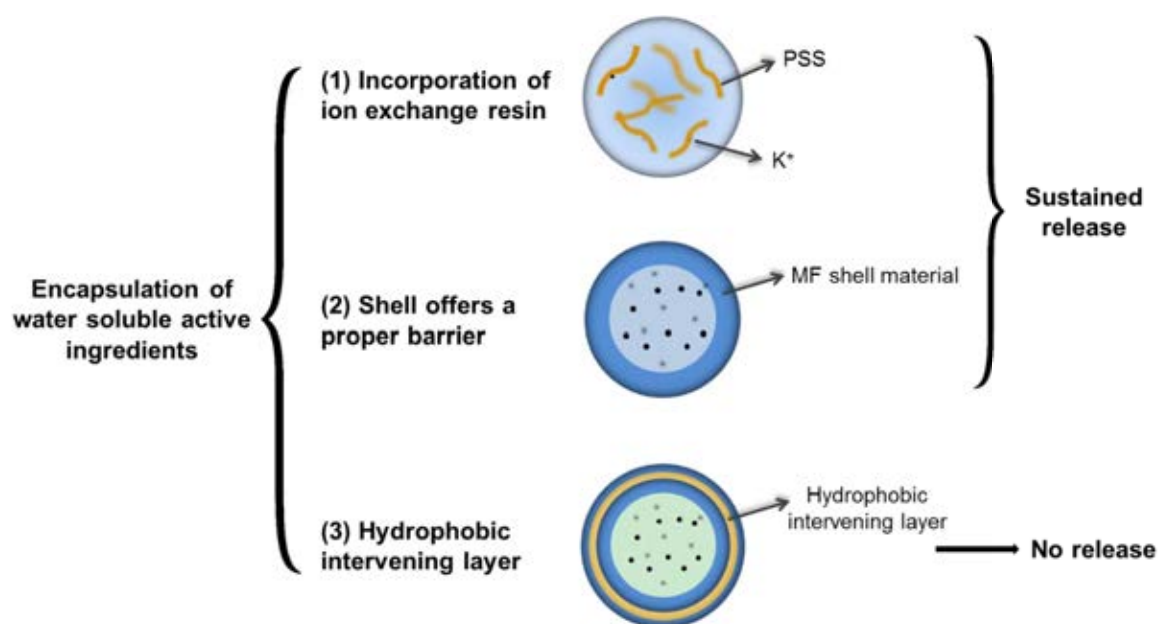
Scheme 7.1 Schematic summary of the three methods to encapsulate water soluble ingredients for long-term sustained/no release in water.

1. Incorporation of oppositely charged ion exchange resins (**Chapter 4**)

A novel type of organic-inorganic composite solid microsphere, comprised of polystyrene sulfonate and silica (PSS-SiO$_2$), has been synthesised from polystyrene sulfonic acid and tetraethyl ortrhosilicate. It reveals a sustained release of K$^+$ ions in aqueous environment for over 48 hours, with a high encapsulation efficiency of $93 \pm 1\%$. The key to achieve the sustained release of ions is the incorporation of oppositely charged ion exchange resins with the active ingredient in the microparticle matrix, where the active ingredients are interacted with the PSS resins. In this case, the release rate of active ingredient is thus delayed, attributed to the interaction between resin and active ingredient. Moreover, the release rates can be controlled by the addition of different amounts of silicon source. A novel dual-release mechanism of the salt from the microspheres, which leads to the sustained release, is proposed and this delivery system may therefore have potential applicability for the controlled and prolonged release of other actives.

2. Melamine formaldehyde based shell materials offering a desirable barrier to the encapsulated active ingredients. (**Chapter 5**)

A novel type of melamine formaldehyde based microcapsules with a desirable barrier has been developed to encapsulate water soluble ingredients, including KCl and allura red (dye) as models of inorganic salt and organic molecule, respectively, *via* an *in situ* polymerisation method. In addition, the melamine formaldehyde based microcapsules were designed to be fabricated in combination with biocompatible shellac or oppositely charged ion exchange resin (polystyrene sulfonate, PSS). They all showed a sustained release of KCl and allura red for 12 h and >10 days in aqueous environment, respectively. The encapsulation efficiency of the

formed MF based microcapsules reached 74 ($\pm$ 4) % and 95 ($\pm$ 2) % for KCl and allura red, respectively.

The MF based microcapsules/microspheres fabricated without copolymer displayed a lower encapsulation efficiency and higher release rate of payloads due to the poor MF shell barrier fabricated without using the copolymer. MF-shellac microspheres exhibited a higher encapsulation efficiency than the rest batches of samples, which may be ascribed to the coating of shellac and the integration of copolymer in the MF materials. MF^{wtc}-PSS microspheres synthesised with the incorporation of PSS ion exchange resin displayed a fast release rate of K^+ ions within 30 min, following by the sustained release up to 12 h. In addition, the formed MF microcapsules displayed Young`s modulus values in the order of GPa, revealing a strong stiffness of the material. Therefore, the developed MF formation method may provide a new way to deliver different types of water soluble ingredients in a sustained way, which may have applications in various areas of scientific research and industry.

3. Hydrophobic intervening layer embedded in the shell material. (**Chapter 6**)

A novel approach to encapsulate small water-soluble ingredients including K^+ ions and allura red molecules has been developed based on the formation of melamine formaldehyde-octadecyltrichlorosilane-melamine formaldehyde (MOM) microcapsules, achieving no release in aqueous environment for 1 month. Two morphological types of MF microcapsules including "acorn" and core-shell structure, can be fabricated via the adjusting the amounts of surfactant. The key for the microcapsules to provide the excellent barrier property to entrap the active ingredients is profited from the sandwich of the hydrophobic material between two melamine formaldehyde shells.

135

It is a breakthrough to prevent the leakage of small water soluble ingredients from the carrier, which is of great significance for their long-term storage until they are delivered to a target place via triggered release in many applications. Also, it is the first time to fabricate the microcapsules with a hydrophobic layer embedded in the shell materials, applied in the delivery of hydrophilic active ingredients. The mechanism to form the MOM microcapsules and their characterisation results have been presented here. The novel encapsulation may afford vast applications in academic research and industries.

7.2 Recommendations for future works

For the microencapsulation, the selection of shell material is very important, since it is strongly related to the end-use of the microcapsules. Biodegradable materials should be considered as the shell materials to fabricate the microcapsules carrying the water soluble active ingredients. Regarding the shell materials embedded with an intervening hydrophobic layer, other types of materials with excellent biocompatibilities, such as calcium based biomaterials, silica, polycaprolactone and organosilicon can be used.

Size and size distribution are significant physical properties for the designed microcapsules, and they strongly affect the end use of the final products, such as payloads, mechanical properties and even release profiles. The wide size distribution of the MOM microcapsules synthesised and presented in Chapter 6, which is attributed to the aggregation of the formed microcapsules, can be reduced by some other methods, e.g. using membrane emulsification. The procedure of the microencapsulation technique needs to be improved for the fabrication of well dispersed microcapsules. The aggregation of the MO microcapsules might be reduced by adding less amount of OTS or utilising another type of hydrophobic materials. Also, the issue may be solved by increasing the stirring speed or using a homogeniser.

Moreover, the mechanical properties of the formed MOM microcapsules should be desirable, which should be confirmed *via* using the micromanipulation technique, and the microcapsules can be designed with different shell thickness by using different F/M (molar ratio) as shell materials, exhibiting different mechanical properties. The microcapsules can be further designed to be ruptured by certain force ranges, which can be applied in different industrial products.

Finally, the no release of the two active ingredients from MOM microcapsules should be demonstrated for a longer period of time, e.g. up to 12 months. In this case, appropriate accelerated release experiments relevant to end applications should be designed. The MOM microcapsules may also be used to achieve the sustained release of active ingredients by adjusting the property of the hydrophobic layer embedded in the shell. The content of OTS solution can be decreased, leading to a thinner or an incontinuous hydrophobic intervening layer. Alternatively, some other types of hydrophobic materials exhibiting lower water contact angle can be selected to be the intervening layer to achieve a sustained release in aqueous environment.

References

1   Ciriminna, R. & Pagliaro, M. Sol-gel microencapsulation of odorants and flavors: opening the route to sustainable fragrances and aromas. *Chem Soc Rev* **42**, 9243-9250 (2013).

2   Ciriminna, R., Sciortino, M., Alonzo, G., de Schrijver, A. & Pagliaro, M. From Molecules to Systems: Sol-Gel Microencapsulation in Silica-Based Materials. *Chem Rev* **111**, 765-789 (2011).

3   Mitragotri, S., Burke, P. A. & Langer, R. Overcoming the challenges in administering biopharmaceuticals: formulation and delivery strategies. *Nat Rev Drug Discov* **13**, 655-672 (2014).

4   Ross, C., Murdoch, L. C., Freedman, D. L. & Siegrist, R. L. Characteristics of potassium permanganate encapsulated in polymer. *Journal of Environmental Engineering* **131**, 1203-1211 (2005).

5   Kang, N., Hua, I. & Rao, P. S. C. Production and characterization of encapsulated potassium permanganate for sustained release as an in situ oxidant. *Ind Eng Chem Res* **43**, 5187-5193 (2004).

6   Vericella, J. J. *et al.* Encapsulated liquid sorbents for carbon dioxide capture. *Nat Commun* **6**, 6124 (2015).

7   Green, B. K. & Scheicher, L. Pressure Sensitive Record Materials. *US Patent*, no. 2(217):507, Ncr C. (1955).

8   Madene, A., Jacquot, M., Scher, J. & Desobry, S. Flavour encapsulation and controlled release - a review. *Int J Food Sci Tech* **41**, 1-21 (2006).

9   Doinikov, A. A. & Dayton, P. A. Spatio-temporal dynamics of an encapsulated gas bubble in an ultrasound field. *J Acoust Soc Am* **120**, 661-669 (2006).

10   Loscertales, I. G. *et al.* Micro/nano encapsulation via electrified coaxial liquid jets. *Science* **295**, 1695-1698 (2002).

11   Bansode, S. S., Banarjee, S. K., Gaikwad, D. D., Jadhav, S. L. & Thorat, R. M. MICROENCAPSULATION : A REVIEW. *Rev.fac.nal.agr.medellín* **63**, 181-189 (2010).

12   Anders, A. Approaches to rid cathodic arc plasmas of macro- and nanoparticles: a review. *Surf Coat Tech* **120**, 319-330 (1999).

13   Trojer, M. A., Nordstierna, L., Nordin, M., Nyden, M. & Holmberg, K. Encapsulation of actives for sustained release. *Phys Chem Chem Phys* **15**, 17727-17741 (2013).

14   Leonard, A. *et al.* Whole-cell based hybrid materials for green energy production, environmental remediation and smart cell-therapy. *Chem Soc Rev* **40**, 860-885 (2011).

15   Wang, X. L., Zhou, W. Z., Cao, J., Liu, W. C. & Zhu, S. P. Preparation of core-shell $CaCO_3$ capsules via Pickering emulsion templates. *J Colloid Interf Sci* **372**, 24-31 (2012).

16   Zhang, J. *et al.* One-Step Fabrication of Supramolecular Microcapsules from Microfluidic Droplets. *Science* **335**, 690-694 (2012).

17   Fujii, S. *et al.* Hydroxyapatite-armored poly(epsilon-caprolactone) microspheres and hydroxyapatite microcapsules fabricated via a Pickering emulsion route. *J Colloid Interf Sci* **374**, 1-8 (2012).

18   Zhou, W. Z., Cao, J., Liu, W. C. & Stoyanov, S. How Rigid Rods Self-Assemble at Curved Surfaces. *Angew Chem Int Edit* **48**, 378-381 (2009).

19   Desai, K. G. H. & Park, H. J. Recent developments in microencapsulation of food ingredients. *Dry Technol* **23**, 1361-1394 (2005).

20   Lachman, L., Lieberman, H. A. & Kanig, J. L. *The theory and practice of industrial pharmacy*. (Lea and Febiger, 1986).

21   Gibbs, B. F., Kermasha, S., Alli, I. & Mulligan, C. N. Encapsulation in the food industry: a review. *Int J Food Sci Nutr* **50**, 213-224 (1999).

22   Shekhar, K., Madhu, M. N., Pradeep, B. & Banji, D. A review on microencapsulation. *Int. J. Pharm. Sci. Rev. Res* **5**, 58-62 (2010).

23   Beristain, C. I., Vazquez, A., Garcia, H. S. & Vernon-Carter, E. J. Encapsulation of orange peel oil by co-crystallization. *Lwt-Food Sci Technol* **29**, 645-647 (1996).

24   Goubet, I., Le Quere, J.-L. & Voilley, A. Retention of aroma compounds by carbohydrates: influence of their physicochemical characteristics and of their physical state. A review. *J Agr Food Chem* **46**, 1981-1990 (1998).

25   Green, B. K.   (Google Patents, 1955).

26   Dziezak, J. D. Microencapsulation and Encapsulated Ingredients. **42**, 136-151 (1988).

27   Madene, A., Jacquot, M., Scher, J. & Desobry, S. Flavour encapsulation and controlled release– a review. *International journal of food science & technology* **41**, 1-21 (2006).

28   Lakkis, D. J. M. Encapsulation and Controlled Release Technologies in Food Systems, 2nd Edition.

29   Boh, B. & Frère, Y. *Microencapsulation by chemical methods: a solution for the past or future*, <http://bioencapsulation.net/index2-select-newsletter-nl-BI_2013_03.html> (2013).

30   Long, Y., Vincent, B., York, D., Zhang, Z. & Preece, J. A. Organic-inorganic double shell composite microcapsules. *Chem Commun (Camb)* **46**, 1718-1720, doi:10.1039/b911266a (2010).

31   Yuan, L., Liang, G., Xie, J., Li, L. & Guo, J. Preparation and characterization of poly (urea-formaldehyde) microcapsules filled with epoxy resins. *Polymer* **47**, 5338-5349 (2006).

32   Tong, X.-M., Zhang, T., Yang, M.-Z. & Zhang, Q. Preparation and characterization of novel melamine modified poly (urea–formaldehyde) self-repairing microcapsules. *Colloids and Surfaces A: Physicochemical and Engineering Aspects* **371**, 91-97 (2010).

33   Zhang, H. & Wang, X. Fabrication and performances of microencapsulated phase change materials based on n-octadecane core and resorcinol-modified melamine–formaldehyde shell. *Colloids and Surfaces A: Physicochemical and Engineering Aspects* **332**, 129-138 (2009).

34   Chao, H. Y. In-situ polymerization process for producing epoxy microcapsules. (1992).

35   Bône, S. *et al.* Microencapsulated fragrances in melamine formaldehyde resins. *Chimia* **65**, 177-181 (2010).

36   Long, Y., York, D., Zhang, Z. & Preece, J. A. Microcapsules with low content of formaldehyde: Preparation and characterization. *J Mater Chem* **19**, 6882-6887 (2009).

37   Mittal, V. *Encapsulation Nanotechnologies*. (Wiley, 2013).

38   Arshady, R. *Microspheres Microcapsules & Liposomes: Preparation & Chemical Applications*. (Citus Books, 1999).

39   Blythe, D., Churchill, D., Glanz, K. & Stutz, J. Microcapsules for carbonless copy paper: Industrial and commercial aspects. *MML SERIES* **1**, 419 (1999).

40   Šumiga, B. *et al.* Production of Melamine-Formaldehyde PCM Microcapsules with Ammonia Scavenger used for Residual Formaldehyde Reduction. *Acta Chimica Slovenica* **58** (2011).

41   Li, W., Zhang, X.-X., Wang, X.-C. & Niu, J.-J. Preparation and characterization of microencapsulated phase change material with low remnant formaldehyde content. *Mater Chem Phys* **106**, 437-442 (2007).

42   Brown, E. N., Kessler, M. R., Sottos, N. R. & White, S. R. In situ poly (urea-formaldehyde) microencapsulation of dicyclopentadiene. *J Microencapsul* **20**, 719-730 (2003).

43   Mishra, M. *Handbook of encapsulation and controlled release*. (CRC Press, 2015).

44   Perignon, C., Ongmayeb, G., Neufeld, R., Frere, Y. & Poncelet, D. Microencapsulation by interfacial polymerisation: membrane formation and structure. *J Microencapsul* **32**, 1-15 (2015).

45   Chang, T. M. Semipermeable microcapsules. *Science* **146**, 524-525 (1964).

46   Tiwari, S. & Verma, P. Microencapsulation technique by solvent evaporation method (Study of effect of process variables). *International journal of pharmacy & life sciences* **2** (2011).

47   Freitas, S., Merkle, H. P. & Gander, B. Microencapsulation by solvent extraction/evaporation: reviewing the state of the art of microsphere preparation process technology. *J Control Release* **102**, 313-332 (2005).

48   Chung, T.-W., Huang, Y.-Y. & Liu, Y.-Z. Effects of the rate of solvent evaporation on the characteristics of drug loaded PLLA and PDLLA microspheres. *Int J Pharm* **212**, 161-169 (2001).

49   Chung, T.-W., Huang, Y.-Y., Tsai, Y.-L. & Liu, Y.-Z. Effects of solvent evaporation rate on the properties of protein-loaded PLLA and PDLLA microspheres fabricated by emulsion-solvent evaporation process. *J Microencapsul* **19**, 463-471 (2002).

50   Kim, T. K., Yoon, J. J., Lee, D. S. & Park, T. G. Gas foamed open porous biodegradable polymeric microspheres. *Biomaterials* **27**, 152-159 (2006).

51   Leo, E., Pecquet, S., Rojas, J., Couvreur, P. & Fattal, E. Changing the pH of the external aqueous phase may modulate protein entrapment and delivery from poly (lactide-co-glycolide) microspheres prepared by aw/o/w solvent evaporation method. *J Microencapsul* **15**, 421-430 (1998).

52   Yang, Y.-Y., Chia, H.-H. & Chung, T.-S. Effect of preparation temperature on the characteristics and release profiles of PLGA microspheres containing protein fabricated by double-emulsion solvent extraction/evaporation method. *J Control Release* **69**, 81-96 (2000).

53   Donath, E., Sukhorukov, G. B., Caruso, F., Davis, S. A. & Möhwald, H. Novel hollow polymer shells by colloid‐templated assembly of polyelectrolytes. *Angewandte Chemie International Edition* **37**, 2201-2205 (1998).

54   Sukhorukov, G. B. *et al.* Stepwise polyelectrolyte assembly on particle surfaces: a novel approach to colloid design. *Polym Advan Technol* **9**, 759-767 (1998).

55   Caruso, F., Caruso, R. A. & Möhwald, H. Nanoengineering of inorganic and hybrid hollow spheres by colloidal templating. *Science* **282**, 1111-1114 (1998).

56   Shchukina, E. M. & Shchukin, D. G. LbL coated microcapsules for delivering lipid-based drugs. *Adv Drug Deliver Rev* **63**, 837-846 (2011).

57   Grigoriev, D., Bukreeva, T., Möhwald, H. & Shchukin, D. New method for fabrication of loaded micro-and nanocontainers: emulsion encapsulation by polyelectrolyte layer-by-layer deposition on the liquid core. *Langmuir* **24**, 999-1004 (2008).

58   Volodkin, D. V., Larionova, N. I. & Sukhorukov, G. B. Protein encapsulation via porous CaCO3 microparticles templating. *Biomacromolecules* **5**, 1962-1972, doi:Doi 10.1021/Bm049669e (2004).

59   Sukhorukov, G. B. *et al.* Porous calcium carbonate microparticles as templates for encapsulation of bioactive compounds. *J Mater Chem* **14**, 2073-2081 (2004).

60   Volodkin, D. V., Petrov, A. I., Prevot, M. & Sukhorukov, G. B. Matrix polyelectrolyte microcapsules: new system for macromolecule encapsulation. *Langmuir* **20**, 3398-3406 (2004).

61   Baschong, W. *et al.* Dedication - Delivery System Handbook for Personal Care and Cosmetic Products. *Delivery System Handbook for Personal Care & Cosmetic Products*, III (2005).

62   Rosen, M. *Delivery system handbook for personal care and cosmetic products: technology, applications and formulations*. (William Andrew, 2005).

63   Xue, J. & Zhang, Z. B. Physical, Structural, and Mechanical Characterization of Calcium-Shellac Microspheres as a Carrier of Carbamide Peroxide. *J Appl Polym Sci* **113**, 1619-1625 (2009).

64   White, M. A. The chemistry behind carbonless copy paper. *J Chem Educ* **75**, 1119-1120 (1998).

65   Kromidas, L., Perrier, E., Flanagan, J., Rivero, R. & Bonnet, I. Release of antimicrobial actives from microcapsules by the action of axillary bacteria. *Int J Cosmetic Sci* **28**, 103-108 (2006).

66   Paramonov, S. E. *et al.* Fully acid-degradable biocompatible polyacetal microparticles for drug delivery. *Bioconjugate Chem* **19**, 911-919 (2008).

67   Wang, Z., Qian, L., Wang, X., Yang, F. & Yang, X. Construction of hollow DNA/PLL microcapsule as a dual carrier for controlled delivery of DNA and drug. *Colloids and Surfaces A: Physicochemical and Engineering Aspects* **326**, 29-36 (2008).

68   Wells, J. I. *Pharmaceutical Technology: Controlled Drug Release Vol 2: Controlled Drug Release*. Vol. 2 (CRC Press, 1991).

69   Huang, S.-L. Liposomes in ultrasonic drug and gene delivery. *Adv Drug Deliver Rev* **60**, 1167-1176 (2008).

70   Shchukin, D. G., Grigoriev, D. O. & Möhwald, H. Application of smart organic nanocontainers in feedback active coatings. *Soft Matter* **6**, 720-725 (2010).

71   Esser-Kahn, A. P., Sottos, N. R., White, S. R. & Moore, J. S. Programmable microcapsules from self-immolative polymers. *J Am Chem Soc* **132**, 10266-10268 (2010).

72   Fomina, N., McFearin, C., Sermsakdi, M., Edigin, O. & Almutairi, A. UV and near-IR triggered release from polymeric nanoparticles. *J Am Chem Soc* **132**, 9540-9542 (2010).

73   Qi, W. *et al.* Triggered release of insulin from glucose-sensitive enzyme multilayer shells. *Biomaterials* **30**, 2799-2806 (2009).

74   Lu, Z. *et al.* Magnetic switch of permeability for polyelectrolyte microcapsules embedded with Co@ Au nanoparticles. *Langmuir* **21**, 2042-2050 (2005).

75   Shi, X.-Y. & Tan, T.-W. Preparation of chitosan/ethylcellulose complex microcapsule and its application in controlled release of Vitamin D 2. *Biomaterials* **23**, 4469-4473 (2002).

76   Floyd, J. A., Galperin, A. & Ratner, B. D. Drug encapsulated polymeric microspheres for intracranial tumor therapy: a review of the literature. *Adv Drug Deliver Rev* **91**, 23-37 (2015).

77   Loira-Pastoriza, C., Todoroff, J. & Vanbever, R. Delivery strategies for sustained drug release in the lungs. *Adv Drug Deliver Rev* **75**, 81-91 (2014).

78   Sun, T. *et al.* Engineered nanoparticles for drug delivery in cancer therapy. *Angewandte Chemie International Edition* **53**, 12320-12364 (2014).

79   Maderuelo, C., Zarzuelo, A. & Lanao, J. M. Critical factors in the release of drugs from sustained release hydrophilic matrices. *J Control Release* **154**, 2-19 (2011).

80   Bassindale, A. R., Pourny, M., Taylor, P. G., Hursthouse, M. B. & Light, M. E. Fluoride‐Ion Encapsulation within a Silsesquioxane Cage. *Angewandte Chemie International Edition* **42**, 3488-3490 (2003).

81   Liu, M., Saman, W. & Bruno, F. Review on storage materials and thermal performance enhancement techniques for high temperature phase change thermal storage systems. *Renewable and Sustainable Energy Reviews* **16**, 2118-2132 (2012).

82   Oró, E., De Gracia, A., Castell, A., Farid, M. & Cabeza, L. Review on phase change materials (PCMs) for cold thermal energy storage applications. *Applied Energy* **99**, 513-533 (2012).

83   Munin, A. & Edwards-Lévy, F. Encapsulation of natural polyphenolic compounds; a review. *Pharmaceutics* **3**, 793-829 (2011).

84   Caruso, F., Trau, D., Möhwald, H. & Renneberg, R. Enzyme encapsulation in layer-by-layer engineered polymer multilayer capsules. *Langmuir* **16**, 1485-1488 (2000).

85   Yu, A., Wang, Y., Barlow, E. & Caruso, F. Mesoporous Silica Particles as Templates for Preparing Enzyme‐Loaded Biocompatible Microcapsules. *Adv Mater* **17**, 1737-1741 (2005).

86   Natarajan, J. V., Nugraha, C., Ng, X. W. & Venkatraman, S. Sustained-release from nanocarriers: a review. *J Control Release* **193**, 122-138 (2014).

87   Ul‐Islam, M., Khan, S., Ullah, M. W. & Park, J. K. Structure, Chemistry and Pharmaceutical Applications of Biodegradable Polymers. *Handbook of Polymers for Pharmaceutical Technologies: Biodegradable Polymers, Volume 3*, 517-540 (2015).

88   Nair, L. S. & Laurencin, C. T. Biodegradable polymers as biomaterials. *Progress in polymer science* **32**, 762-798 (2007).

89   Sairam, M., Babu, V. R., Naidu, B. V. K. & Aminabhavi, T. M. Encapsulation efficiency and controlled release characteristics of crosslinked polyacrylamide particles. *Int J Pharm* **320**, 131-136 (2006).

90   Song, W., He, Q., Möhwald, H., Yang, Y. & Li, J. Smart polyelectrolyte microcapsules as carriers for water-soluble small molecular drug. *Journal of Controlled Release* **139**, 160-166 (2009).

91   Chavanpatil, M. D., Khdair, A. & Panyam, J. Surfactant-polymer nanoparticles: a novel platform for sustained and enhanced cellular delivery of water-soluble molecules. *Pharm Res* **24**, 803-810 (2007).

92   Zhao, Y. *et al.* A Preloaded Amorphous Calcium Carbonate/Doxorubicin@ Silica Nanoreactor for pH‑Responsive Delivery of an Anticancer Drug. *Angewandte Chemie International Edition* **54**, 919-922 (2015).

93   Gilbert, N.   (Nature Publishing Group, 2009).

94   Chechik, V., Zhao, M. & Crooks, R. M. Self-assembled inverted micelles prepared from a dendrimer template: phase transfer of encapsulated guests. *J Am Chem Soc* **121**, 4910-4911 (1999).

95   Meier, W. Polymer nanocapsules. *Chem Soc Rev* **29**, 295-303 (2000).

96   Keen, P. H., Slater, N. K. & Routh, A. F. Encapsulation of amylase in colloidosomes. *Langmuir* **30**, 1939-1948 (2014).

97   Khan, N. & Mukhtar, H. Tea polyphenols for health promotion. *Life sciences* **81**, 519-533 (2007).

98   Shutava, T. G. *et al.* Layer-by-layer-coated gelatin nanoparticles as a vehicle for delivery of natural polyphenols. *Acs Nano* **3**, 1877-1885 (2009).

99   Zhou, H. *et al.* Fabrication of biopolymeric complex coacervation core micelles for efficient tea polyphenol delivery via a green process. *Langmuir* **28**, 14553-14561 (2012).

100   Liang, J. *et al.* Synthesis, characterization and cytotoxicity studies of chitosan-coated tea polyphenols nanoparticles. *Colloids and Surfaces B: Biointerfaces* **82**, 297-301 (2011).

101   Srivastava, A. K. *et al.* Synthesis of PLGA nanoparticles of tea polyphenols and their strong in vivo protective effect against chemically induced DNA damage. *Int J Nanomed* **8**, 1451 (2013).

102   Shao, S. *et al.* Controlled green tea polyphenols release from electrospun PCL/MWCNTs composite nanofibers. *Int J Pharm* **421**, 310-320 (2011).

103   Zou, L.-q. *et al.* Characterization and bioavailability of tea polyphenol nanoliposome prepared by combining an ethanol injection method with dynamic high-pressure microfluidization. *J Agr Food Chem* **62**, 934-941 (2014).

104   Lu, Q., Li, D.-C. & Jiang, J.-G. Preparation of a tea polyphenol nanoliposome system and its physicochemical properties. *J Agr Food Chem* **59**, 13004-13011 (2011).

105   Fang, J.-Y., Hwang, T.-L., Huang, Y.-L. & Fang, C.-L. Enhancement of the transdermal delivery of catechins by liposomes incorporating anionic surfactants and ethanol. *Int J Pharm* **310**, 131-138 (2006).

106   Fang, J.-Y., Lee, W.-R., Shen, S.-C. & Huang, Y.-L. Effect of liposome encapsulation of tea catechins on their accumulation in basal cell carcinomas. *Journal of dermatological science* **42**, 101-109 (2006).

107   Zheng, L., Ding, Z., Zhang, M. & Sun, J. Microencapsulation of bayberry polyphenols by ethyl cellulose: Preparation and characterization. *J Food Eng* **104**, 89-95 (2011).

108   Harris, R., Lecumberri, E., Mateos-Aparicio, I., Mengíbar, M. & Heras, A. Chitosan nanoparticles and microspheres for the encapsulation of natural antioxidants extracted from Ilex paraguariensis. *Carbohyd Polym* **84**, 803-806 (2011).

109   Taylor, J., Taylor, J. R., Belton, P. S. & Minnaar, A. Kafirin microparticle encapsulation of catechin and sorghum condensed tannins. *J Agr Food Chem* **57**, 7523-7528 (2009).

110   Gavini, E., Alamanni, M., Cossu, M. & Giunchedi, P. Tabletted microspheres containing Cynara scolymus (var. Spinoso sardo) extract for the preparation of controlled release nutraceutical matrices. *J Microencapsul* **22**, 487-499 (2005).

111   Sosa, M., Rodríguez-Rojo, S., Mattea, F., Cismondi, M. & Cocero, M. Green tea encapsulation by means of high pressure antisolvent coprecipitation. *The Journal of Supercritical Fluids* **56**, 304-311 (2011).

112   Xue, J. & Zhang, Z. Preparation and characterization of calcium-shellac spheres as a carrier of carbamide peroxide. *J Microencapsul* **25**, 523-530 (2008).

113   Xue, J. & Zhang, Z. Physical, structural, and mechanical characterization of calcium–shellac microspheres as a carrier of carbamide peroxide. *J Appl Polym Sci* **113**, 1619-1625 (2009).

114   Bednarz, S., Ryś, B. & Bogdał, D. Application of hydrogen peroxide encapsulated in silica xerogels to oxidation reactions. *Molecules* **17**, 8068-8078 (2012).

115   Murillo, M., Gamazo, C., Goñi, M., Irache, J. M. & Blanco-Príeto, M. Development of microparticles prepared by spray-drying as a vaccine delivery system against brucellosis. *Int J Pharm* **242**, 341-344 (2002).

116   Jamnongkan, T. & Kaewpirom, S. Potassium release kinetics and water retention of controlled-release fertilizers based on chitosan hydrogels. *Journal of Polymers and the Environment* **18**, 413-421 (2010).

117   Tronto, J. *et al.* In vitro release of citrate anions intercalated in magnesium aluminium layered double hydroxides. *J Phys Chem Solids* **65**, 475-480 (2004).

118   Gowda, D. & Shivakumar, H. Preparation and evaluation of waxes/fat microspheres loaded with lithium carbonate for controlled release. *Indian Journal of Pharmaceutical Sciences* **69**, 251-256 (2007).

119   Wu, P.-C., Huang, Y.-B., Chang, J.-I., Tsai, M.-J. & Tsai, Y.-H. Preparation and evaluation of sustained release microspheres of potassium chloride prepared with ethylcellulose. *Int J Pharm* **260**, 115-121 (2003).

120   Wu, P.-C., Huang, Y.-B., Chang, J.-S., Tsai, M.-J. & Tsai, Y.-H. Design and evaluation of sustained release microspheres of potassium chloride prepared by Eudragit®. *Eur J Pharm Sci* **19**, 115-122 (2003).

121   Wu, P.-C., Tsai, M.-J., Huang, Y.-B., Chang, J.-S. & Tsai, Y.-H. In vitro and in vivo evaluation of potassium chloride sustained release formulation prepared with saturated polyglycolyed glycerides matrices. *Int J Pharm* **243**, 119-124 (2002).

122   Jarosiewicz, A. & Tomaszewska, M. Controlled-release NPK fertilizer encapsulated by polymeric membranes. *J Agr Food Chem* **51**, 413-417 (2003).

123   Bonnet, M. *et al.* Release rate profiles of magnesium from multiple W/O/W emulsions. *Food Hydrocolloid* **23**, 92-101 (2009).

124   Bonnet, M., Cansell, M., Placin, F., Anton, M. & Leal-Calderon, F. Impact of sodium caseinate concentration and location on magnesium release from multiple W/O/W emulsions. *Langmuir* **26**, 9250-9260 (2010).

125   Bonnet, M. *et al.* Influence of the oil globule fraction on the release rate profiles from multiple W/O/W emulsions. *Colloids and Surfaces B: Biointerfaces* **78**, 44-52 (2010).

126   Herzi, S., Essafi, W., Bellagha, S. & Leal-Calderon, F. Influence of the inner droplet fraction on the release rate profiles from multiple W/O/W emulsions. *Colloids and Surfaces A: Physicochemical and Engineering Aspects* **441**, 489-495 (2014).

127   Cohen-Sela, E., Chorny, M., Koroukhov, N., Danenberg, H. D. & Golomb, G. A new double emulsion solvent diffusion technique for encapsulating hydrophilic molecules in PLGA nanoparticles. *J Control Release* **133**, 90-95 (2009).

128   Edelstein, A. S. & Cammaratra, R. *Nanomaterials: synthesis, properties and applications*. (CRC press, 1998).

129   Chitnis, G., Ding, Z., Chang, C.-L., Savran, C. A. & Ziaie, B. Laser-treated hydrophobic paper: an inexpensive microfluidic platform. *Lab Chip* **11**, 1161-1165 (2011).

130   Bozzola, J. J. & Russell, L. D. *Electron microscopy: principles and techniques for biologists*. (Jones & Bartlett Learning, 1999).

131   Pluta, M. & Maksymilian, P. *Advanced light microscopy*. Vol. 1 (Elsevier Amsterdam, 1988).

132   Zimmermann, H. *et al.* Fabrication of homogeneously cross-linked, functional alginate microcapsules validated by NMR-, CLSM-and AFM-imaging. *Biomaterials* **24**, 2083-2096 (2003).

133   Cheeke, J. D. N. *Fundamentals and applications of ultrasonic waves*. (CRC press, 2012).

134   Huber, A. J., Keilmann, F., Wittborn, J., Aizpurua, J. & Hillenbrand, R. Terahertz near-field nanoscopy of mobile carriers in single semiconductor nanodevices. *Nano Lett* **8**, 3766-3770 (2008).

135   Jensen, E. Types of Imaging, Part 3: Atomic Force Microscopy. *The Anatomical Record* **296**, 179-183 (2013).

136   Weisenburger, S. & Sandoghdar, V. Light microscopy: an ongoing contemporary revolution. *Contemporary Physics* **56**, 123-143 (2015).

137   Evers, C. H., Luiken, J. A., Bolhuis, P. G. & Kegel, W. K. Self-assembly of microcapsules via colloidal bond hybridization and anisotropy. *nature* **534**, 364 (2016).

138   Ye, C. *et al.* Robust microcapsules with controlled permeability from silk fibroin reinforced with graphene oxide. *Small* **10**, 5087-5097 (2014).

139   Zhang, Y. *et al.* Investigation on the uniformity and stability of sunflower oil/water emulsions prepared by a Shirasu porous glass membrane. *Ind Eng Chem Res* **47**, 6412-6417 (2008).

140   Aryanti, N., Hou, R. & Williams, R. A. Performance of a rotating membrane emulsifier for production of coarse droplets. *J Membrane Sci* **326**, 9-18 (2009).

141   Webb, P. A. in *Micromeritics Instrument Corp, Technical Workshop Series: Introduction to the Latest, ANSI/ISO Standard for Laser Particle Size Analysis.*

142   Cao, Z., Landfester, K. & Ziener, U. Preparation of dually, pH-and thermo-responsive nanocapsules in inverse miniemulsion. *Langmuir* **28**, 1163-1168 (2011).

143   Rahman, M. M. & Elaissari, A. A versatile method for the preparation of rigid submicron hollow capsules containing a temperature responsive shell. *J Mater Chem* **22**, 1173-1179 (2012).

144   Gray, A., Egan, S., Bakalis, S. & Zhang, Z. Determination of microcapsule physicochemical, structural, and mechanical properties. *Particuology* **24**, 32-43 (2016).

145   Chen, J., Jo, S. & Park, K. Polysaccharide hydrogels for protein drug delivery. *Carbohyd Polym* **28**, 69-76 (1995).

146   Poncelet, D. & Neufeld, R. J. Shear breakage of nylon membrane microcapsules in a turbine reactor. *Biotechnol Bioeng* **33**, 95-103 (1989).

147   Santos, V. *et al.* Relevance of rheological properties of gel beads for their mechanical stability in bioreactors. *TOWARDS THE INTEGRATION OF OXIDATIVE AND REDUCTIVE ACTIVITIES: APPLICATION TO NITROGEN REMOVAL BY CO-IMMOBILIZED MICROORGANISMS*, 131 (1997).

148   Neubauer, M. P., Poehlmann, M. & Fery, A. Microcapsule mechanics: From stability to function. *Adv Colloid Interfac* **207**, 65-80 (2014).

149   Neuman, K. C. & Nagy, A. Single-molecule force spectroscopy: optical tweezers, magnetic tweezers and atomic force microscopy. *Nature methods* **5**, 491 (2008).

150   Lefebvre, Y., Leclerc, E., Barthès-Biesel, D., Walter, J. & Edwards-Lévy, F. Flow of artificial microcapsules in microfluidic channels: a method for determining the elastic properties of the membrane. *Physics of Fluids* **20**, 123102 (2008).

151   She, S., Xu, C., Yin, X., Tong, W. & Gao, C. Shape deformation and recovery of multilayer microcapsules after being squeezed through a microchannel. *Langmuir* **28**, 5010-5016 (2012).

152   Hochmuth, R. M. Micropipette aspiration of living cells. *Journal of biomechanics* **33**, 15-22 (2000).

153   Kim, D.-H., Wong, P. K., Park, J., Levchenko, A. & Sun, Y. Microengineered platforms for cell mechanobiology. *Annual review of biomedical engineering* **11**, 203-233 (2009).

154   Dieluweit, S. *et al.* Mechanical properties of bare and protein-coated giant unilamellar phospholipid vesicles. A comparative study of micropipet aspiration and atomic force microscopy. *Langmuir* **26**, 11041-11049 (2010).

155   Olbrich, K., Rawicz, W., Needham, D. & Evans, E. Water permeability and mechanical strength of polyunsaturated lipid bilayers. *Biophysical Journal* **79**, 321-327 (2000).

156   Ratanabanangkoon, P., Gropper, M., Merkel, R., Sackmann, E. & Gast, A. P. Mechanics of streptavidin-coated giant lipid bilayer vesicles: A micropipet study. *Langmuir* **19**, 1054-1062 (2003).

157   Rawicz, W., Olbrich, K., McIntosh, T., Needham, D. & Evans, E. Effect of chain length and unsaturation on elasticity of lipid bilayers. *Biophysical Journal* **79**, 328-339 (2000).

158   Butt, H.-J. Measuring electrostatic, van der Waals, and hydration forces in electrolyte solutions with an atomic force microscope. *Biophysical Journal* **60**, 1438-1444 (1991).

159   Ducker, W. A., Senden, T. J. & Pashley, R. M. Direct measurement of colloidal forces using an atomic force microscope. *nature* **353**, 239 (1991).

160   Sheng, S., Czajkowsky, D. & Shao, Z. AFM tips: how sharp are they? *Journal of microscopy* **196**, 1-5 (1999).

161   Skulason, H. & Frisbie, C. D. Rupture of hydrophobic microcontacts in water: correlation of pull-off force with AFM tip radius. *Langmuir* **16**, 6294-6297 (2000).

162   Zhang, Z., Ferenczi, M., Lush, A. & Thomas, C. A novel micromanipulation technique for measuring the bursting strength of single mammalian cells. *Appl Microbiol Biot* **36**, 208-210 (1991).

163   Hu, J., Chen, H.-Q. & Zhang, Z. Mechanical properties of melamine formaldehyde microcapsules for self-healing materials. *Mater Chem Phys* **118**, 63-70 (2009).

164   Stenekes, R. J. *et al.* Pore sizes in hydrated dextran microspheres. *Biomacromolecules* **1**, 696-703 (2000).

165   Zhang, Z. Mechanical strength of single microcapsules determined by a novel micromanipulation technique. *J Microencapsul* **16**, 117-124 (1999).

166   Zhang, Z., Ferenczi, M. & Thomas, C. A micromanipulation technique with a theoretical cell model for determining mechanical properties of single mammalian cells. *Chemical Engineering Science* **47**, 1347-1354 (1992).

167   Zhao, L. & Zhang, Z. Mechanical characterization of biocompatible microspheres and microcapsules by direct compression. *Artificial cells, blood substitutes, and biotechnology* **32**, 25-40 (2004).

168   Dipietro, E. *et al.* Comparison of an inductively coupled plasma-atomic emission spectrometry method for the determination of calcium, magnesium, sodium, potassium, copper and zinc with atomic absorption spectroscopy and flame photometry methods. *Sci Total Environ* **74**, 249-262 (1988).

169   Skoog, D. A., Holler, F. J. & Crouch, S. R. *Principles of instrumental analysis*. (Cengage learning, 2017).

170   Henderson, R. K. *et al.* Fluorescence as a potential monitoring tool for recycled water systems: a review. *Water Res* **43**, 863-881 (2009).

171   Szczepanowicz, K. *et al.* Biocompatible long-sustained release oil-core polyelectrolyte nanocarriers: from controlling physical state and stability to biological impact. *Adv Colloid Interfac* **222**, 678-691 (2015).

172   Wang, X., Zhou, W., Cao, J., Liu, W. & Zhu, S. Preparation of core–shell CaCO3 capsules via Pickering emulsion templates. *J Colloid Interf Sci* **372**, 24-31 (2012).

173   Ciriminna, R., Sciortino, M., Alonzo, G., Schrijver, A. d. & Pagliaro, M. From molecules to systems: Sol– gel microencapsulation in silica-based materials. *Chemical reviews* **111**, 765-789 (2010).

174   Tang, F., Li, L. & Chen, D. Mesoporous silica nanoparticles: synthesis, biocompatibility and drug delivery. *Adv Mater* **24**, 1504-1534 (2012).

175   Chen, D. *et al.* Micro–Nanocomposites in Environmental Management. *Adv Mater* **28**, 10443-10458 (2016).

176   Ge, J. *et al.* Advanced sorbents for Oil‐Spill cleanup: Recent advances and future perspectives. *Adv Mater* **28**, 10459-10490 (2016).

177   Ruan, C., Ai, K., Li, X. & Lu, L. A superhydrophobic sponge with excellent absorbency and flame retardancy. *Angewandte Chemie International Edition* **53**, 5556-5560 (2014).

178   Ford, B. J. From Dilettante to Diligent Experimenter, a Reappraisal of Leeuwenhoek as microscopist and investigator. *Biology History* **5**, 5-6 (1992).

179   Goodwin, P. C. A primer on the fundamental principles of light microscopy: Optimizing magnification, resolution, and contrast. *Molecular Reproduction & Development* **82**, 502 (2015).

180   Goldstein, J. Scanning Electron Microscopy and X-ray Microanalysis: Third Edition. (2003).

181   Goldstein, J. I. *et al.* in *Scanning Electron Microscopy and X-Ray Microanalysis*   271-296 (Springer, 2003).

182   Xu, R. *Particle characterization: light scattering methods*. Vol. 13 (Springer Science & Business Media, 2001).

183   Xu, R. Books-PARTICLE CHARACTERIZATION: LIGHT SCATTERING METHODS. Kluwer Academic Publishers, Dordrecht/Boston/London (2000), 432,(Particle Technology Series, No. 13) Hardbound, ISBN 0-7923-6300-0, US $172. *China Particuology* **1**, 271 (2003).

184   Kissa, E. *Dispersions: Characterization, testing, and measurement*. Vol. 84 (CRC Press, 1999).

185   Brown, W., Johansson, K. & Almgren, M. Threadlike micelles from cetyltrimethylammonium bromide in aqueous sodium naphthalenesulfonate solutions studied by static and dynamic light scattering. *The Journal of Physical Chemistry* **93**, 5888-5894 (1989).

186   Berzina-Cimdina, L. & Borodajenko, N. in *Infrared Spectroscopy-Materials Science, Engineering and Technology*   (InTech, 2012).

187   Chai, L., Wang, X. & Wu, D. Development of bifunctional microencapsulated phase change materials with crystalline titanium dioxide shell for latent-heat storage and photocatalytic effectiveness. *Applied Energy* **138**, 661-674 (2015).

188   Moore, Z. *Application of x-ray diffraction methods and molecular mechanics simulations to structure determination and cotton fiber analysis*, University of New Orleans, (2008).

189   Qiao, R., Zhang, X. L., Qiu, R., Li, Y. & Kang, Y. S. Fabrication of superparamagnetic cobalt nanoparticles-embedded block copolymer microcapsules. *The Journal of Physical Chemistry C* **111**, 2426-2429 (2007).

190   Marangoni, A. G. *Structure-function analysis of edible fats*. (AOCS Press Urbana, 2012).

191   Sankar, G. *et al.* Combined QuEXAFS-XRD: a new technique in high-temperature materials chemistry; an illustrative in situ study of the zinc oxide-enhanced solid-state production of cordierite from a precursor zeolite. *The Journal of Physical Chemistry* **97**, 9550-9554 (1993).

192   Esteves, L. P. On the hydration of water-entrained cement–silica systems: combined SEM, XRD and thermal analysis in cement pastes. *Thermochimica Acta* **518**, 27-35 (2011).

193   Sacksteder, C. & Barry, B. A. FOURIER TRANSFORM INFRARED SPECTROSCOPY: A MOLECULAR APPROACH TO AN ORGANISMAL QUESTION. *Journal of Phycology* **37**, 197–199 (2001).

194   Wang, J. *et al.* Near‐Infrared‐Light‐Mediated Imaging of Latent Fingerprints based on Molecular Recognition. *Angewandte Chemie* **126**, 1642-1646 (2014).

195   Mwaikambo, L. Y. & Ansell, M. P. Chemical modification of hemp, sisal, jute, and kapok fibers by alkalization. *J Appl Polym Sci* **84**, 2222-2234 (2002).

196   Fivga, A. *Comparison of the effect of pre-treatment and catalysts on liquid quality from fast pyrolysis of biomass*, Aston University, (2012).

197   Lee, H., Cho, J.-L., Yoon, E.-S., Cho, M. & Kim, D.-G. Assessment of Mass Fraction and Melting Temperature for the Application of Limestone Concrete and Siliceous Concrete to Nuclear Reactor Basemat Considering Molten Core–Concrete Interaction. *Nuclear Engineering and Technology* **48**, 448-456 (2016).

198   principles, I. D. P. T. o. p. P. G. ISO/FDIS 11358-1 - Plastics -- Thermogravimetry (TG) of polymers -- Part 1: General principles.

199   Goldstein, J. I. *et al. Scanning electron microscopy and X-ray microanalysis*. (Springer, 2017).

200   Bertin, E. P. *Principles and practice of X-ray spectrometric analysis*. (Springer Science & Business Media, 2012).

201   Gu, X., Xie, X., Li, N., Zheng, Y. & Qin, L. In vitro and in vivo studies on a Mg–Sr binary alloy system developed as a new kind of biodegradable metal. *Acta Biomater* **8**, 2360-2374 (2012).

202   Barr, T. L. *Modern ESCAThe Principles and Practice of X-Ray Photoelectron Spectroscopy*. (CRC press, 1994).

203   Van Grieken, R. & Markowicz, A. *Handbook of X-ray Spectrometry*. (CRC press, 2001).

204   Istone, W. K. *X-ray photoelectron spectroscopy (XPS)*. (CRC Press, 1995).

205 Gao, M.-R. *et al.* An efficient molybdenum disulfide/cobalt diselenide hybrid catalyst for electrochemical hydrogen generation. *Nat Commun* **6**, 5982 (2015).

206 Thomas, H. R. & O'Malley, J. J. Surface studies on multicomponent polymer systems by X-ray photoelectron spectroscopy. Polystyrene/poly (ethylene oxide) diblock copolymers. *Macromolecules* **12**, 323-329 (1979).

207 Maeda, S., Gill, M., Armes, S. P. & Fletcher, I. W. Surface characterization of conducting polymer-silica nanocomposites by X-ray photoelectron spectroscopy. *Langmuir* **11**, 1899-1904 (1995).

208 Schroder, D. K. *Semiconductor material and device characterization*. (John Wiley & Sons, 2006).

209 Ge, J. *et al.* Joule-heated graphene-wrapped sponge enables fast clean-up of viscous crude-oil spill. *Nature nanotechnology* **12**, 434 (2017).

210 Liu, B., He, Y., Fan, Y. & Wang, X. Fabricating super‐hydrophobic lotus‐leaf‐like surfaces through soft‐lithographic imprinting. *Macromol Rapid Comm* **27**, 1859-1864 (2006).

211 Feng, X. & Jiang, L. Design and creation of superwetting/antiwetting surfaces. *Adv Mater* **18**, 3063-3078 (2006).

212 Sun, T., Feng, L., Gao, X. & Jiang, L. Bioinspired surfaces with special wettability. *Accounts Chem Res* **38**, 644-652 (2005).

213 Young, T. III. An essay on the cohesion of fluids. *Philosophical transactions of the royal society of London* **95**, 65-87 (1805).

214 Girifalco, L. & Good, R. J. A theory for the estimation of surface and interfacial energies. I. Derivation and application to interfacial tension. *The Journal of Physical Chemistry* **61**, 904-909 (1957).

215 Yuan, Y. & Lee, T. R. in *Surface science techniques*   3-34 (Springer, 2013).

216 Robinson, J. W. *Atomic spectroscopy*. (CRC Press, 1996).

217 Thomas, O. & Burgess, C. *UV-visible spectrophotometry of water and wastewater*. (Elsevier, 2017).

218 Shchukina, E. M. & Shchukin, D. G. Layer-by-layer coated emulsion microparticles as storage and delivery tool. *Curr Opin Colloid In* **17**, 281-289, doi:DOI 10.1016/j.cocis.2012.06.003 (2012).

219 Liu, K. *et al.* Simple Peptide-Tuned Self-Assembly of Photosensitizers towards Anticancer Photodynamic Therapy. *Angew Chem Int Edit* **55**, 3036-3039, doi:10.1002/anie.201509810 (2016).

220 Cui, J. W. *et al.* Monodisperse Polymer Capsules: Tailoring Size, Shell Thickness, and Hydrophobic Cargo Loading via Emulsion Templating. *Adv Funct Mater* **20**, 1625-1631, doi:DOI 10.1002/adfm.201000209 (2010).

221 Jyothi, N. V. N. *et al.* Microencapsulation techniques, factors influencing encapsulation efficiency. *J Microencapsul* **27**, 187-197, doi:Doi 10.3109/02652040903131301 (2010).

222 Long, Y., Vincent, B., York, D., Zhang, Z. B. & Preece, J. A. Organic-inorganic double shell composite microcapsules. *Chem Commun* **46**, 1718-1720 (2010).

223 Long, Y., York, D., Zhang, Z. B. & Preece, J. A. Microcapsules with low content of formaldehyde: preparation and characterization. *J Mater Chem* **19**, 6882-6887, doi:Doi 10.1039/B902832c (2009).

224 Yang, Y. Y., Chung, T. S. & Ng, N. P. Morphology, drug distribution, and in vitro release profiles of biodegradable polymeric microspheres containing protein fabricated by double-emulsion solvent extraction/evaporation method. *Biomaterials* **22**, 231-241, doi:Doi 10.1016/S0142-9612(00)00178-2 (2001).

225 Keen, P. H. R., Slater, N. K. H. & Routh, A. F. Encapsulation of Amylase in Colloidosomes. *Langmuir* **30**, 1939-1948 (2014).

226 Elabbadi, A., Jeckelmann, N., Haefliger, O. P. & Ouali, L. Complexation/encapsulation of green tea polyphenols in mixed calcium carbonate and phosphate micro-particles. *J Microencapsul* **28**, 1-9 (2011).

227   Sui, C. *et al.* Synthesis of Mesoporous Calcium Phosphate Microspheres by Chemical Transformation Process: Their Stability and Encapsulation of Carboxymethyl Chitosan. *Cryst Growth Des* **13**, 3201-3207 (2013).

228   Zhao, Y. *et al.* A Preloaded Amorphous Calcium Carbonate/Doxorubicin@Silica Nanoreactor for pH-Responsive Delivery of an Anticancer Drug. *Angew Chem Int Edit* **54**, 919-922, doi:DOI 10.1002/anie.201408510 (2015).

229   Zhang, H., Fei, J. B., Yan, X. H., Wang, A. H. & Li, J. B. Enzyme-Responsive Release of Doxorubicin from Monodisperse Dipeptide-Based Nanocarriers for Highly Efficient Cancer Treatment In Vitro. *Adv Funct Mater* **25**, 1193-1204, doi:10.1002/adfm.201403119 (2015).

230   Bassindale, A. R., Pourny, M., Taylor, P. G., Hursthouse, M. B. & Light, M. E. Fluoride-ion encapsulation within a silsesquioxane cage. *Angew Chem Int Edit* **42**, 3488-3490, doi:10.1002/anie.200351249 (2003).

231   Behzadi, S. *et al.* Osmotic pressure-dependent release profiles of payloads from nanocontainers by co-encapsulation of simple salts. *Nanoscale* **8**, 12998-13005, doi:10.1039/c6nr01882c (2016).

232   Fiore, A. *et al.* Controlling the Maillard Reaction by Reactant Encapsulation: Sodium Chloride in Cookies. *J Agr Food Chem* **60**, 10808-10814, doi:10.1021/jf3026953 (2012).

233   Oro, E., de Gracia, A., Castell, A., Farid, M. M. & Cabeza, L. F. Review on phase change materials (PCMs) for cold thermal energy storage applications. *Appl Energ* **99**, 513-533, doi:10.1016/j.apenergy.2012.03.058 (2012).

234   Wu, P. C., Huang, Y. B., Chang, J. I., Tsai, M. J. & Tsai, Y. H. Preparation and evaluation of sustained release microspheres of potassium chloride prepared with ethylcellulose. *Int J Pharm* **260**, 115-121, doi:Doi 10.1016/S0378-5173(03)00255-2 (2003).

235   Wu, P. C., Huang, Y. B., Chang, J. S., Tsai, M. J. & Tsai, Y. H. Design and evaluation of sustained release microspheres of potassium chloride prepared by Eudragit (R). *Eur J Pharm Sci* **19**, 115-122, doi:10.1016/S0928-0987(03)00069-1 (2003).

236   Wu, P. C., Tsai, M. J., Huang, Y. B., Chang, J. S. & Tsai, Y. H. In vitro and in vivo evaluation of potassium chloride sustained release formulation prepared with saturated polyglycolyed glycerides matrices. *Int J Pharm* **243**, 119-124, doi:Pii S0378-5173(02)00264-8

Doi 10.1016/S0378-5173(02)00264-8 (2002).

237   Varshney, K. G., Pandith, A. H. & Gupta, U. Synthesis and characterization of zirconium aluminophosphate. A new cation exchanger. *Langmuir* **14**, 7353-7358, doi:Doi 10.1021/La970464j (1998).

238   Jung, W. M., Kang, S. H., Kim, K. S., Kim, W. S. & Choi, C. K. Precipitation of calcium carbonate particles by gas-liquid reaction: Morphology and size distribution of particles in Couette-Taylor and stirred tank reactors. *J Cryst Growth* **312**, 3331-3339, doi:10.1016/j.jcrysgro.2010.08.026 (2010).

239   Zhao, Y. *et al.* Templating Synthesis of Preloaded Doxorubicin in Hollow Mesoporous Silica Nanospheres for Biomedical Applications. *Adv Mater* **22**, 5255-5259, doi:10.1002/adma.201002395 (2010).

240   Almeida, R. M. & Pantano, C. G. Structural Investigation of Silica-Gel Films by Infrared-Spectroscopy. *J Appl Phys* **68**, 4225-4232, doi:Doi 10.1063/1.346213 (1990).

241   Bertoluzza, A., Fagnano, C., Morelli, M. A., Gottardi, V. & Guglielmi, M. Raman and Infrared-Spectra on Silica-Gel Evolving toward Glass. *J Non-Cryst Solids* **48**, 117-128, doi:Doi 10.1016/0022-3093(82)90250-2 (1982).

242   Galeener, F. L. Band Limits and the Vibrational-Spectra of Tetrahedral Glasses. *Phys Rev B* **19**, 4292-4297, doi:DOI 10.1103/PhysRevB.19.4292 (1979).

243   Fan, W. G. & Gao, L. Synthesis of silica hollow spheres assisted by ultrasound. *J Colloid Interf Sci* **297**, 157-160, doi:10.1016/j.jcis.2005.10.021 (2006).

244 Jang, J., Ha, J. & Cho, J. Fabrication of water-dispersible polyaniline-poly(4-styrenesulfonate) nanoparticles for inkjet-printed chemical-sensor applications. *Adv Mater* **19**, 1772-+, doi:10.1002/adma.200602127 (2007).

245 Lu, X. Y. & Weiss, R. A. Development of Miscible Blends of Polyamide-6 and Manganese Sulfonated Polystyrene Using Specific Interactions. *Macromolecules* **24**, 4381-4385, doi:Doi 10.1021/Ma00015a021 (1991).

246 Zundel, G. *Hydration and intermolecular interaction; infrared investigations with polyelectrolyte membranes*. (Academic Press, 1969).

247 Nasef, M. M., Saidi, H. & Nor, H. M. Cation exchange membranes by radiation-induced graft copolymerization of styrene onto PFA copolymer films. III. Thermal stability of the membranes. *J Appl Polym Sci* **77**, 1877-1885, doi:Doi 10.1002/1097-4628(20000829)77:9<1877::Aid-App3>3.0.Co;2-X (2000).

248 Bunchman, T. E. *et al.* Pretreatment of Formula with Sodium Polystyrene Sulfonate to Reduce Dietary Potassium Intake. *Pediatr Nephrol* **5**, 29-32 (1991).

249 Mahltig, B. & Bottcher, H. Modified silica sol coatings for water-repellent textiles. *J Sol-Gel Sci Techn* **27**, 43-52, doi:Doi 10.1023/A:1022627926243 (2003).

250 Tamaki, R. & Chujo, Y. Synthesis of polystyrene and silica gel polymer hybrids utilizing ionic interactions. *Chem Mater* **11**, 1719-1726, doi:Doi 10.1021/Cm9810741 (1999).

251 Fritz, E. Measurement of cation exchange capacity (CEC) of plant cell walls by X-ray microanalysis (EDX) in the transmission electron microscope. *Microsc Microanal* **13**, 233-244, doi:10.1017/S1431927607070420 (2007).

252 Zhang, Z., Saunders, R. & Thomas, C. R. Mechanical strength of single microcapsules determined by a novel micromanipulation technique. *J Microencapsul* **16**, 117-124 (1999).

253 Casanova, F. & Santos, L. Encapsulation of cosmetic active ingredients for topical application - a review. *J Microencapsul* **33**, 1-17 (2016).

254 Kim, B. J. *et al.* Cytoprotective Alginate/Polydopamine Core/Shell Microcapsules in Microbial Encapsulation. *Angew Chem Int Edit* **53**, 14443-14446 (2014).

255 Lee, H. *et al.* Encapsulation and Enhanced Retention of Fragrance in Polymer Microcapsules. *Acs Appl Mater Inter* **8**, 4007-4013 (2016).

256 Windbergs, M., Zhao, Y., Heyman, J. & Weitz, D. A. Biodegradable Core-Shell Carriers for Simultaneous Encapsulation of Synergistic Actives. *J Am Chem Soc* **135**, 7933-7937 (2013).

257 Abdekhodaie, M. J., Cheng, J. & Wu, X. Y. Effect of formulation factors on the bioactivity of glucose oxidase encapsulated chitosan-alginate microspheres: In vitro investigation and mathematical model prediction. *Chem Eng Sci* **125**, 4-12 (2015).

258 Dogan, E. M., Sudur Zalluhoglu, F. & Orbey, N. Effect of potassium ion on the stability and release rate of hydrogen peroxide encapsulated in silica hydrogels. *AIChE Journal* **63**, 409-417, doi:10.1002/aic.15406 (2017).

259 Bhaumik, J. *et al.* Bioinspired nanotheranostic agents: synthesis, surface functionalization, and antioxidant potential. *Acs Biomater Sci Eng* **1**, 382-392 (2015).

260 Sui, C., Preece, J. A. & Zhang, Z. Novel polystyrene sulfonate-silica microspheres as a carrier of a water soluble inorganic salt (KCl) for its sustained release, via a dual-release mechanism. *RSC Advances* **7**, 478-481, doi:10.1039/C6RA25488H (2017).

261 Nadian, A. & Lindblom, L. Studies on the development of a microencapsulated delivery system for norbormide, a species-specific acute rodenticide. *Int J Pharm* **242**, 63-68, doi:Pii S0378-5173(02)00142-4

Doi 10.1016/S0378-5173(02)00142-4 (2002).

262 Pearnchob, N., Dashevsky, A. & Bodmeier, R. Improvement in the disintegration of shellac-coated soft gelatin capsules in simulated intestinal fluid. *J Control Release* **94**, 313-321, doi:DOI 10.1016/j.jconrel.2003.10.004 (2004).

263   Sheorey, D. S., Shastri, A. S. & Dorle, A. K. Effect of Variables on the Preparation of Shellac Microcapsules by Solvent Evaporation Technique .1. *Int J Pharm* **68**, 19-23, doi:Doi 10.1016/0378-5173(91)90122-5 (1991).

264   Xue, J. & Zhang, Z. B. Preparation and characterization of calcium-shellac spheres as a carrier of carbamide peroxide. *J Microencapsul* **25**, 523-530, doi:Pii 792371718

Doi 10.1080/02652040802049638 (2008).

265   Lakshminarayanan, T. & Gupta, M. Nature of cure of shellac – amino resin blends. *J Appl Polym Sci* **22**, 3035-3037 (1978).

266   Chen, D. *et al.* Micro-Nanocomposites in Environmental Management. *Adv Mater* **28**, 10443-10458, doi:10.1002/adma.201601486 (2016).

267   Ge, J. *et al.* Advanced Sorbents for Oil-Spill Cleanup: Recent Advances and Future Perspectives. *Adv Mater* **28**, 10459-10490, doi:10.1002/adma.201601812 (2016).

268   Ruan, C. P., Ai, K. L., Li, X. B. & Lu, L. H. A Superhydrophobic Sponge with Excellent Absorbency and Flame Retardancy. *Angew Chem Int Edit* **53**, 5556-5560 (2014).

269   White, M. A. The chemistry behind carbonless copy paper. *J Chem Educ* **75**, 1119 (1998).

270   Ghaemi, A. *et al.* Mechanical behaviour of micro-capsules and their rupture under compression. *Chem Eng Sci* **142**, 236-243 (2016).

271   Mercade-Prieto, R. *et al.* Failure of elastic-plastic core-shell microcapsules under compression. *Aiche Journal* **58**, 2674-2681 (2012).

272   Pretzl, M. *et al.* Formation and Mechanical Characterization of Aminoplast Core/Shell Microcapsules. *Acs Appl Mater Inter* **4**, 2940-2948 (2012).

273   Schrade, A., Landfester, K. & Ziener, U. Pickering-type stabilized nanoparticles by heterophase polymerization. *Chem Soc Rev* **42**, 6823-6839 (2013).

274   Merline, D. J., Vukusic, S. & Abdala, A. A. Melamine formaldehyde: curing studies and reaction mechanism. *Polym J* **45**, 413 (2013).

275   He, X. D., Ge, X. W. W., Wang, M. Z. & Zhang, Z. C. Polystyrene/melamine-formaldehyde hollow microsphere composite by self-assembling of latex particles at emulsion droplet interface. *Polymer* **46**, 7598-7604 (2005).

276   Hong, K. & Park, S. Melamine resin microcapsules containing fragrant oil: synthesis and characterization. *Mater Chem Phys* **58**, 128-131 (1999).

277   Seetapan, N., Limparyoon, N. & Kiatkamjornwong, S. Effect of fire retardant on flammability of acrylamide and 2-acrylamido-2-methylpropane sodium sulfonate copolymer composites. *Polym Degrad Stabil* **96**, 1927-1933 (2011).

278   Lanthong, P., Nuisin, R. & Kiatkamjornwong, S. Graft copolymerization, characterization, and degradation of cassava starch-g-acrylamide/itaconic acid superabsorbents. *Carbohyd Polym* **66**, 229-245 (2006).

279   Liu, M. *Understanding the mechanical strength of microcapsules and their adhesion on fabric surfaces*, University of Birmingham, (2010).

280   Su, J. F., Qiu, J., Schlangen, E. & Wang, Y. Y. Investigation the possibility of a new approach of using microcapsules containing waste cooking oil: In situ rejuvenation for aged bitumen. *Constr Build Mater* **74**, 83-92 (2015).

281   Mercade-Prieto, R. *et al.* Compression of elastic-perfectly plastic microcapsules using micromanipulation and finite element modelling: Determination of the yield stress. *Chem Eng Sci* **66**, 1835-1843 (2011).

282   Bhatia, D., Sarkar, P. & Alam, M. Specular reflectance and derivative spectrometric studies on lac-melamine formaldehyde (MF) resin blends. *Pigment & resin technology* **35**, 260-269 (2006).

283   Benita, S. Microencapsulation: Methods and Industrial Applications. *Crc Press* (2006).

284   Desai, T. & Shea, L. D. Advances in islet encapsulation technologies. *Nature Reviews Drug Discovery* (2016).

285   Orive, G., Emerich, D. & De Vos, P. Encapsulate this: the do's and don'ts. *Nature medicine* **20**, 233-233 (2014).

286   Lakkis, J. M. *Encapsulation and controlled release technologies in food systems*. (John Wiley & Sons, 2016).

287   Bhujbal, S. V., de Vos, P. & Niclou, S. P. Drug and cell encapsulation: alternative delivery options for the treatment of malignant brain tumors. *Advanced drug delivery reviews* **67**, 142-153 (2014).

288   Parikh, D. M. *Handbook of pharmaceutical granulation technology*. (CRC Press, 2016).

289   Ulbrich, K. *et al.* Targeted drug delivery with polymers and magnetic nanoparticles: covalent and noncovalent approaches, release control, and clinical studies. *Chemical reviews* **116**, 5338-5431 (2016).

290   Bandeira, N. A. *et al. Microencapsulation: innovative applications*. (Walter de Gruyter GmbH & Co KG, 2015).

291   Martins, I. M., Barreiro, M. F., Coelho, M. & Rodrigues, A. E. Microencapsulation of essential oils with biodegradable polymeric carriers for cosmetic applications. *Chemical Engineering Journal* **245**, 191-200 (2014).

292   Sagis, L. M. *Microencapsulation and microspheres for food applications*. (Academic Press, 2015).

293   Hirayama, F. & Uekama, K. Cyclodextrin-based controlled drug release system. *Advanced drug delivery reviews* **36**, 125-141 (1999).

294   Augustin, M. A. & Hemar, Y. Nano-and micro-structured assemblies for encapsulation of food ingredients. *Chemical Society Reviews* **38**, 902-912 (2009).

295   Ciriminna, R. & Pagliaro, M. Sol–gel microencapsulation of odorants and flavors: opening the route to sustainable fragrances and aromas. *Chemical Society Reviews* **42**, 9243-9250 (2013).

296   Dolgin, E. Encapsulate this. *Nature medicine* **20**, 9-11 (2014).

297   McHugh, K. J. *et al.* Fabrication of fillable microparticles and other complex 3D microstructures. *Science* **357**, 1138-1142 (2017).

298   Jiang, Z.-R. *et al.* Coating sponge with a hydrophobic porous coordination polymer containing a low-energy CF 3-decorated surface for continuous pumping recovery of an oil spill from water. *NPG Asia Materials* **8**, e253 (2016).

299   Mercadé-Prieto, R. *et al.* Determination of the elastic properties of single microcapsules using micromanipulation and finite element modeling. *Chemical Engineering Science* **66**, 2042-2049 (2011).

300   Solans, C., Izquierdo, P., Nolla, J., Azemar, N. & Garcia-Celma, M. Nano-emulsions. *Current opinion in colloid & interface science* **10**, 102-110 (2005).

301   He, X., Xuewu, W. G., Wang, M. & Zhang, Z. Polystyrene/melamine-formaldehyde hollow microsphere composite by self-assembling of latex particles at emulsion droplet interface. *Polymer* **46**, 7598-7604 (2005).

302   Pham, V. H. & Dickerson, J. H. Superhydrophobic silanized melamine sponges as high efficiency oil absorbent materials. *ACS applied materials & interfaces* **6**, 14181-14188 (2014).

303   Ulman, A. *An Introduction to Ultrathin Organic Films: From Langmuir--Blodgett to Self--Assembly*. (Academic press, 2013).

304   Kulkarni, S. A., Mirji, S., Mandale, A. & Vijayamohanan, K. P. Thermal stability of self-assembled octadecyltrichlorosilane monolayers on planar and curved silica surfaces. *Thin Solid Films* **496**, 420-425 (2006).

305   Sui, C., Preece, J. A. & Zhang, Z. Novel polystyrene sulfonate–silica microspheres as a carrier of a water soluble inorganic salt (KCl) for its sustained release, via a dual-release mechanism. *RSC Advances* **7**, 478-481 (2017).